Universidad Nacional Autónoma de México

FACULTAD DE CIENCIAS

Relaxation and thermalization in nonlinear lattices: beyond the Fermi-Pasta-Ulam-Tsingou model

T E S I S

QUE PARA OPTAR POR EL GRADO DE:

Físico

PRESENTA:

José Ángel Aké Jiménez

DIRECTOR DE TESIS:
Dr. Gerardo García Naumis

Ciudad de México, 2025

1. Datos del alumno
Aké
Jiménez
José Ángel
9381261136
Universidad Nacional Autónoma de México
Facultad de Ciencias
Física
421059650

2. Datos del tutor
Dr
Gerardo
García
Naumis

3. Datos del sinodal 1
Dr
Carlos
Villareal
Luján

4. Datos del sinodal 2
Dr
Francisco Javier
Mandujano
Sánchez

5. Datos del sinodal 3
Dr
Luis
Benet
Fernández

6. Datos del sinodal 4
Dr
Francisco
Nettel
Rueda

7. Datos del trabajo escrito
Relaxation and thermalization in nonlinear lattices: beyond the Fermi-Pasta-Ulam-Tsingou model
pages
2025

Agradecimientos

Aquellos que me conocen saben que soy un sarcástico, un cínico, a veces un pesado, rudo, serio y amargado. Y aquellos que me conocen aún mejor saben que solo soy un alma sensible y melancólica, que intentar entender el sufrimiento que a todos nos une a todos los humanos. Con esto en mente, me gustaría aprovechar este minúsculo instante para intentar expresar aquello que no puede ser expresado en palabras. Pues aunque al final, todas estas palabras desaparecerán, igual que lágrimas en la lluvia, las acciones se quedan con nosotros.

A mis padres, quienes enfrentaron monstruos invisibles como la pobreza, el hambre y la desigualdad, y, aun así, salir adelante, junto a mí y a mi hermano, en busca de un mejor porvenir.

A mi hermano, quien desde que llegó a mi vida ha sido mi más grande compañero, juntos en los momentos más duros, cuando nuestros padres no estuvieron junto a nosotros, y quien ha sido mi mayor motor para salir adelante junto a él.

A mis abuelos, tíos, primos, y a toda mi familia que, de mencionarlos a todos, no cabría en este minúsculo pedazo de existencia. Para mostrarles al mundo que es posible iniciar desde lo más bajo y llegar a lo más alto.

A mis amigos, desde quien me conoce desde muy joven hasta los que me conocieron en la carrera. En particular, a estos, les debo más que mi gratitud. Desde quien empezó conmigo y ya no está, hasta quienes conocí hasta el final. Gracias a ellos, a quienes logré encontré un hogar en esta ciudad de realidades, miserias y aventuras, viendo más allá de la región más transparente, al haber llegado aquí sin conocer nada ni a nadie. Ustedes, aunque sus nombres no los diga, saben quiénes son.

A Azaneth González. Quien, aunque no estuvo presente durante los últimos años, estuvo en el momento necesario para escribir estas palabras.

A aquellos que por mi culpa me he infligido un daño en el corazón, y a quienes también se los he infligido.

A mis profesores de la carrera. A la Dra. Mirna Villavicencio, a los doctores Víctor Romero, Alberto Vázquez, Ricardo Atahualpa, Reyes Coronado, Francisco Mandujano, Eric Vázquez, Jorge Seman y Rafael Barrio, por ayudarme a acercarme un poco más al ideal de físico que deseo ser.

Por último, pero no por ello menos importante, al Dr. Gerardo García Naumis. Quien me ha acogido como su pupilo y me dio la oportunidad de trabajar y de aprender con él. Quien me ha dejado ver un poco más allá de su figura de mentor para ver a un ser humano con sus gustos, pasiones y preocupaciones, y a quien espero no haberle defraudado, poder seguir trabajando con él en el futuro y seguir aprendiendo de él.

Declaración de autenticidad

Por la presente declaro que, salvo cuando se haga referencia específica al trabajo de otras personas, el contenido de esta tesis es original y no se ha presentado total o parcialmente para su consideración para cualquier otro título o grado en esta o cualquier otra Universidad. Esta tesis es resultado de mi propio trabajo y no incluye nada que sea el resultado de algún trabajo realizado en colaboración, salvo que se indique específicamente en el texto.

José Ángel Aké Jiménez. Ciudad de México, 2025

Insert random quote here...

Resumen/Abstract

In the early 1950s, a study was conducted by four scientists from Los Alamos to address a seemingly simple question:

What happens when a small nonlinearity is introduced into a system of coupled oscillators?

Through their research, unexpected behavior was discovered in thermalization, energy localization, and recurrence in the system, ultimately leading to a fundamental challenge to the principles of statistical physics.

More than half a century later, the problem, now known as the Fermi-Pasta-Ulam-Tsingou problem, is still regarded as a cornerstone of nonlinear dynamics and computational physics. In this work, the problem is revisited, and its framework is extended to alternating mass/spring systems, exploring its consequences, with a focus on its effects on relaxation dynamics and energy localization.

Although the case of alternanting masses was previously studied in the literature, the case of different spring constants has not been studied before. This last case is interesting as it is a model for polymers and topological insulators. In this thesis, site dependent spring constants are considered.

Índice general

Introduction

Los Alamos, 1954. The war had ended, but a new scientific era had begun. With the Cold War fueling technological advances, modern computers emerged, offering unprecedented opportunities for scientific exploration. Among the European scientists who remained in the United States were Enrico Fermi, John Pasta, and Stanislaw Ulam, who, in this fertile intellectual environment, posed a seemingly simple question:

What happens when a system of masses and springs is perturbed with a slight nonlinearity?

At the time, classical statistical mechanics predicted that energy should eventually spread across all degrees of freedom, a consequence of the ergodic hypothesis (cite). For the first time, computers provided a way to test this assumption. Mary Tsingou, tasked with running the simulations, played a crucial role in obtaining the results—though her contributions remained unrecognized for decades [1].

When the results arrived, they were stunning: Energy failed to spread, the ergodic hypothesis appeared to break down, and the system did not reach thermal equilibrium. These findings raised fundamental questions. Was this a failure of statistical mechanics? Or just an anomaly?

Before these questions could be answered, Fermi passed away in 1954, and the group abandoned the study [2]. Years later, the preprint resurfaced in Fermi's unpublished works, laying the foundation for computational physics and nonlinear dynamics.

Even today, the Fermi-Pasta-Ulam-Tsingou (FPUT) problem remains central to discussions of thermalization, equipartition, and statistical mechanics [3, 4]. Some view it as a paradox that challenges fundamental assumptions, while others regard it as a computational curiosity with far-reaching implications.

Beyond its theoretical significance, the FPUT framework has influenced modern physics, particularly in glasses [5, 6] and metamaterials [7]. Extensions to site dependent systems have fueled research on energy localization and transport, making further generalizations of the model essential for understanding the interplay of nonlinearity, site dependent, and energy dynamics.

Despite decades of research, fundamental questions remain. Does the system truly fail to thermalize? Is the FPUT problem a genuine challenge to statistical physics, or simply an exceptional case? This thesis explores these questions, focusing on the role of site dependent, high nonlinearity regimes, and various initial and boundary conditions.

Chapter 1 develops the theoretical foundation, from classical oscillations to coupled nonlinear systems, motivating extensions to site dependent systems.

Chapter 2 examines relaxation dynamics in an FPUT system with varying masses, analyzing different initial and boundary conditions.

Chapter 3 extends this study to an FPUT system with varying spring constants, following a similar approach.

Chapter 4 presents conclusions and future directions.

By addressing these aspects, this work takes a step toward understanding the fundamental mechanisms of energy transport and thermalization in nonlinear and site dependent systems.

Capítulo 1

Mathematical and Physical Foundations

To address the problem at hand, it is essential to establish a solid theoretical foundation. This chapter begins with a review of the Fermi-Pasta-Ulam-Tsingou (FPUT) problem, outlining the fundamental mathematical framework governing nonlinear lattices. Key analytical tools are introduced, starting from the linear case and extending to the nonlinear regime, where mode interactions and energy transfer mechanisms play a crucial role. Additionally, these concepts are expanded to incorporate systems with alternating masses and springs, providing a broader perspective on their implications for thermalization, wave turbulence, and statistical mechanics.

1.1. Foundations of the Fermi-Pasta-Ulam-Tsingou Problem

1.1.1. The linear case

Before introducing the original problem, it is useful to consider the Hamiltonian governing a one-dimensional chain of N coupled oscillators:

$$H = \sum_{i=1}^{N} \frac{p_i^2}{2m} + \frac{1}{2}\kappa \sum_{i=1}^{N} (q_{i+1} - q_i)^2, . \tag{1.1}$$

where q_i and p_i are the position and momentum of the i-th mass, m is the (identical) mass of each particle, and κ is the uniform spring constant.

From Eq. (1.1), the equations of motion follow:

$$\dot{q}_i = \frac{p_i}{m}, . \tag{1.2}$$

$$\dot{p}_i = \kappa(q_{i+1} - 2q_i + q_{i-1}).. \tag{1.3}$$

Combining these, the system satisfies the next equation:

$$m\ddot{q}_i = \kappa \left(q_{i+1} - 2q_i + q_{i-1}\right) .. \tag{1.4}$$

To solve for the system's normal modes, we assume a solution of the form $q_i = A_i e{-}i\omega t$ yielding:

$$-\omega^2 m A_i = \kappa \left(A_{i+1} - 2A_i + A_{i-1}\right) .. \tag{1.5}$$

where ω is the frequency of oscillation of the system. This can be rewritten in matrix form:

$$\mathbf{KA} = \lambda \mathbf{A}, . \tag{1.6}$$

where $\lambda = \omega^2/\omega_0^2$, with $\omega_0^2 = \kappa/m$, $\mathbf{A}$ is the matrix of coefficients of A_i and

$$\mathbf{K} = \begin{bmatrix} 2 & -1 & 0 & \dots & 0 \\ -1 & 2 & -1 & \dots & 0 \\ 0 & & \ddots & & \vdots \\ \vdots & & -1 & 2 & -1 \\ 0 & \dots & 0 & -1 & 2 \end{bmatrix} . \tag{1.7}$$

The eigenvectors of $\mathbf{K}$ correspond to the normal coordinates, forming the transformation matrix $\mathbf{V}$. Using this transformation, the positions and momenta can be rewritten as

$$\mathbf{q} = m^{-1/2}\mathbf{V}\mathbf{u}, . \tag{1.8}$$

where $\mathbf{u}$ represents the normal mode coordinates for position. Similarly, the momentum satisfies

$$\mathbf{p} = m^{1/2}\mathbf{V}\mathbf{P}, . \tag{1.9}$$

where $\mathbf{P}$ corresponds to the normal mode coordinates for momentum.

By substituting Eqs. (1.8) and (1.9) into Eq. (1.1), the Hamiltonian in normal coordinates takes the form

$$H = \frac{1}{2} \sum_{k=1}^{N} \left(P_k^2 + \omega_k^2 u_k^2\right) , . \tag{1.10}$$

which represents the total energy of the system expressed in terms of normal modes. Each normal mode behaves as an independent harmonic oscillator, confirming that in the linear case, energy remains separable among the modes. Moreover, it is clear that thermal equipartition can not be achieved as there is now way to share energy between the modes and this requires the addition of non-linear terms to the Hamiltonian.

1.1.1.1. The nonlinear case

In their original article, Fermi, Pasta, Ulam and Tsingou took the Hamiltonian (1.1), studying the case where $\kappa = 1$, $m = 1$ and modified it adding a cubic term, and later a quartic

term, giving now

$$H = \sum_{i=1}^{N} \frac{1}{2}p_i^2 + (q_{i+1} - q_i)^2 + \frac{1}{3}\alpha(q_{i+1} - q_i)^3 + \frac{1}{4}\beta(q_{i+1} - q_i)^4. \tag{1.11}$$

Here, α is a coupling parameter indicating the strength of the cubic nonlinear interaction, similarly β is a coupling indicating the strength of the quartic nonlinear term.

The equation (1.2) remains unchanged. However, the equation (1.3) is modified, giving

$$-\dot{p}_i = -\kappa\left[(q_{i+1} - q_i) + (q_{i-1} - q_i)\right] - \alpha\left[(q_{i+1} - q_i)^2 - (q_{i-1} - q_i)\right] - \beta\left[(q_{i+1} - q_i)^3 + (q_{i-1} - q_i)^3\right]. \tag{1.12}$$

Similar with the linear case, it is possible to write the Hamiltonian in terms of normal modes of the system, using the equations (1.8) and (1.9) and applying the same change of variables. Then we found the following equation for the case $\alpha \neq 0, \beta = 0$,

$$H = \sum_{k=1}^{N} \frac{1}{2}\left(P_k^2 + \omega_k^2 u_k\right) + \frac{\alpha}{3} \sum_{k,l,m=1}^{N} c_{klm} u_k u_l u_m \omega_k \omega_l \omega_m. \tag{1.13}$$

where c_{klm} are the coefficients between coupling for each mode. For the case, $\alpha = 0, \beta \neq 0$, something similar can be made,

$$H = \sum_{k=1}^{N} \frac{1}{2}\left(P_k^2 + \omega_k^2 u_k\right) + \frac{\beta}{4} \sum_{j,k,l,m=1}^{N} d_{jklm} u_j u_k u_l u_m \omega_j \omega_k \omega_l \omega_m. \tag{1.14}$$

where d_{jklm} are, again, the coefficients of coupling for each mode. Both equations, (1.13) and (1.14), tell us that the nonlinear terms cause mode coupling. As a consequence, energy can be transferred from one mode to several modes. A more general approach for mode coupling in different systems can be found in [8, 9]. The case where $\beta = 0$, $\alpha \neq 0$ is called an $\alpha-$FPUT chain, and the case for $\beta \neq 0$, $\alpha = 0$ is called an $\beta-$FPUT chain.

It is enough to ignore the additional terms due to the nonlinear factor α (for the case $\alpha \neq 0$, $\beta = 0$ and the case $\beta \neq 0$, $\alpha = 0$) and for other nonlinear factors of higher order. The linear terms are called the harmonic energies. This is due to the values of ω_k^2 compared to the nonlinear terms [2]. Therefore, it is possible to approximate the energy of the system in terms of normal modes using (1.13) and (1.14) using only the harmonic energies.

1.1.2. Relaxation and nonlinearity

In their original work, Fermi, Pasta, Ulam, and Tsingou studied the energy per harmonic mode at a certain time t of a monoatomic chain with equal masses and springs. In our study, this corresponds to study the energy per normal modes given by Eqs. (1.13) and (1.14).

$$E_k(t) = \frac{P_k^2}{2} + \omega_k^2 u_k^2, . \tag{1.15}$$

and as the nonlinear terms are assumed small relative to the harmonic terms, $H \approx \sum_k E_k(t)$ to a good approximation [2]. FPUT calculated the average energy $< E_k(t) >$ for a given mode from the begining up to an elapsed time t of the simulation,

$$\langle E_k(t) \rangle = \frac{1}{t} \int_0^t E_k(t) dt. \tag{1.16}$$

To quantify the energy distribution across modes, different definitions of spectral entropy have been introduced in the literature. Following [10] and [4], we introduce the spectral entropy as:

$$S(t) = -\sum_{k=1}^{N} e_k(t) \ln e_k(t), . \tag{1.17}$$

where the normalized mode energy $e_k(t)$ is defined as in [4]:

$$e_k(t) = \frac{E_k(t)}{\sum_k E_k(t)}.. \tag{1.18}$$

However, in nonlinear chains such as the FPUT system, the spectral entropy exhibits significant oscillations due to recurrence effects. To mitigate this, Livi et al. [11] proposed to compute $E_k(t)$ over a local time window $(t - \Delta T, t + \Delta T)$ where ΔT encompases several simulation time steps. This ensures that $E_k(t)$ evolves smoothly, preventing large entropy fluctuations. Therefore, we define

$$\bar{E}_k(t) = \frac{1}{T} \int_{t-\Delta T}^{t+\Delta T} E_k(t') dt'.. \tag{1.19}$$

Without this averaging, entropy oscillations would be more pronounced, making it harder to assess the thermalization process. We can also support this idea from [11], in which it is established the idea that, on the long rung $\bar{E} \to \frac{E}{N}$. Therefore, in this thesis we compute the entropy using the formula,

$$S(t) = -\sum_{k=1}^{N} \bar{e}_k(t) \ln \bar{e}_k(t), . \tag{1.20}$$

where the local time averaged normalized mode energy $e_k(t)$ is defined as:

$$\bar{e}_k(t) = \frac{\bar{E}_k(t)}{\sum_k \bar{E}_k(t)}.. \tag{1.21}$$

with, $\bar{E}_k(t)$ defined as in (1.19. A first approximation for thermalization occurs when $\frac{dS}{dt} \to 0$. Also and to define when thermalization has been effectively reached, we impose an asymptotic threshold, when $\frac{dS}{dt} < 10^{-7}$. This criterion ensures a more reliable estimate of thermalization, accounting for recurrence effects in the system.

However, the thermalized value of the entropy as defined above depends upon the number of masses [11]. To avoid this and to look for the equipartition, a parameter $\eta(t)$ is defined as [12],

$$\eta = \frac{S(t) - S_{max}}{S(0) - S_{max}}. \tag{1.22}$$

where $S(t)$ is the spectral entropy defined as (1.20), $S(0)$ is the spectral entropy at time $t = 0$ and S_{max} is the maximum value of entropy during the simulation. From there one can define a global average $\langle\eta(t)\rangle$ from the beginning up to an elapsed time t of the simulation,

$$\langle\eta(t)\rangle = \frac{1}{t}\int_0^t \eta(t)dt. \tag{1.23}$$

in order to compute the thermalization time. This quantity goes from 1 (initial state) to 0 (equipartition reached). In practice, a threshold for thermalization is imposed.

1.2. Generalized Fermi-Pasta-Ulam chains

1.2.1. Linear chain with site dependent masses and springs

Consider now a system of coupled oscillators, given by the equation

$$H = \sum_{i=1}^{N} \frac{p_i^2}{2m_i} + \kappa_i(q_{i+1} - q_i)^2. \tag{1.24}$$

where κ_i is the spring between particle i and particle $i+1$ and m_i being the mass of the particle i.

For this case, equation (1.3) is transformed into,

$$\frac{\partial H}{\partial q_i} = -\dot{p}_i = -\kappa_i(q_{i+1} - q_i) + \kappa_{i-1}(q_i - q_{i-1}). \tag{1.25}$$

the equation (1.2) remains unchanged.

The resulting equation of motion is

$$m_i\ddot{q}_i = \kappa_i(q_{i+1} - q_i) - \kappa_{i-1}(q_i - q_{i-1}). \tag{1.26}$$

Such as in the original case, one could try to write (1.24) in terms of normal modes. For this, we can transform this equation in terms of mass-weighted coordinates: Defining mass-weighted coordinates u_i as

$$u_i = \sqrt{m_i}q_i. \tag{1.27}$$

or in matrix notation

$$\mathbf{u} = \mathbf{M}^{1/2}\mathbf{q}. \tag{1.28}$$

where, $\mathbf{M}$ in this case, is a diagonal matrix consisting of the masses of the system,

The equations of motion in terms of q_i become

$$\ddot{u}_i = \frac{1}{\sqrt{m_i}}\left(k_{i-1}\left(\frac{u_{i-1}}{\sqrt{m_{i-1}}} - \frac{u_i}{\sqrt{m_i}}\right) - k_i\left(\frac{u_i}{\sqrt{m_i}} - \frac{u_{i+1}}{\sqrt{m_{i+1}}}\right)\right). \tag{1.29}$$

$$\ddot{u}_i = -\left(\frac{k_{i-1}+k_i}{m_i}\right)u_i + \frac{k_i}{\sqrt{m_i m_{i+1}}}u_{i+1} + \frac{k_{i-1}}{\sqrt{m_i m_{i-1}}}u_{i-1}. \tag{1.30}$$

In matrix form, (1.30) becomes

$$\ddot{\mathbf{u}} = -\mathbf{M}^{-1/2}\mathbf{K}\mathbf{M}^{-1/2}\mathbf{u}. \tag{1.31}$$

Now, the dynamical matrix becomes

$$\mathbf{D} = \mathbf{M}^{-1/2}\mathbf{K}\mathbf{M}^{-1/2}. \tag{1.32}$$

The matrix is symmetric as long as $\mathbf{K}$ is symmetric. Now, for implementing a numerical version, we write this equation in matrix form, and for this, we must take into account the different boundary conditions to be studied

For fixed boundary conditions we have, $q_0 = q_{N+1} = 0$. Therefore, the matrix $\mathbf{D}$ has components

$$\begin{pmatrix} \frac{\kappa_1}{m_1} & -\frac{\kappa_1}{\sqrt{m_1 m_2}} & 0 & \dots & 0 \\ -\frac{\kappa_1}{\sqrt{m_1 m_2}} & \frac{\kappa_1+\kappa_2}{m_2} & -\frac{\kappa_2}{\sqrt{m_2 m_3}} & \dots & 0 \\ 0 & & \ddots & & \vdots \\ \vdots & & & \ddots & -\frac{\kappa_N}{\sqrt{m_{N-1} m_N}} \\ 0 & \dots & 0 & -\frac{\kappa_N}{\sqrt{m_{N-1} m_N}} & \frac{\kappa_N}{m_N} \end{pmatrix}. \tag{1.33}$$

.

On the other hand, in the case of periodic boundary conditions, the dynamical matrix is similar to the case with fixed boundary conditions, but now $q_0 = q_N$.

$$\begin{pmatrix} \frac{\kappa_1+\kappa_N}{m_1} & -\frac{\kappa_1}{\sqrt{m_1 m_2}} & 0 & \dots & -\frac{\kappa_N}{\sqrt{m_N m_1}} \\ -\frac{\kappa_1}{\sqrt{m_1 m_2}} & \frac{\kappa_1+\kappa_2}{m_2} & -\frac{\kappa_2}{\sqrt{m_2 m_3}} & \dots & 0 \\ 0 & & \ddots & & \vdots \\ \vdots & & & \ddots & -\frac{\kappa_{N-1}}{\sqrt{m_{N-1} m_N}} \\ -\frac{\kappa_N}{\sqrt{m_N m_1}} & \dots & 0 & -\frac{\kappa_N}{\sqrt{m_{N-1} m_N}} & \frac{\kappa_{N-1}+\kappa_N}{m_N} \end{pmatrix}. \tag{1.34}$$

The decomposition into normal modes of the system can be performed using the following formulation

$$\mathbf{u} = \mathbf{M}^{-1/2}\mathbf{W}\mathbf{v}. \tag{1.35}$$

$$\dot{\mathbf{u}} = \mathbf{M}^{-1/2}\mathbf{W}\dot{\mathbf{v}}. \tag{1.36}$$

where $\mathbf{u}$ is the displacement vector, $\mathbf{W}$ is the matrix of normal modes (normalized to the masses) and $\mathbf{v}$ are the normal coordinates.

Using equations (1.35) and (1.36 the Hamiltonian (1.24 can be written in matrix notation form

$$H = \frac{1}{2}\dot{\mathbf{u}}^T\mathbf{M}\dot{\mathbf{u}} + \frac{1}{2}\mathbf{u}^T\mathbf{K}\mathbf{u}. \tag{1.37}$$

to a normal modes approach, resulting in

$$H = \frac{1}{2}\sum_{i=1}^{N}(\dot{v}_i^2 + \omega_i^2 v_i^2).. \tag{1.38}$$

where v_i are the components of vector $\mathbf{v}$. Thus, the total energy is given by equation (1.38).

1.2.2. Fermi-Pasta-Ulam-Tsingou chain with site dependent masses and springs

A more general case of the (1.11) equation is treated here. Now consider a one-dimensional disordered chain. The Hamiltonian of this system is given by

$$H = \sum_{i=1}^{N}\frac{p_i^2}{2m_i} + \frac{1}{2}\kappa_i(q_{i+1}-q_i)^2 + \frac{1}{3}\alpha\kappa_i(q_{i+1}-q_i)^2 + \frac{1}{4}\beta\kappa_i(q_{i+1}-q_i)^4. \tag{1.39}$$

From which the equations of motion are obtained

$$\frac{\partial H}{\partial p_i} = \dot{q}_i = \frac{p_i}{m}. \tag{1.40}$$

$$\begin{aligned}\frac{\partial H}{\partial q_i} &= -\dot{p}_i \\ &= -\kappa_i(q_{i+1}-q_i) + \kappa_{i-1}(q_i - q_{i-1}) \\ &\quad - \alpha\kappa_i(q_{i+1}-q_i)^2 + \alpha\kappa_{i-1}(q_{i-1}-q_i)^2 \\ &\quad - \beta\kappa_i(q_{i+1}-q_i)^3 + \beta\kappa_{i-1}(q_{i-1}-q_i)^3\end{aligned}. \tag{1.41}$$

The analysis for the energies in terms of normal modes can be performed using the same tools for the disordered linear case. An important thing to notice is the incorporation of nonlinear terms in a disordered system and how this is done. In most papers, it is assumed that the strength of nonlinear terms is homogeneous, and only changing the masses [13-15].

We remark here that the case of alternanting masses was previously studied in the literature [13-15] while the case of different spring constants has not been studied before. This last case is interesting as it is a model for polymers and topological insulators. Here we take a further important step, incorporating nonlinear terms in the spring variations.

1.3. Effects in the generalized Fermi-Pasta-Ulam-Tsingou chains

In the standard FPUT system, all masses and springs are identical, and energy spreads across different modes due to nonlinear interactions (shown by Equation (1.13) and (1.14).

However, introducing position dependent masses or springs modifies the normal modes. The study of these cases is relevant for the modelling of different materials [16, 17]. A key feature of the FPUT system is resonance, particularly in low-frequency modes. Exciting one low-frequency mode generates resonances with others, driving the system toward thermalization [18]. However, introducing mass variations Δm can delay or prevent thermalization by changing energy recurrence and localization for certain modes. Understanding these effects is crucial for explaining observed recurrence behavior and thermalization time, how these are affected by introducing mass/spring alternance, and possible implications and applications given the previous literature.

1.3.1. Predictions on thermalization time

In the uniform FPUT system, the thermalization time τ_{th} depends primarily on the nonlinearity strength α or β, and the energy of the system E [19]. In contrast, alternating chains introduce an additional dependence on alternance strength, characterized by mass or spring variations, which we call D:

$$D(m) = \frac{|m_2 - m_1|}{m_1 + m_2}, \quad D(\kappa) = \frac{|\kappa_2 - \kappa_1|}{\kappa_2 + \kappa_1}.. \tag{1.42}$$

and we define two important parameters,

$$\Delta m = m_2 - m_1, \Delta\kappa = \kappa_2 - \kappa_1. \tag{1.43}$$

For $D = 0$, the system reduces to the uniform FPUT model. When $D \neq 0$, the normal mode frequencies split into acoustic and optical branches, separated by a frequency gap that affects energy transfer. A special case of these quantities are studied here, using adimensional masses such that $m_1 = 1 + \Delta m$, $m_2 = 1 - \Delta m$, $\kappa_1 = 1 + \Delta\kappa$ and $\kappa_2 = 1 - \Delta\kappa$. For these cases, (1.42 is reduced to

$$D(m) = \Delta m \quad D(\kappa) = \Delta\kappa. \tag{1.44}$$

Therefore, it is enough to study $\Delta\kappa$ and Δm for a diatomic chain if we choose $m_1 = 1 + \Delta m$, $m_2 = 1 - \Delta m$, $\kappa_1 = 1 + \Delta\kappa$ and $\kappa_2 = 1 - \Delta\kappa$. From here, we will study these kind of systems unless specified otherwise.

1.3.1.1. Effect on dispersion and resonances of diatomic case

Let's imagine a chain of atoms vibrating harmonically. If the chain is uniform (equal masses and springs), the dispersion relation follows:

$$\omega_k = ck. \tag{1.45}$$

where k is the wave number and c the velocity of the wave. But what happens if the chain is not uniform?. An interesting case is the chain with alternating masses or with alternating springs. These cases are both referred to as diatomic chains.

For a diatomic chain with alternating masses m_1 and m_2 (see Fig. 1.1), the dispersion

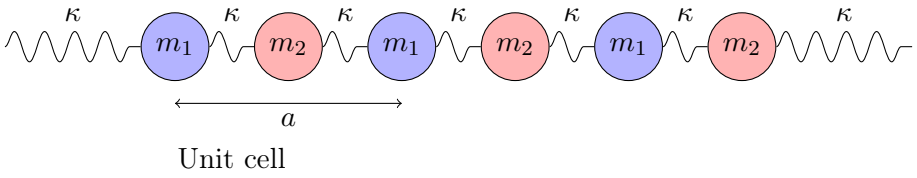

Fig. 1.1: Diatomic chain with alternating masses m_1 and m_2, connected by springs with spring constant κ. The unit cell has a length a.

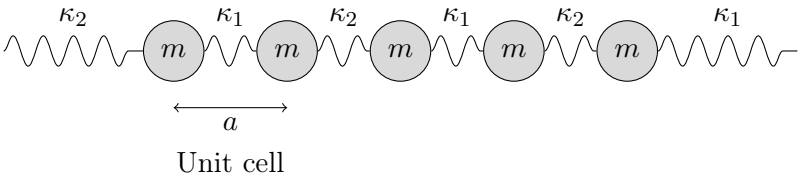

Fig. 1.2: Diatomic chain with alternating springs κ_1 and κ_2, connected by equal masses m. The unit cell has a length a.

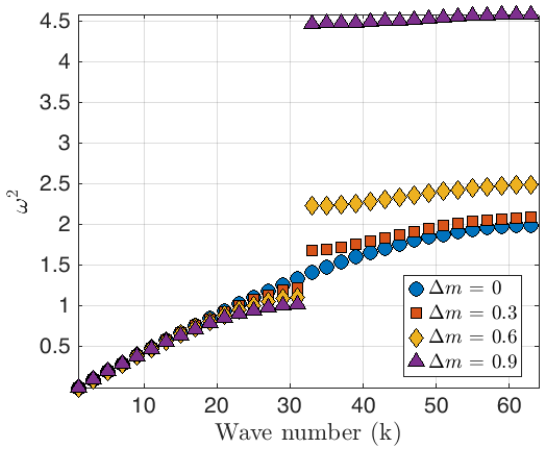

a) Dispersion relation respect to corresponding wave number k computed numerically for the case of a diatomic chain with different masses with $N = 64$ particles.

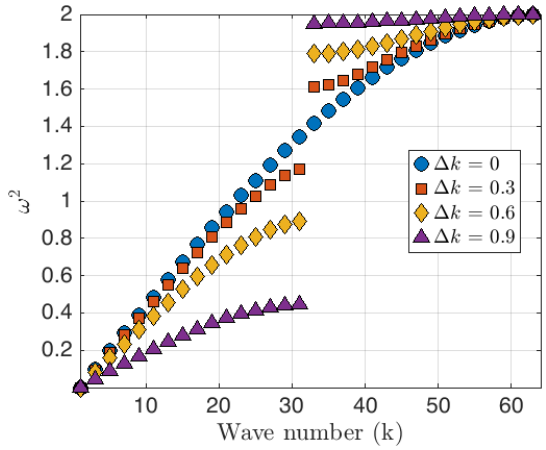

b) Dispersion relation respect to corresponding wave number k computed numerically for the case of a diatomic chain with different springs with $N = 64$ particles.

Fig. 1.3: Dispersion relations for a diatomic chain computed numerically using the values of ω obtained from Eq. (1.38.

relation is given by the formula [20]

$$\omega^2 = \frac{\kappa}{m_1 m_2}\left(m_1 + m_2 \pm \sqrt{(m_1+m_2)^2 - 4m_1 m_2 \sin^2(ka/2)}\right). \tag{1.46}$$

where a is the size of the unit cell. If we consider the following change of variables,

$$M = m_1 + m_2 \quad . \tag{1.47}$$

$$\frac{1}{\mu} = \frac{1}{m_1} + \frac{1}{m_2}. \tag{1.48}$$

where M and μ are the total and reduced mass of the system respectively, we can express Eq.

(1.46 as follows

$$\omega^2 = \kappa \left(\frac{1}{\mu} \pm \sqrt{\left(\frac{1}{\mu}\right)^2 - \frac{4\sin^2(ka)}{\mu M}} \right). \tag{1.49}$$

Similarly, for a diatomic chain with alternating springs κ_1 and κ_2 (see Fig. 1.2), we have

$$\omega^2 = \frac{\kappa_1 + \kappa_2}{m} \pm \frac{1}{m}\sqrt{(k_1 + k_2)^2 - 4\kappa_1\kappa_2 \sin^2(ka/2)}. \tag{1.50}$$

and introducing the following change of variables

$$\bar{\kappa} = \frac{\kappa_1 + \kappa_2}{2}. \tag{1.51}$$

$$\frac{1}{\kappa_{red}} = \frac{1}{\kappa_1} + \frac{1}{\kappa_2}. \tag{1.52}$$

the (1.50) becomes

$$\omega^2 = \frac{2\bar{\kappa}}{m} \left(1 \pm \sqrt{1 - \frac{\kappa_{\text{red}}}{\bar{\kappa}\sin^2(ka)}} \right). \tag{1.53}$$

In both cases, the frequencies with the + sign correspond to the so-called optical modes, while those with the − sign are the acoustic modes. Dispersion relations are presented in figures1.3a) and 1.3b).

If we look at the limit of small k (long waves), we can expand the expression (1.49) and obtain

$$\omega^2 = \frac{a^2\kappa}{2M}k^2 - \frac{a^4\kappa\mu}{24M^2}k^4 + ... \tag{1.54}$$

and then, we can identify the velocity of the acoustic mode as

$$c_{ac} = a\sqrt{\frac{\kappa}{2M}}. \tag{1.55}$$

We can see, therefore, the dependence of mass-ratio in Eqs. (1.49) and (1.55).

In this thesis, we will consider adimensional masses such that $m_1 = 1 + \Delta m$ and $m_2 = 1 - \Delta m$. Then $M = m_1 + m_2 = 2$, $m_1 m_2 = 1 - (\Delta m)^2$ and $\mu = (1 - (\Delta m)^2)/2$. Using this, Eqs (1.49) and (1.55)

$$\omega^2 = \frac{2\kappa}{1 - (\Delta m)^2} \left(1 \pm \sqrt{1 - (1 - (\Delta m)^2 \sin^2(ka)} \right). \tag{1.56}$$

Therefore c_{ac} does not depend on Δm, but the second order term of k^4 does. With this in mind, we can write

$$\omega^2_{k(\text{ac})} \approx c^2_{ac}k^2 + \delta(k, \Delta m), . \tag{1.57}$$

where $\delta(k, \Delta m)$ is given by

$$\delta(k, \Delta m) = -\frac{a^4 \kappa}{24}\left[\frac{1}{8}\left(1 - (\Delta m)^2\right)\right] k^4 + ... \tag{1.58}$$

and the rest of higher order terms given in (1.54), and quantifies the shift from the uniform case.

Similarly, we can do the same thing with a diatomic chain with alternating springs κ_1 and κ_2.

$$\omega^2 = \frac{2}{m}\left(1 \pm \sqrt{1 - (1 - (\Delta\kappa)^2)\sin^2(ka)}\right). \tag{1.59}$$

Expanding the cosine term around $k = 0$ in (1.50) we have

$$\omega_{ac}^2 = \frac{\kappa_{\text{red}}}{4m}(qa)^2 - \frac{\kappa_{\text{red}}}{48m}\left(1 - \frac{\kappa_{\text{red}}}{2\kappa_{\text{avg}}}\right)(qa)^4 + ... \tag{1.60}$$

and using (1.51) and (1.52)

$$\omega_{ac}^2 = \frac{1 - (\Delta\kappa)^2}{4m}(ka)^2 - \frac{(1 - (\Delta\kappa)^4)}{96m}(ka)^4 + ... \tag{1.61}$$

Again, we can see the dependence of constants dependence of spring-ratio in Eq. (1.59), but in this case velocity of sound does depend on springs even for a system of alternating springs. Therefore, for this case, we can write

$$\omega_{k(\text{ac})}^2 \approx c_{ac}^2(\Delta\kappa)k^2 + \delta(k, \Delta\kappa), . \tag{1.62}$$

where $\delta(k, \kappa)$ is given by

$$\delta(k, \Delta\kappa) = -\frac{\kappa_{\text{red}}}{48m}\left(1 - \frac{\kappa_{\text{red}}}{2\kappa_{\text{avg}}}\right)(ka)^4 + ... \tag{1.63}$$

The rest of higher order terms given in (1.54), quantifies the shift in the dispersion relation from the uniform case.

In the uniform FPUT model, quasi-resonances occur for cubic and quartic nonlinearities [21, 22]. For the cubic nonlinear term, we have

$$\omega_{k_1} \pm \omega_{k_2} \pm \omega_{k_3} = 0, \quad (\alpha\text{-FPUT}). \tag{1.64}$$

In alternating chains, mismatch due to $\delta(k, \Delta m)$ or $\delta(k, \Delta\kappa)$ alters this balance, reducing available resonant interactions [23, 24]. Then, a measure of mismatch for a three-wave coupling is

$$|\omega_{k_1} + \omega_{k_2} - \omega_{k_3}| > \delta(\Delta m) \quad |\omega_{k_1} + \omega_{k_2} - \omega_{k_3}| > \delta(\Delta\kappa) \quad . \tag{1.65}$$

Therefore, to drive energy from a low mode up to the next, it must happen in both cases that

$$|\omega_{k_1} + \omega_{k_2} - \omega_{k_3}| \approx 0 \quad . \tag{1.66}$$

in the case of a three-Wave resonance. Resonance, according to [17] can occur only if the ratio between two heavy and light masses is less than 3 in the case of an $\alpha-$FPUT chain and in 3-wave interactions (in particular, interaction between two acoustic and one optical mode). In this case, thermalization can occur faster than the monoatomic case, as interactions between acoustic and optical modes are mediated by the values of Δm or $\Delta\kappa$.

For a Four-Wave resonance, the idea is similar and we get, [21, 22]

$$\omega_{k_1} \pm \omega_{k_2} \pm \omega_{k_3} \pm \omega_{k_4} = 0, \quad (\beta\text{-FPUT})..\tag{1.67}$$

and from a similar argument we have,

$$|\omega_{k_1} + \omega_{k_2} + \omega_{k_3} - \omega_{k_4}| > \delta(\Delta m) \quad |\omega_{k_1} + \omega_{k_2} + \omega_{k_3} - \omega_{k_4}| > \delta(\Delta\kappa) \quad .\tag{1.68}$$

This shift affects the resonance conditions, crucial for energy transfer. It is worth noting that if $\delta(k, \Delta m), \delta(k, \Delta\kappa) \sim 0$, then resonances for uniform FPUT are recovered.

For the special case of $m_1 = 1 + \Delta m$ and $m_2 = 1 - \Delta m$, we found that $\Delta m < \frac{1}{2}$. Therefore, it is expected that for $\Delta m < \frac{1}{2}$ the thermalization time decreases and once this condition is broken, the thermalization time remains the same or even increases.

1.3.1.2. Thermalization Time Scaling

Following [19], we estimate thermalization time using the Fourier-transformed Hamiltonian for an alternating linear chain. Reference [19] introduces the next canonical transformation

$$q_n = \sqrt{\frac{2}{N+1}} \sum_{k=1}^{N} \left[\frac{z_k - z_k^*}{i\sqrt{2\omega_k}}\right] \sin\left(\frac{\pi k n}{N+1}\right), \quad p_n = \sqrt{\frac{2}{N+1}} \sum_{k=1}^{N} \left[\sqrt{\frac{\omega_k}{2}}(z_k + z_k^*)\right] \sin\left(\frac{\pi k n}{N+1}\right)..\tag{1.69}$$

and then Eq. (1.11) with $\beta = 0$ (α-FPUT case) can be rewritten as

$$H = \sum_k \omega_k |z_k|^2 + H_{\text{int}}(z, z^*),.\tag{1.70}$$

where

$$H_{int}(z, z^*) = \frac{i\alpha}{12\sqrt{N+1}} \sum_{k_1,k_2,k_3=1}^{N} S_{k_1 k_2 k_3} \Pi_{j=1}^{3} \sqrt{\omega_{k_j}}(z_{k_1} - z_{k_1}^*),.\tag{1.71}$$

and

$$S_{k_1 k_2 k_3} \equiv \delta_{k_1+k_2-k_3,0} + \delta_{k_1-k_2+k_3,0} + \delta_{k_1-k_2-k_3,0} - \delta_{k_1+k_2+k_3,2N+2}..\tag{1.72}$$

A full rewriting of this canonical transformation can be seen in [25]. Now, we define the specific energy as:

$$\varepsilon = \frac{E}{N},.\tag{1.73}$$

and estimate the highest excited mode k_c in which equipartition can be achieved over time. According to [19] and [26] it follows the next equation for the homogeneous α-FPUT chain:

$$k_c \sim \alpha^{-1/2}\varepsilon^{-1/4}.. \tag{1.74}$$

After a canonical transformation of (1.70 of the form,

$$z_k = \exp\left(\frac{i\pi k}{N+1}t\right)\xi_k \quad z_k^* = \exp\left(\frac{i\pi k}{N+1}t\right)\xi_k^* \quad . \tag{1.75}$$

we obtain a Hamiltonian of the form

$$\bar{K} = \sum_k \Omega_k |\xi_k|^2 + \bar{H}_3(\xi, \xi^*). \tag{1.76}$$

where $\bar{H}_3$ defines the nonlinear terms in the new canonical transformation (see [17, 19] for a complete derivation) . With this expression it is possible to compute the resulting thermalization time [19], given by:

$$\tau_{\text{th}} \sim \frac{|\xi_k|^2}{\left|\frac{\partial \bar{H}_3}{\partial \xi_k^*}\right|^2}.. \tag{1.77}$$

which is a measure of how strong are the nonlinear terms and coupling terms, given by ξ_k in respect to the linear terms $\left|\frac{\partial \bar{H}_3}{\partial \xi_k^*}\right|^2$. For the homogeneous $\alpha-$FPUT case, it has been found that an estimation for the thermalization time takes the next form:

$$\tau_{\text{th}} \sim \frac{1}{\alpha^{3/2}\varepsilon^{3/4}}.. \tag{1.78}$$

Meanwhile, for a $\beta-$FPUT chain, the thermalization time has been found to follow a similar law, supported by numerical simulations [27]

$$\tau_{\text{th}} \sim \frac{1}{\varepsilon^p}.. \tag{1.79}$$

where $p = 1, 2, 4$ depending on the values of ε (we can find then two regimes for thermalization time depending on the energy).

However, in an alternating chain, the energy transfer is limited by the acoustic-optical gap, requiring nonlinear interactions to compensate for missing resonances [23, 25, 28]. The bigger Δm or $\Delta\kappa$, the acoustic-optical gap is bigger and therefore there are fewer resonances.

With this background in mind, we can guess the thermalization time τ_{th} will grow up in respect to the acoustic-optical gap. Therefore, a first ansatz could be

$$\tau_{th} \sim \tau_{(0)th} \cdot g(\Delta m), . \tag{1.80}$$

where $\tau_{(0)th}$ is the thermalization time for the homogeneous case ($\Delta\kappa = 0, \Delta m = 0$), and $g(\Delta m)$ is a function depending on Δm. Using (1.54) as a first approximation, we can try to fit $g(\Delta m)$ as

a quadratic function of Δm, given by

$$g(\Delta m) = 1 + A(\Delta m) + B(\Delta m)^2. \tag{1.81}$$

in a regime for weak Δm, and in the limit $\Delta m \to 0$, the homogeneous case should be recovered, and A, B are coefficients to determine, such as its dependence of other parameters. This idea can be extrapolated to different springs,

$$\tau_{th} \sim \tau_{(0)th} \cdot h(\Delta\kappa), . \tag{1.82}$$

where $h(\Delta m)$ is a function depending on $\Delta\kappa$, and similarly

$$h(\Delta\kappa) = 1 + C(\Delta\kappa) + D(\Delta\kappa)^2. \tag{1.83}$$

in a regime for weak $\Delta\kappa$, and being C, D coefficients to determine. An important point to clarify here is the importance of small values of α, β, as referred to in [17] for the validity of this expression. If this condition breaks the calculations for thermalization times could not be validated at all. Therefore, the importance of small values of $\Delta k/\Delta m$ and α is crucial.

For the case of a β-FPUT chain, studies [18] have shown that the thermalization time scaling remained the same as for the monoatomic case. This is reasonable because with quartic interactions, the leading energy transfer process is still a four-wave interaction. Simply having two branches (acoustic/optical) may not create any new three-wave processes (since the nonlinearity order forbids them), and the four-wave resonant networks might still be similarly sparse.

These results suggest that the introduction of alternating masses/springs inhibits equipartition, significantly delaying or even preventing energy redistribution. If numerical results show increased recurrence and lower entropy once alternating masses or springs are introduced, analytical predictions can be confirmed.

Capítulo 2

On the relaxation for the case of different masses

Building upon the theoretical framework developed in earlier chapters, this chapter examines the relaxation dynamics of a modified Fermi-Pasta-Ulam-Tsingou (FPUT) system incorporating mass heterogeneity. The study is conducted under both fixed and periodic boundary conditions, with the system initialized using excitations in low- and high-frequency modes to explore their distinct thermalization pathways.

The chapter begins by analyzing the case of fixed boundary conditions. After revisiting the original FPUT problem to establish a reference, the dynamics of low-frequency excitations are explored, revealing that resonance phenomena play a central role in energy redistribution. Thermalization time is quantified using spectral entropy, demonstrating that stronger mass asymmetry enhances energy localization and delays thermalization. The analysis then shifts to high-frequency excitations, which disrupt recurrence patterns and generate energy cascades. This behavior excites a broader range of modes and leads to higher entropy values, illustrating the complex interplay between mass alternance and nonlinear interactions.

The second part of the chapter focuses on periodic boundary conditions. In this context, low-frequency excitations exhibit modified resonance behavior due to the modification of boundary constraints, often resulting in persistent energy localization. High-frequency excitations, meanwhile, continue to exhibit broad spectral spreading and more rapid entropy growth.

Through numerical simulations and entropy-based diagnostics, this study demonstrates the critical role of boundary conditions and excitation modes in determining thermalization behavior. These results deepen our understanding of energy transport, recurrence, and relaxation in nonlinear lattices with structural alternance of masses, offering new insights into the FPUT problem when mass heterogeneity is introduced.

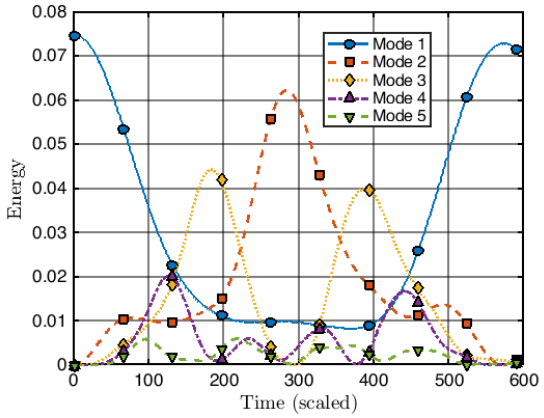

a) Energy per modes over time, integrating the equations of motion (1.40) and (1.41) for $N = 32$ particles and $\alpha = 0.25$.

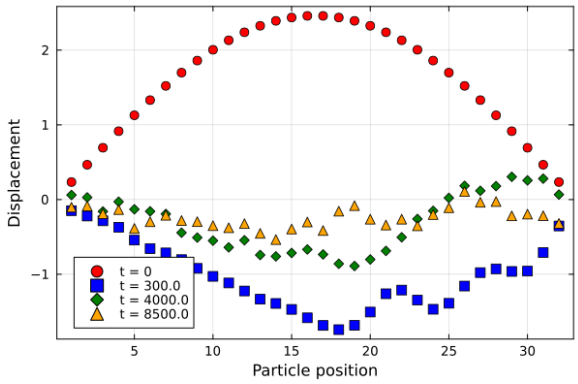

b) Displacement of the FPUT system for different times, integrating Eqs. (1.40) and (1.41) for $N = 32$ particles and $\alpha = 1.0$ with fixed boundary conditions.

Fig. 2.1: Selected results for the α-FPUT system. Figure 2.1a) presents the evolution of energy distribution across normal modes over time, while Figure 2.1b) illustrates the displacement of particles in the system. These results closely follow the original findings reported in [3], capturing the recurrence behavior characteristic of the FPUT problem.

2.1. Fixed Boundary Conditions

2.1.1. The Original Fermi-Pasta-Ulam-Tsingou Problem

Before delving into the study of a Fermi-Pasta-Ulam-Tsingou Chain with different masses, it is important to review some key aspects of the original FPUT system. These key aspects involve the transfer of energy between normal modes, the recurrence phenomena and conditions to relaxation of the system.

Figure 2.1a) shows the energy per modes for an α-FPUT system with particular initial parameters as studied in [3]. This system is given by Eq. (1.11). Figure 2.1a) illustrates transfer of energy between different modes as a consequence of the introduction of a nonlinear term, as pointed out in Eq. (1.13). The consequence of this coupling in the motion of the system is shown in Fig. 2.1b) where one can see the motion of the system for different time steps.Furthermore, we can see that the system seems to return to the initial state after certain time. This is the recurrence phenomena observed by Fermi, Pasta, Ulam and Tsingou.

Another critical observation is the energy transfer between uniquely the first 5 modes of vibration, leaving the subsequent modes without energy transfer. This can be observed in Fig 2.1a), where beyond the third mode, energy transfer is barely noticeable. This suggests a lack of ergodicity in the original problem. Fermi et al. initially assumed that introducing a nonlinear term would induce chaos, ensuring ergodicity. However, as shown in Figure 2.1a), energy remains confined to the first few modes, indicating that nonlinearity alone is insufficient to guarantee ergodicity.

Connecting these observations, the appearance of recurrence and the lack of ergodicity, suggest a violation of the equipartition theorem, which predicts uniform energy distribution among modes in thermal equilibrium. Instead, the energy remains localized in the first few low-frequency

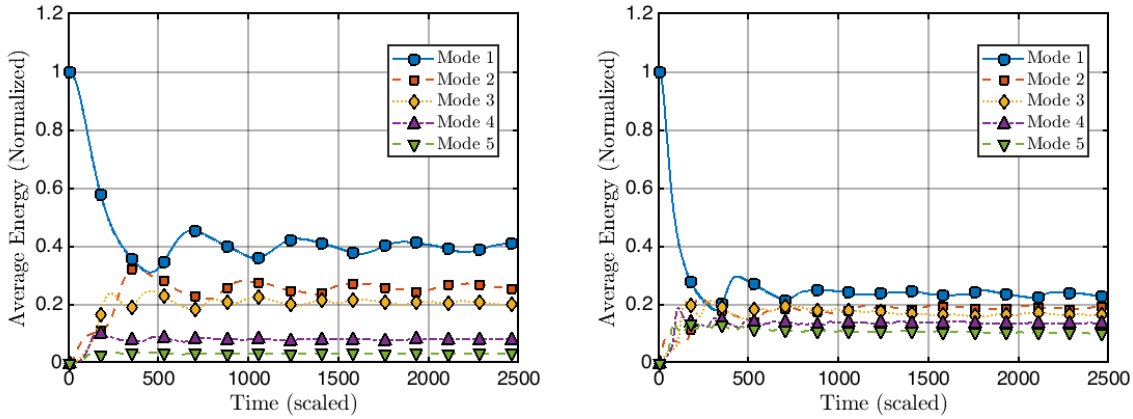

a) Time evolution of the average energy per mode for a system of $N = 32$ particles with $\alpha = 0.25$. The equations of motion (1.40) and (1.41) were integrated with an initial amplitude of $A = 1$.

b) Same as (a) but with an initial amplitude of $A = 10$. It can be observed that energies on the long run tend to reach a stable value, possibly reaching energy equpartition for longer times.

Fig. 2.2: Selected results for the α-FPUT system. Figure 2.1a) presents the evolution of energy distribution across normal modes over time, while Figure 2.1b) illustrates the displacement of particles in the system. These results closely follow the original findings reported in [3], capturing the recurrence behavior characteristic of the FPUT problem.

modes, indicating that the system does not reach a state of thermal equilibrium within the observed timescales. To further investigate this, Fermi et Al. computed the average energy over time for a particular system, given by (1.19). The result is shown in Fig. 2.2a). The decay of average energy for different modes suggests the system is going to relaxation, but energy does not seem to tend to the same value for all modes (The first mode still retains most of the energy despite decay). Further studies [29] showed that equipartition can be achieved if sufficient initial energy is given in the system. (See Fig. 2.2b)).

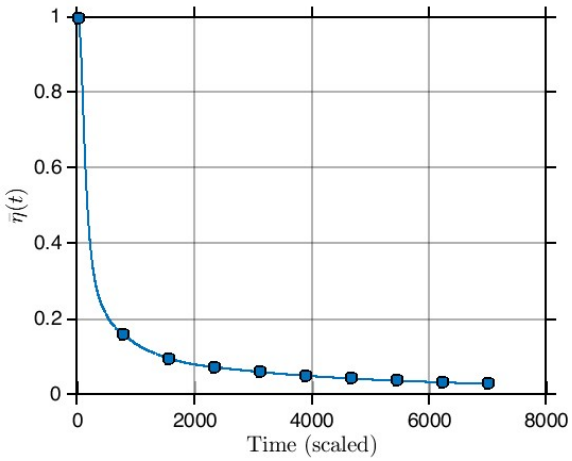

Fig. 2.3: $\langle \eta(t) \rangle$ defines as in (1.23) for a system of $N = 64$ particles with and amplitude of $A = 10$ with fixed boundary conditions. As $t \to \infty$, $\langle \eta(t) \rangle$ tends to zero, indicating the possibility of equipartition on the long run.

Previous studies [4] suggest that energy localization depends on initial conditions, particularly the excited mode, its amplitude, and the strength of nonlinear parameters α and β. Additionally, the system exhibits non-chaotic behavior, remaining confined to low-frequency modes with recurrent dynamics. This challenges the notion that nonlinearity inherently leads

to chaos or ergodicity, highlighting the complex relationship between nonlinear interactions and energy redistribution.

To further investigate thermalization in this chapter, two approaches are considered. First, introducing mass alternance to assess its impact on energy redistribution. By varying the mass distribution along the chain, we aim to explore how structural alternace between masses influences the recurrence phenomena and the transition to thermal equilibrium. Second, modifying initial conditions, particularly by (i) varying the amplitude A of the excited mode and (ii) exciting low and high-frequency modes separately to explore its role in energy transfer. These modifications allow us to study how different energy inputs and mode excitations affect the system's relaxation dynamics and whether they can overcome the observed localization effects.

Building on these approaches, we now turn our attention to the specific dynamics of low-frequency modes and their role in thermalization.

2.1.2. The Role of Low-Frequency Mode Dynamics in Thermalization

In this section, we explore thermalization in a nonlinear chain with alternating masses and fixed boundary conditions. The equations of motion (1.40) and (1.41) are solved numerically in MATLAB (see A). The system consists of alternating masses, $m = 1 \pm \Delta m$, with $0 \leq \Delta m < 1$, introducing heterogeneity that influences energy transport and thermalization. Simulations are performed for various nonlinearity strengths α and β , which control the cubic and quartic interactions. Figures 2.4 and 2.5 display the normalized energy per mode over time for different mass distributions Δm and different values α and β. From this, we can observe certain key behaviors.

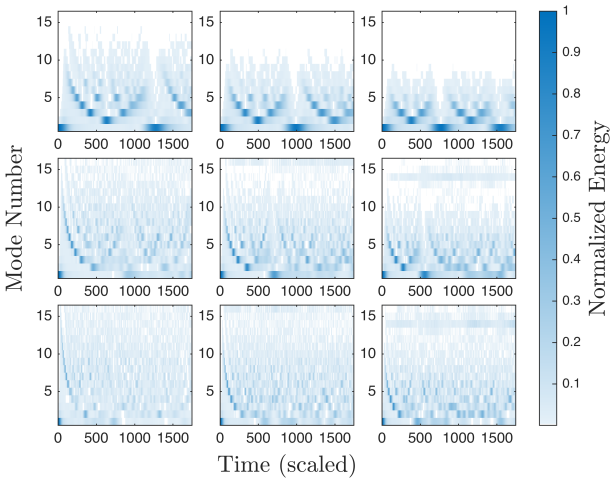

Fig. 2.4: Normalized energy per mode over time for a system of $N = 64$ particles with fixed boundary conditions. The columns represent different mass difference levels: $\Delta m = 0.3, 0.6, 0.9$ (left to right). The rows correspond to varying nonlinearity strengths: $\alpha = 0.3, 0.6, 0.9$ (top to bottom). The system is initialized with energy localized in the second mode with an amplitude of $A = 10$.

Let's start by exploring how mass differences and nonlinearity influence energy dynamics in our system. From Fig. 2.4, we observe that for $\alpha = 0.3, 0.6$. increasing Δm reduces the recurrence time typical of the Fermi-Pasta-Ulam-Tsingou problem. At the same time, energy spreading

across modes diminishes, suggesting that structural heterogeneity localizes energy. However, when nonlinearity α increases closer to 1, energy redistribution accelerates, pushing the system closer to thermalization. Interestingly, thermalization emerges under moderate mass differences and strong nonlinearity, while large Δm inhibits it.

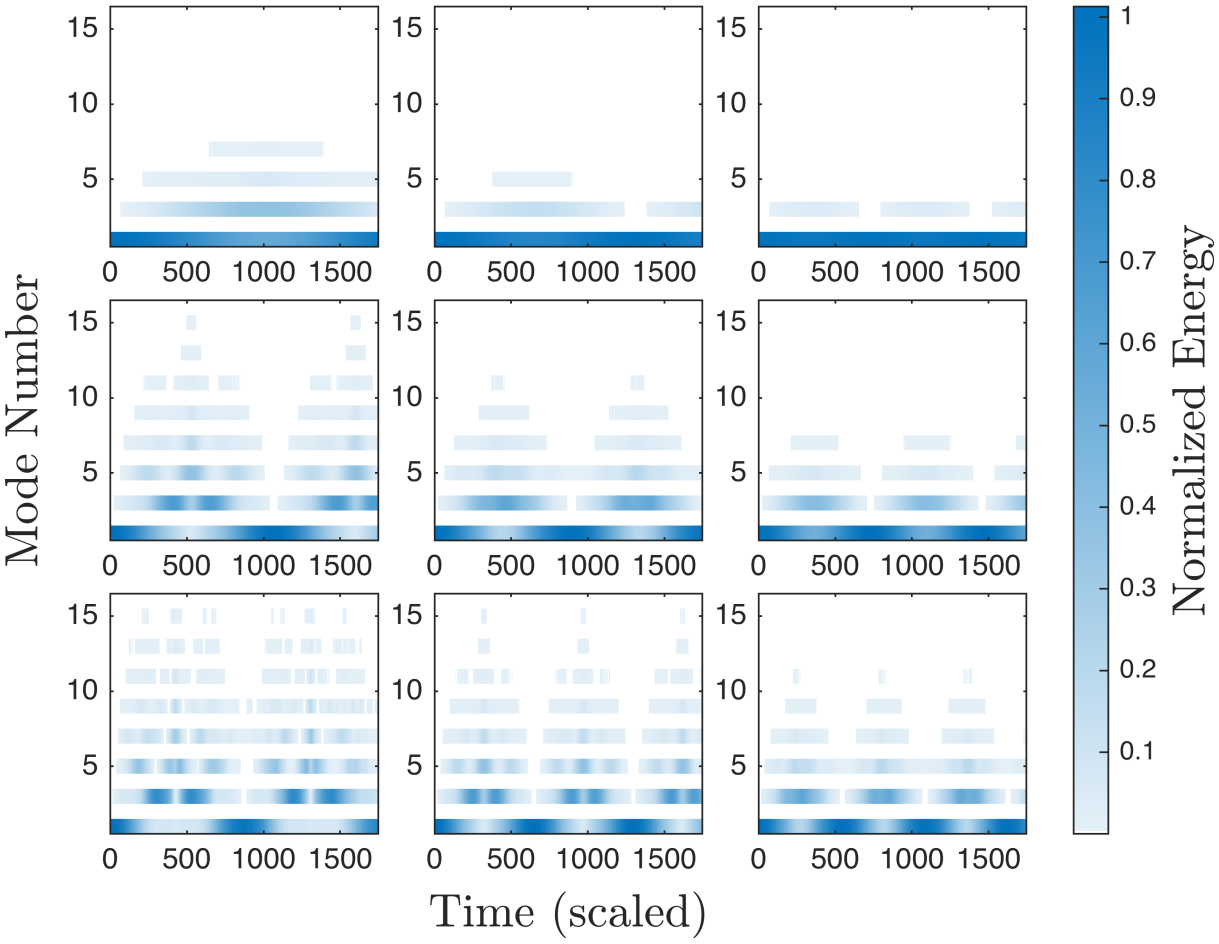

Fig. 2.5: Normalized energy per mode over time for a system of $N = 64$ particles with fixed boundary conditions. The columns represent different mass difference levels: $\Delta m = 0.3, 0.6, 0.9$ (left to right). The rows correspond to varying nonlinearity strengths: $\beta = 1, 3, 5$ (top to bottom). The system is initialized with energy localized in the second mode with an amplitude of $A = 10$.

Now, let's shift our focus to the case where $\alpha = 0$ and $\beta \neq 0$, as shown in Fig. 2.5. Here, the results are less straightforward. For $\Delta m = 0.9$ and $\beta = 1$, the system enters a *sticky state* where relaxation is absent—a phenomenon previously observed in few-mass FPU systems [30]. Even when β increases to 3 or 5, energy sharing improves, but recurrence persists, highlighting the system's resistance to full thermalization.

This means energy remains trapped in specific modes, preventing full thermalization—a behavior consistent with findings in [13, 14], where the introduction of alternating masses generates invariant manifolds, where the motion of the system is trapped, and therefore, showing recurrence according to KAM theorem.

To better understand these effects, we turn to spectral entropy (Equation (1.17), as depicted

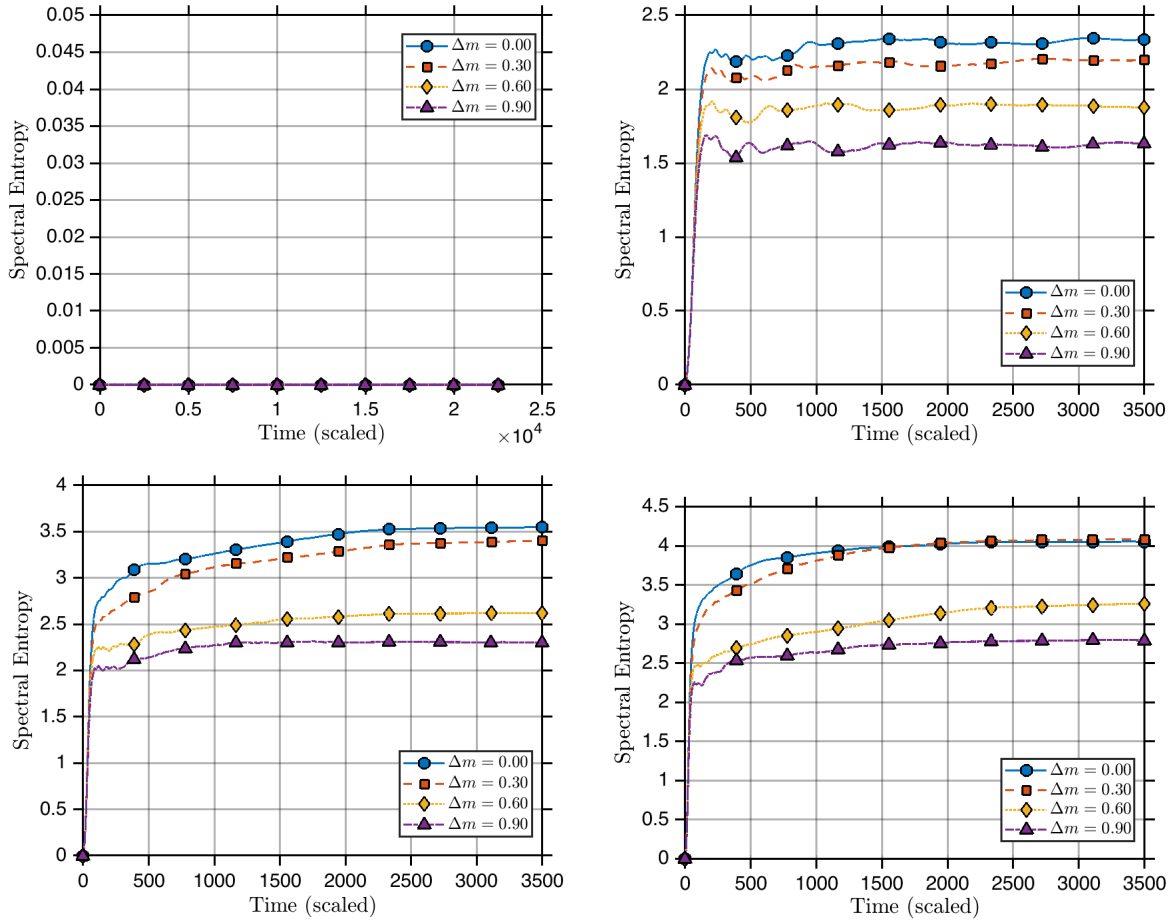

Fig. 2.6: Time evolution of the spectral entropy for a system of $N = 64$ particles with fixed boundary conditions, showing the variation of spectral entropy for different values of Δm. Each panel corresponds to different values of the nonlinear parameter α, increasing from left to right and top to bottom: $\alpha = 0, 0.3, 0.6, 0.9$. The system is initialized with an excitation in the first mode, with an initial amplitude of $A = 10$.

in Figs. 2.6 and 2.7. In systems with alternating masses, and for both cases α and β the spectral entropy stabilizes at lower values, signaling partial energy localization and a lack of equipartition.

The entropy analysis reveals contrasting behaviors between the two systems. For the α-FPUT case, systems with $\alpha = 0.3$ and 0.6 show decreasing maximum entropy values as Δm increases. However, this pattern breaks at $\alpha = 0.9$, where the $\Delta m = 0.3$ configuration achieves entropy values comparable to - and sometimes exceeding - the homogeneous ($\Delta m = 0$) case. The β-FPUT system exhibits markedly different dynamics, with more pronounced oscillations and instability, particularly at $\beta = 3$ and 5. In these cases, entropy systematically decreases with increasing Δm, clearly demonstrating how mass alternation influences the system's accessible states.

In summary, our analysis reveals a delicate balance: while nonlinearity promotes energy redistribution, large mass differences and persistent recurrence hinder thermalization, leaving energy localized and the system far from equilibrium.

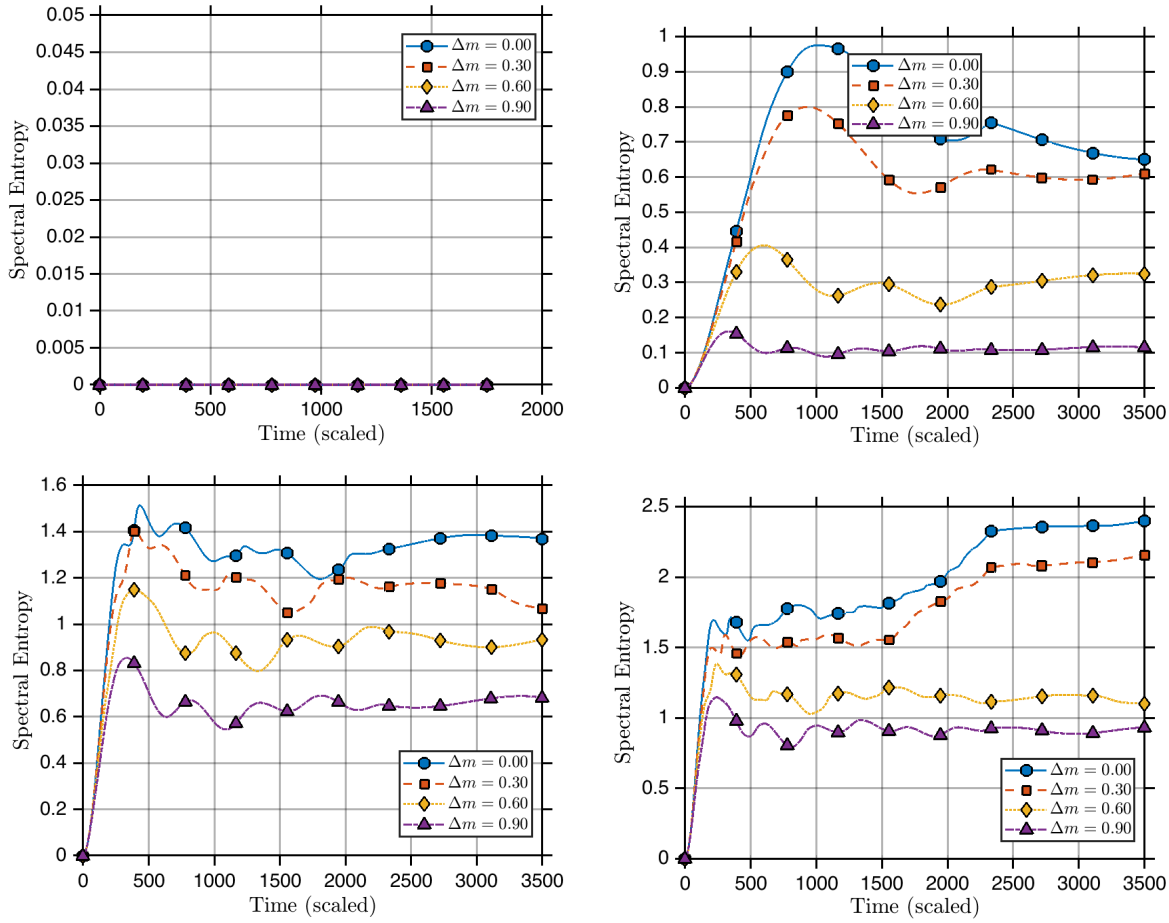

Fig. 2.7: Time evolution of the spectral entropy for a system of $N = 64$ particles with fixed boundary conditions, showing the variation of spectral entropy for different values of Δm. Each panel corresponds to different values of the nonlinear parameter β, increasing from left to right and top to bottom: $\beta = 0, 1, 3, 5$. The system is initialized with an excitation in the first mode, with an initial amplitude of $A = 10$.

2.1.2.1. Analyzing Thermalization Times

Using the last results obtained, we can try to compute a first approximation of the thermalization time of the system, i.e. the minimum value where $\frac{d\langle\eta\rangle}{dt} < 10^{-6}$, as pointed out in section 1.

For the α-FPUT system (Fig. 2.8a)), entropy decreases monotonically with increasing $\Delta\kappa$ for all values of α, with higher nonlinearity leading to initially higher entropy than the homogeneous ($\Delta m = 0$) case, and then, diminishes more steeply. These results indicate that mass heterogeneity suppresses thermalization more effectively in the α-FPUT model compared to the homogeneous case, promoting energy localization across a broad range of nonlinearities.

For the β-FPUT system (Fig. 2.8b)), entropy also decreases with increasing Δm, but follows a more gradual, nearly linear trend. Notably, larger values of β yield higher equilibrium entropy across the range, suggesting delayed localization, while increasing mass difference consistently lowers the final entropy reached. This pattern indicates that although mass heterogeneity reduces

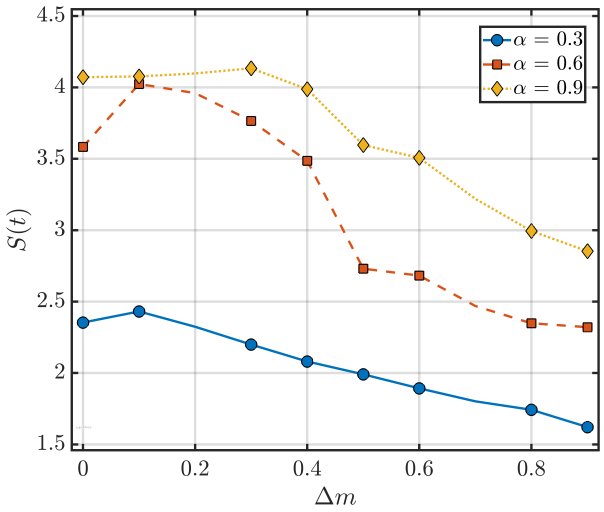

a) Entropy values reached in thermalization for different values of Δm varying values of $\alpha = 0.3, 0.6, 0.9$ with fixed boundary conditions, using the initial conditions of Fig. 2.5.

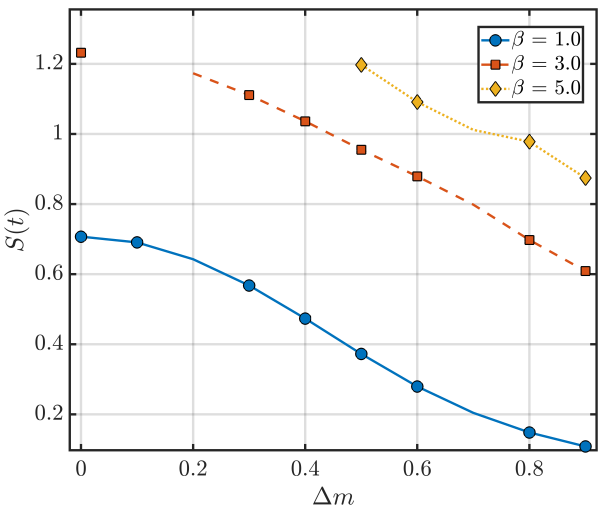

b) Entropy values reached in thermalization for different values of Δm varying values of $\beta = 1.0, 3.0, 5.0$ with fixed boundary conditions, using the initial conditions of Fig. 2.5.

Fig. 2.8: Entropy values reached in thermalization for different values of Δm with fixed boundary conditions. (a) Varying α values. (b) Varying β values.

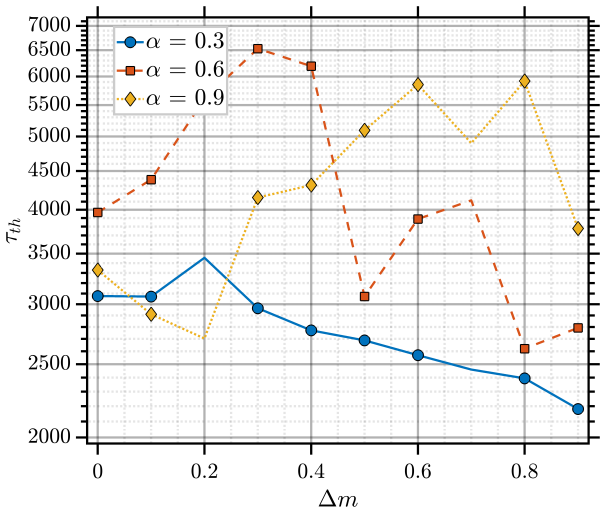

a) Relaxation time vs different values of Δm varying values of $\alpha = 0.3, 0.6, 0.9$ with fixed boundary conditions, using the initial conditions of Fig. 2.5.

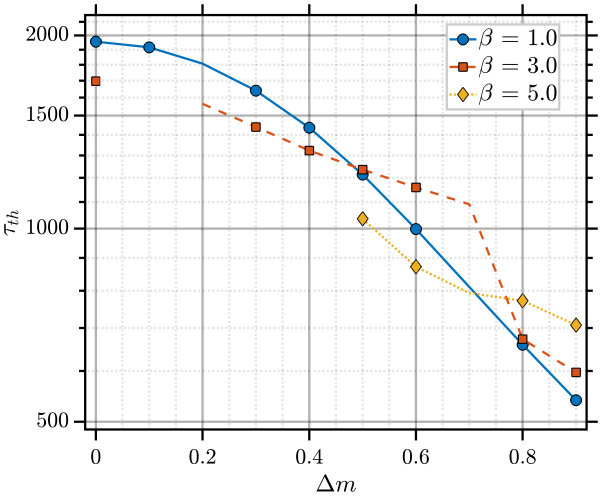

b) Relaxation time vs different values of Δm varying values of $\beta = 1.0, 3.0, 5.0$ with fixed boundary conditions, using the initial conditions of Fig. 2.5.

Fig. 2.9: Relaxation time for different values of Δm with fixed boundary conditions. (a) Varying α values. (b) Varying β values.

thermalization in both systems, the β-FPUT model exhibits a softer suppression, with a less abrupt transition into localized regimes.

In summary, both the α- and β-FPUT systems exhibit reduced entropy as mass difference increases, pointing to a suppression of thermalization and enhanced localization. However, the α-FPUT system shows a stronger and more nonlinear sensitivity to Δm, suggesting a more prominent interplay between nonlinearity and heterogeneity. To verify this, we consider now the thermalization time for each case previously shown, starting with the α-FPUT case.

Figure 2.9a) shows the results for the α-FPUT system. For $\alpha = 0.3$, thermalization time clearly decreases with increasing mass difference Δm. For $\alpha = 0.6$ and $\alpha = 0.9$, the behavior is more complex, with oscillatory patterns. Still, a general trend emerges: thermalization time decreases with Δm for $\alpha = 0.6$, but increases for $\alpha = 0.9$. This suggests a regime shift where increasing Δm can either speed up or slow down thermalization, depending on the nonlinearity.

In Figure 2.9b), the β-FPUT system shows a more consistent decrease in thermalization time as Δm increases. This is especially clear for $\beta = 1.0$. For larger values of β, thermalization at a timescale of 10^3 is not achieved for small Δm; higher mass differences are needed. For example, the decrease begins around $\Delta m = 0.3$ for $\beta = 3.0$ and around $\Delta m = 0.5$ for $\beta = 5.0$, both showing slight oscillations.

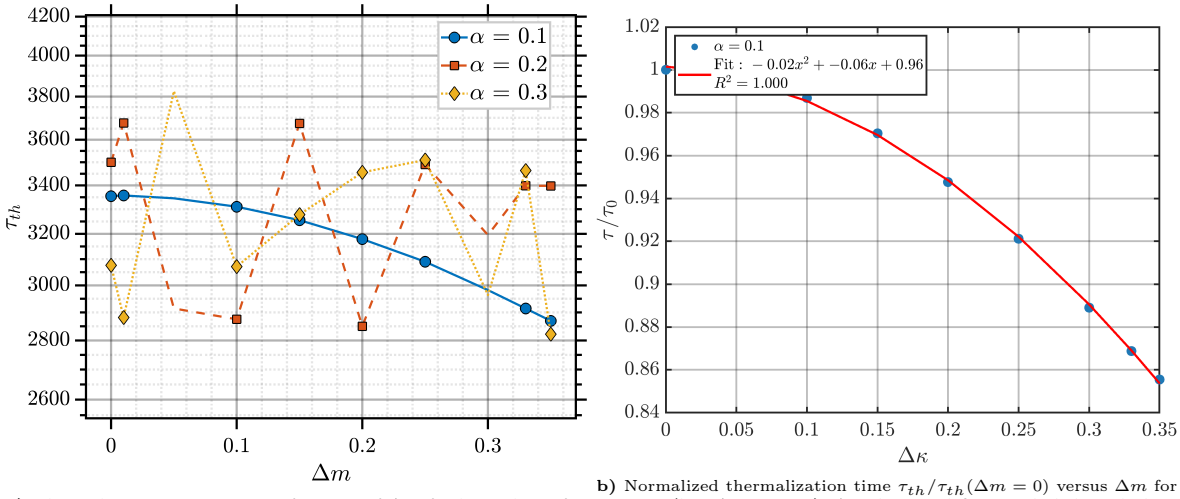

a) Thermalization time τ_{th} as a function of Δm for low values of α and Δm. Initial conditions correspond to those in Fig. 2.9a)

b) Normalized thermalization time $\tau_{th}/\tau_{th}(\Delta m = 0)$ versus Δm for $\alpha = 0.1$ (low Δm regime). A polynomial fit is included, with data points extracted from Fig. 2.10a).

Fig. 2.10: Thermalization dynamics in the low-parameter regime. (a) Dependence of τ_{th} on Δm; (b) Normalized thermalization time with polynomial fit.

As a final result of this section, we can plot τ_{th}/τ_0, where τ_0 is the thermalization time for the homogeneous case exploring the regime of weak values of Δm.

For the case of Δm, we can see a decrease in the thermalization time for $\alpha = 0.1$, showing a clear tendency for decreasing thermalization time around all values of Δm. However, as we increase α, even keeping α in low values, this tendency of a smooth thermalization decay breaks, and an oscillating behavior starts to show in this case. However, for the case $\alpha = 0.3$ if we observe 2.9a) we can see that, for higher values of Δm a decay in thermalization time as Δm increases can be seen. Deeper studies in low values of α are necessary for clearing this behavior.

In the previous case, τ_{th} exhibits a smooth decay compared to other cases for $\alpha = 0.1$. This suggests that Eq. (1.81) describes, as a first approximation, the change on thermalization time when mass difference is introduced and its dependency for a linear and quadratic term of Δm. Further studies are needed to determine the limiting behavior of this phenomenon, as discussed in Chapter 1.

In summary, the α-FPUT system exhibits distinct regimes where thermalization time either decreases or increases with Δm, while the β-FPUT case shows a more uniform decreasing

trend. These results highlight the subtle interplay between nonlinearity and mass heterogeneity in thermalization dynamics.

To better understand the mechanisms behind these thermalization regimes, we now examine how energy redistributes across high frequency modes. In particular, the behavior of high-frequency excitations provides crucial insights into whether energy remains localized or spreads efficiently throughout the system, surprisingly underexplored despite its fundamental importance in nonlinear lattice dynamics applied to fields like solid state.

2.1.3. Exploration of High frequency Mode Dynamics

While acoustic modes have dominated FPUT system studies since their inception, their optical mode counterparts present unique challenges and opportunities. Our analysis of Figs. 2.11 and 2.12 reveals three key distinctions. Let us analyze it the dynamics of energies case by case.

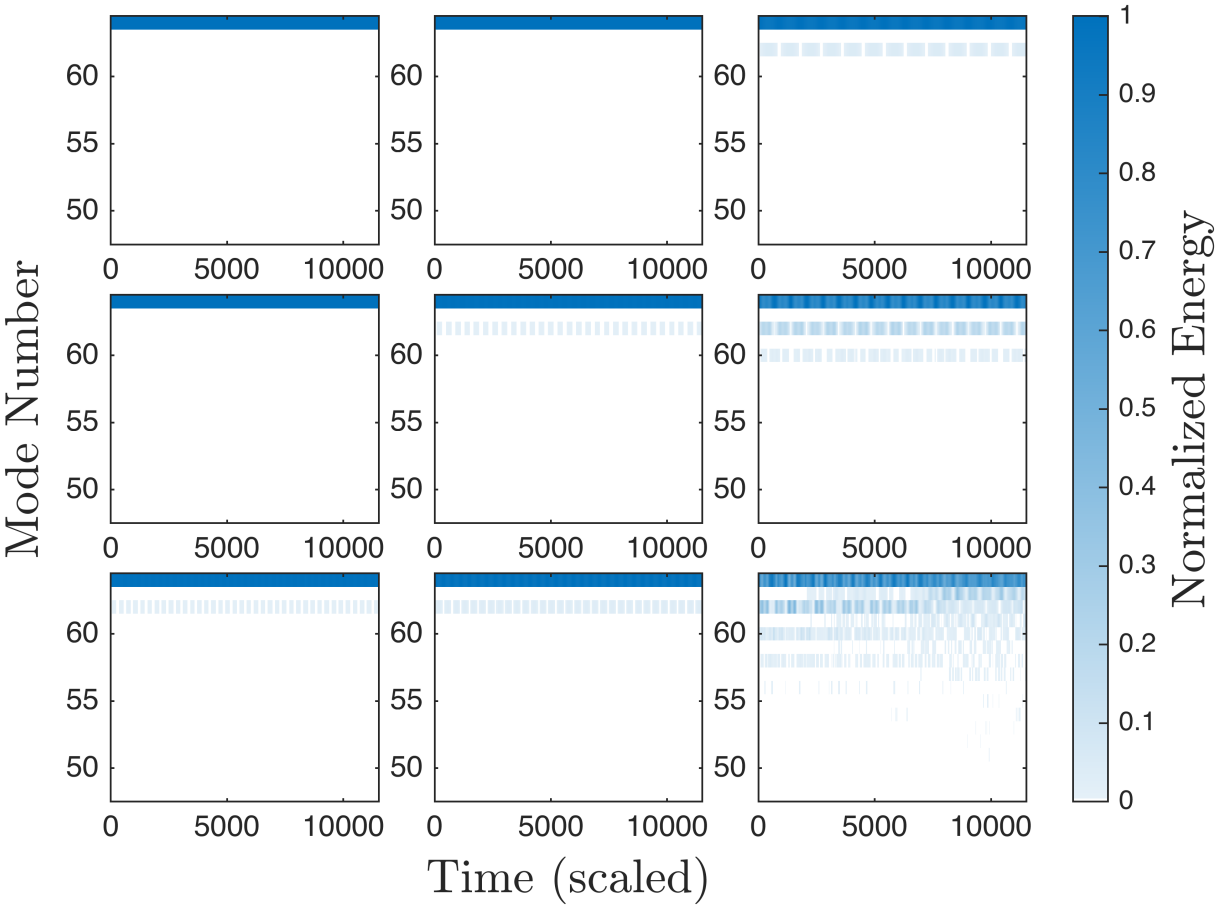

Fig. 2.11: Normalized energy per mode over time for a system of $N = 64$ particles with fixed boundary conditions. The columns represent different spring difference levels: $\Delta m = 0.3, 0.6, 0.9$ (left to right). The rows correspond to varying nonlinearity strengths: $\alpha = 0.3, 0.6, 0.9$ (top to bottom). The system is initialized with energy localized in the last mode with an amplitude of $A = 0.1$.

For the α-FPUT system (Fig. 2.11), mass difference (Δm) proves more influential than nonlinearity (α) in exciting high-frequency modes. The extreme case of $\alpha = 0.9$ with $\Delta m = 0.9$

demonstrates two notable features: a late-time energy cascade characterized by rapid multi-mode excitation, and the potential breakdown of recurrence phenomena.

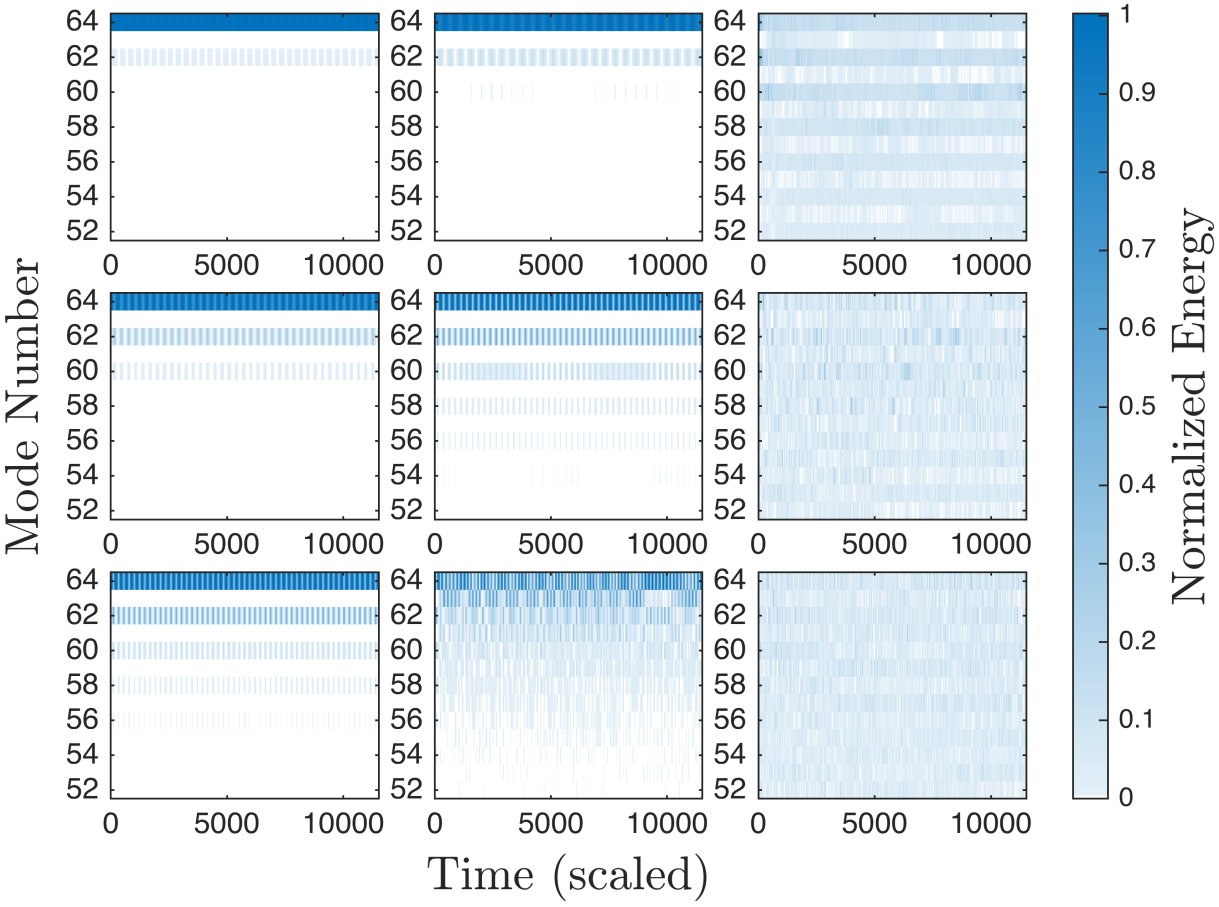

Fig. 2.12: Normalized energy per mode over time for a system of $N = 64$ particles with fixed boundary conditions. The columns represent different spring difference levels: $\Delta m = 0.3, 0.6, 0.9$ (left to right). The rows correspond to varying nonlinearity strengths: $\beta = 1, 3, 5$ (top to bottom). The system is initialized with energy localized in the last mode with an amplitude of $A = 0.1$.

The β-FPUT (see 2.12) system exhibits even more pronounced behavior, where the energy cascade becomes particularly evident at large mass differences. When $\Delta m = 0.9$, the system shows complete disappearance of recurrence and possible transition to chaotic dynamics. Furthermore, increasing β leads to greater mode excitation and significantly reduced recurrence times.

These results demonstrate that while stronger nonlinearities accelerate energy transfer between modes – consistent with known acoustic mode behavior [28, 31] – high-frequency modes display unique characteristics. Moderate mass differences permit partial energy localization, whereas greater alternance promotes mode mixing, especially in β-FPUT systems. Unlike their acoustic counterparts, high-frequency modes maintain persistent energy diffusion rather than exhibiting clear recurrence cycles.

However, these dynamics present computational challenges, as high nonlinearity combined with large mass differences often leads to numerical instabilities. This limitation underscores the need for more robust simulation techniques to properly capture these complex behaviors.

To quantitatively characterize these observed energy dynamics, we compute the spectral entropy $S(t)$. The spectral entropy reveals striking differences from the low-frequency case, providing crucial insights into the system's energy evolution.

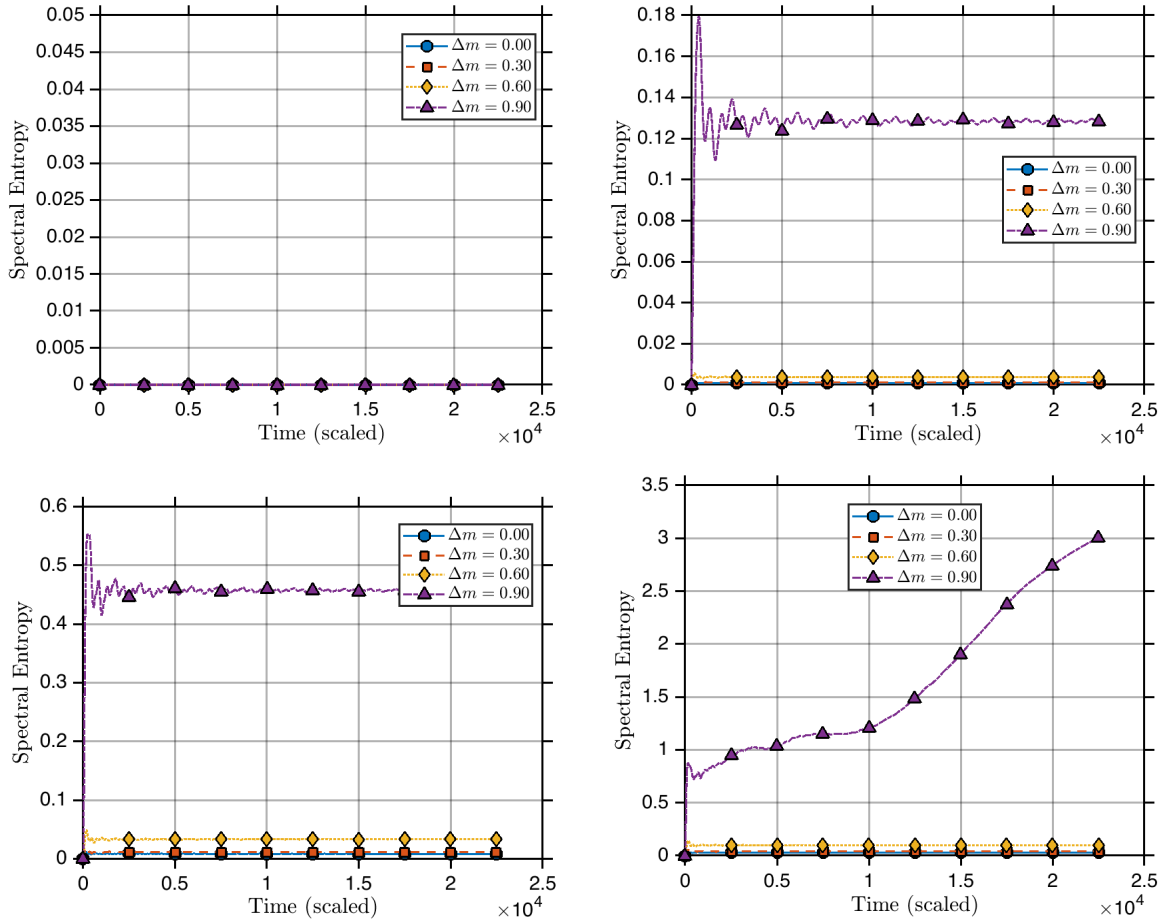

Fig. 2.13: Time evolution of the spectral entropy for a system of $N = 64$ particles with fixed boundary conditions, showing the variation of spectral entropy for different values of Δm. Each panel corresponds to different values of the nonlinear parameter α, increasing from left to right and top to bottom: $\alpha = 0, 0.3.0.6, 0.9$. The system is initialized with an excitation in the last mode, with an initial amplitude of $A = 0.1$.

For the α-FPUT system (Fig. 2.13), the highest entropy values consistently appear at $\Delta m = 0.9$ when $\alpha \neq 0$. The most extreme case ($\alpha = 0.9$, $\Delta m = 0.9$) shows particularly interesting behavior: the entropy becomes unstable within the observed time window and exhibits strong oscillations. These oscillations, present in all $\alpha \neq 0$ cases but most pronounced at $\Delta m = 0.9$, may reflect either numerical stiffness in our simulations or long-timescale recurrent behavior not visible in shorter observations.

Turning to the β-FPUT system (Fig. 2.14), the entropy behavior differs qualitatively. While oscillations persist, they are less prominent than in the α-FPUT case. More significantly, the $\Delta m = 0.9$ configuration shows substantially higher entropy than other mass differences across all β values. The sharp entropy increase between $\Delta m = 0.6$ and 0.9 strongly suggests a dynamical transition, possibly indicating the onset of an energy cascade regime at large mass differences.

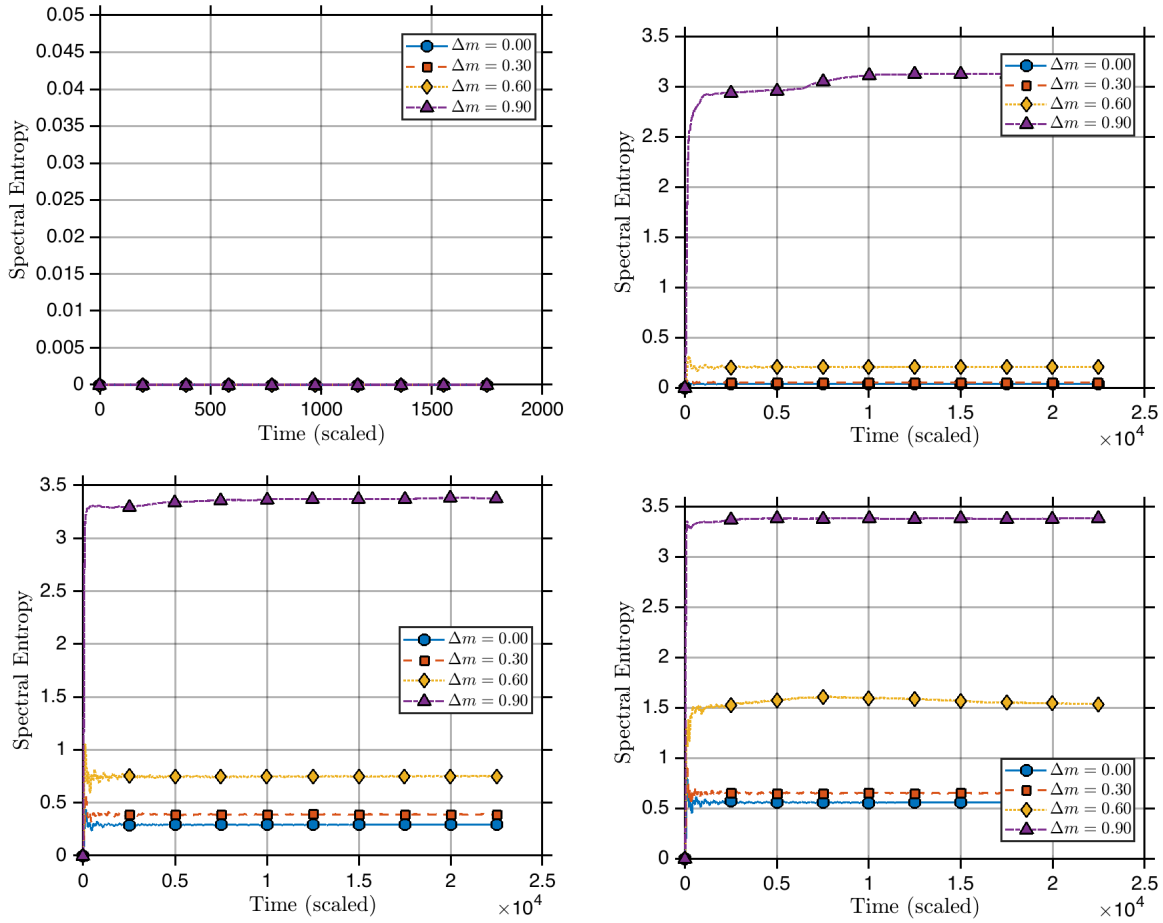

Fig. 2.14: Time evolution of the spectral entropy for a system of $N = 64$ particles with fixed boundary conditions, showing the variation of spectral entropy for different values of Δm. Each panel corresponds to different values of the nonlinear parameter β, increasing from left to right and top to bottom: $\beta = 0, 1, 3, 5$. The system is initialized with an excitation in the last mode, with an initial amplitude of $A = 0.1$.

2.2. Periodic Boundary Conditions

2.2.1. Low Frequency Mode Dynamics and Its Effects

In the original FPUT problem, fixed boundary conditions were considered. However, subsequent studies have also explored periodic boundary conditions due to their relevance in various physical systems, mainly disordered materials. In this work, we extend our analysis to include periodic boundary conditions, allowing us to compare their effects with those of fixed boundaries.

A direct comparison with the case for fixed boundary conditions reveals some points. While fixed boundaries impose constraints leading to stronger energy localization, periodic boundaries reduce confinement effects. This distinction influences the long-term behavior of high-frequency excitations and the rate of energy cascading through nonlinear interactions. The results for periodic boundary conditions are shown in Figs. 2.15 and 2.16.

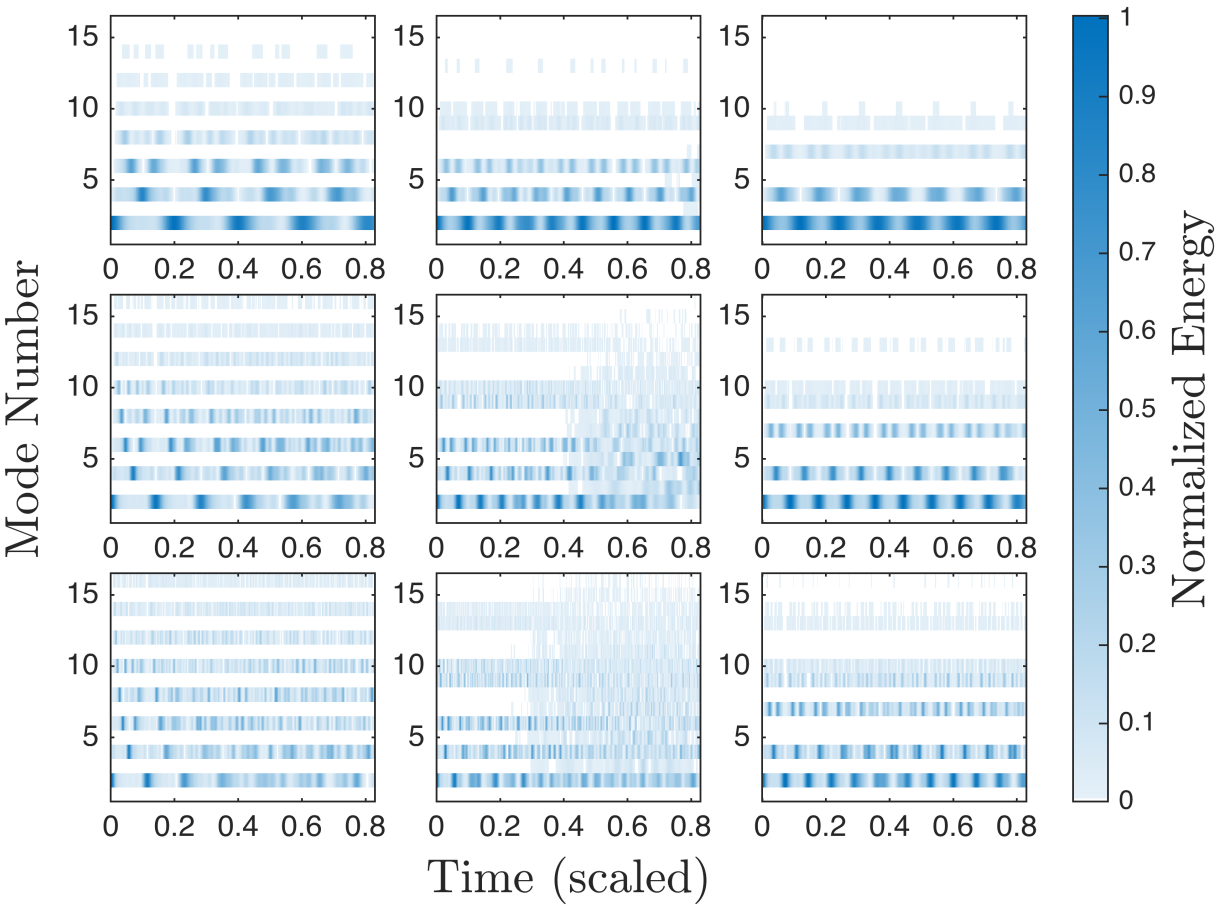

Fig. 2.15: Normalized energy per mode over time for a system of $N = 64$ particles with periodic boundary conditions. The columns represent different mass alternance levels: $\Delta m = 0.3, 0.6, 0.9$ (left to right). The rows correspond to varying nonlinearity strengths: $\alpha = 0.3, 0.6, 0.9$ (top to bottom). The system is initialized with energy localized in the second mode with an initial amplitude of $A = 5$.

For the α-FPUT system (Fig. 2.15), recurrence is observed in most cases. However, for specific parameter combinations—such as $\alpha = 0.6$, $\Delta m = 0.6$ and $\alpha = 0.9$, $\Delta m = 0.6$—recurrence appears to be disrupted by mass differences rather than nonlinearity. This is further supported by the reappearance of recurrence for $\Delta m = 0.9$.

As in the fixed boundary case, increasing nonlinearity reduces energy localization in the first modes, promoting energy redistribution across the system. For the β-FPUT system ($\alpha = 0$), recurrence persists under periodic boundary conditions, except for the case of $\Delta m = 0.9$, $\beta = 1.0$, where a *sticky state* emerges, similar to the fixed boundary scenario. Increasing nonlinearity restores the recurrence phenomenon and shortens the recurrence time. Additionally, higher mass alternance leads to energy spreading, with energy localizing in a pair of modes rather than concentrating in the first few.

These findings have important implications for modeling materials and studying thermalization in systems with alternating masses. They confirm a complex relationship between mass differences, nonlinearity, and thermalization, highlighting how boundary conditions and structural heterogeneity influence energy dynamics.

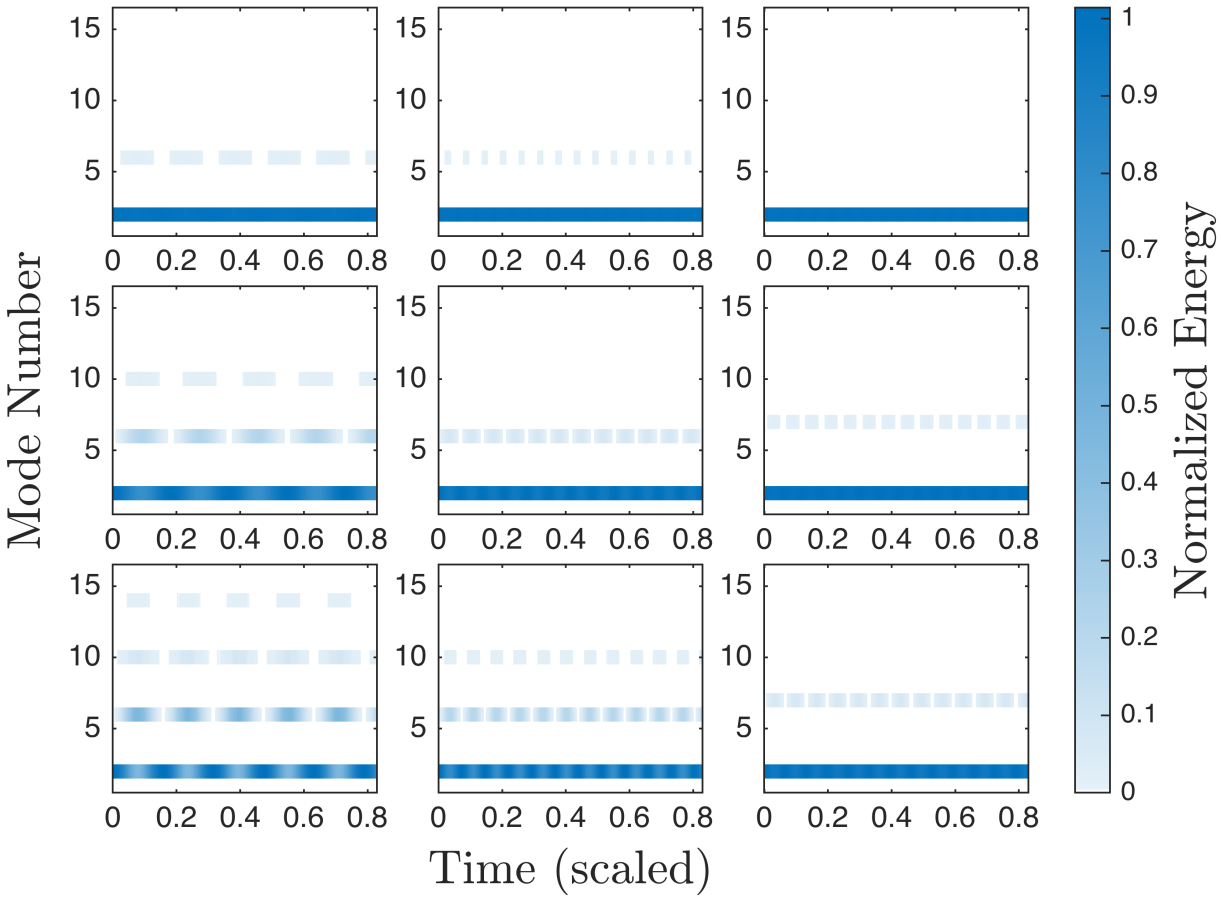

Fig. 2.16: Normalized energy per mode over time for a system of $N = 64$ particles with periodic boundary conditions. The columns represent different mass alternance levels: $\Delta m = 0.3, 0.6, 0.9$ (left to right). The rows correspond to varying nonlinearity strengths: $\beta = 1, 3, 5$ (top to bottom). The system is initialized with energy localized in the second mode with an initial amplitude of $A = 5$.

To further explore these relationships, particularly the interplay between nonlinearity, mass alternance, and boundary conditions, we turn to the spectral entropy as a quantitative measure as we did in the case for fixed boundary conditions. This approach allows us to analyze how energy distributes across modes and provides deeper insights into the system's approach to thermal equilibrium.

For the α-FPUT system, we observe in Fig. 2.17 that at low nonlinearity values, the entropy behavior resembles that of the fixed boundary case. However, as α increases, the entropy for $\Delta m = 0.3$ grows over time, reaching higher values than for $\Delta m = 0$. This may indicate a phase transition near $\Delta m = 0.3$, a hypothesis supported by [25], which reports a resonance phenomenon around the mass ratio $M/m \approx 2$ in diatomic chains. Here, M and m represent the large and small masses, respectively. This mass ratio corresponds to $\Delta m \approx 0.3$ in our study, and it is associated with shorter thermalization times compared to other mass ratios. Future work could employ numerical tools such as Lyapunov exponents and wave turbulence theory to confirm this hypothesis.

Exploring now the β-FPUT system, seen in Fig. 2.18, we observe similar trends at low nonlinearity values ($\beta = 1$), where higher Δm reduces the entropy peak. However, as nonlinearity

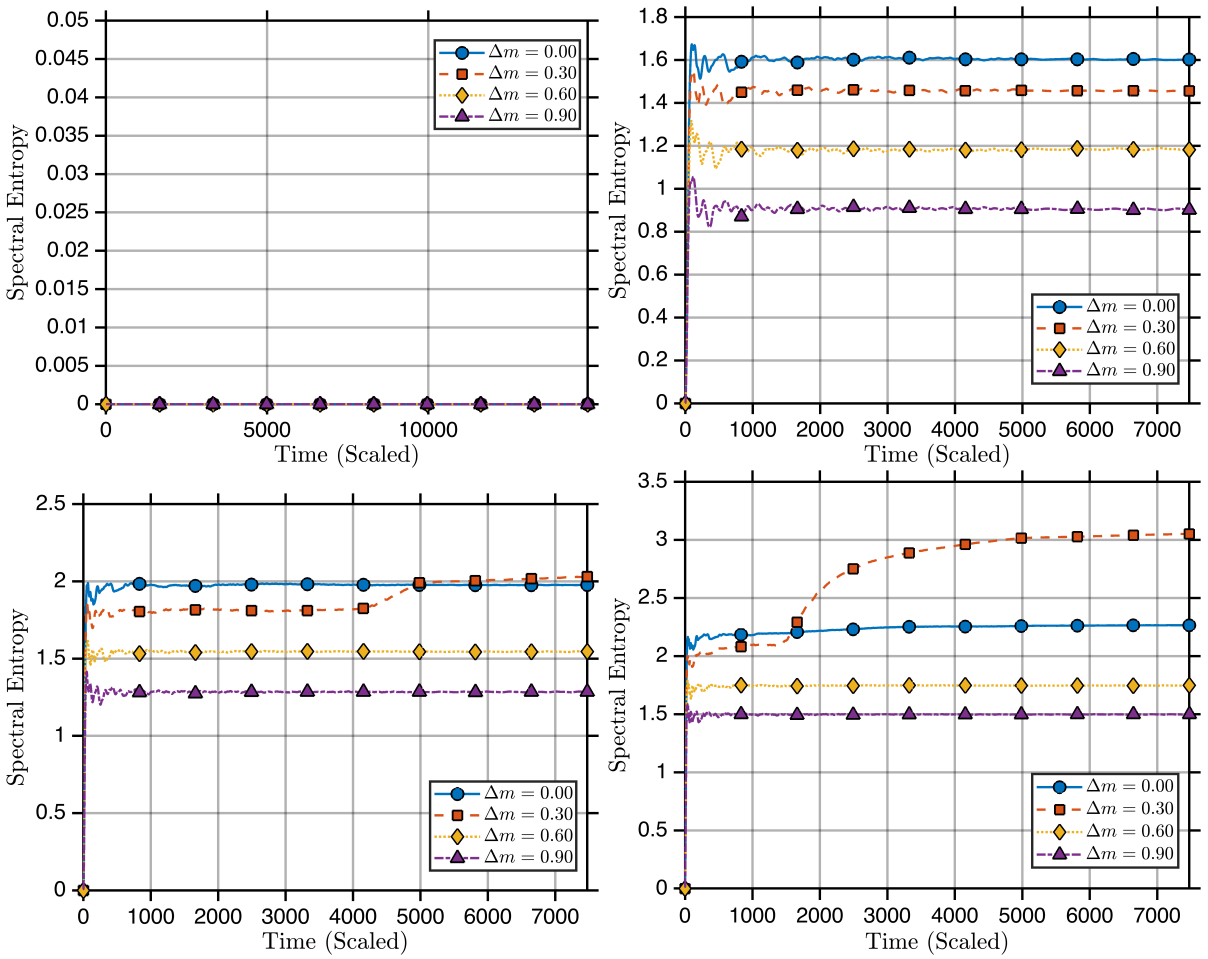

Fig. 2.17: Time evolution of the spectral entropy for a system of $N = 64$ particles with periodic boundary conditions, showing the variation of spectral entropy for different values of Δm. Each panel corresponds to different values of the nonlinear parameter α, increasing from left to right and top to bottom: $\alpha = 0, 0.3, 0.6, 0.90$. The system is initialized with an excitation in the second mode, with an initial amplitude of $A = 5$.

increases, the spectral entropy rises over time, even after reaching an apparent steady state. Notably, for $\beta = 5$ and $\Delta m = 0.3$, the entropy increases after a period of stability, surpassing the values observed for $\Delta m = 0$. This behavior suggests the possibility of a phase transition at specific Δm values or mass ratios $(1 + \Delta m)/(1 - \Delta m) \approx 2$ or $\Delta m \approx 0.3$, consistent with findings in [25].

2.2.2. Exploration of High Frequency Mode Dynamics

For the α-FPUT case, increasing Δm generally leads to excitation of more modes. This effect is particularly pronounced at $\alpha = 0.9$ and $\Delta m = 0.9$, where we observe a distinct mode excitation cascade over time – suggesting accelerated thermalization. Additionally, recurrence time decreases significantly at higher α values.

In contrast, the β-FPUT system exhibits even more dramatic effects. Here, higher values of β enhance mode excitation and further shorten recurrence time. This behavior is particularly

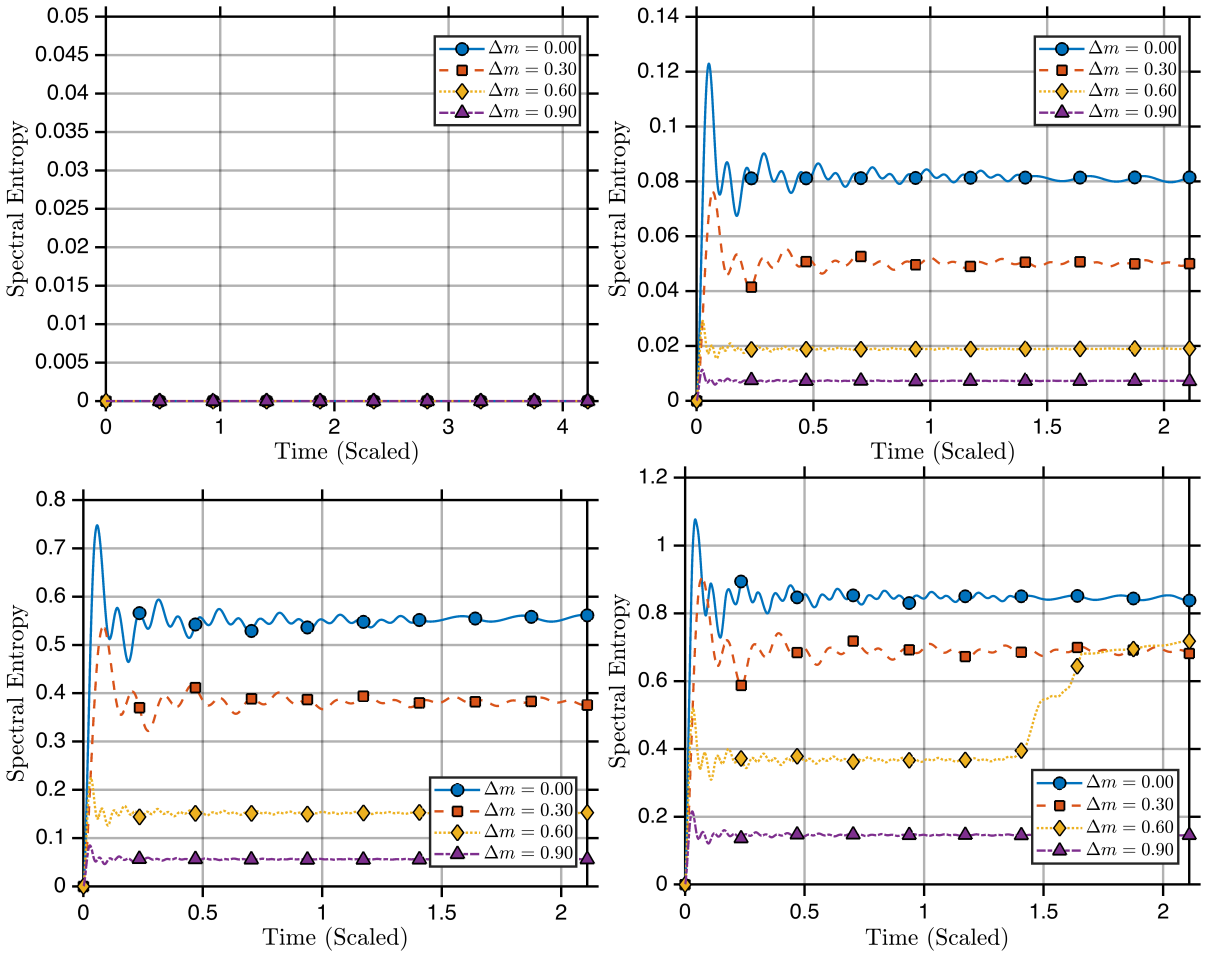

Fig. 2.18: Time evolution of the spectral entropy for a system of $N = 64$ particles with periodic boundary conditions, showing the variation of the spectral entropy for different values of Δm. Each panel corresponds to different values of the nonlinear parameter β, increasing from left to right and top to bottom: $\beta = 0, 1, 3, 5$. The system is initialized with an excitation in the second mode, with an initial amplitude of $A = 5$.

striking as Δm increases: energy spreads faster and more uniformly across the spectrum. At the extreme limit ($\Delta m = 0.9$), we observe a fully developed mode excitation cascade, where nearly all modes participate in energy transfer. Notably, this regime is characterized by an apparent disappearance of recurrence phenomena, suggesting that strong nonlinearity and mass alternance together can suppress long-term energy localization.

This contrast between the α-FPUT and β-FPUT systems underscores how different nonlinear interactions govern energy redistribution in mass-alternating chains. While the α system progressively unlocks new modes, facilitating a gradual transition toward equipartition, the β system exhibits a more abrupt transition into a fully excited state. This distinction suggests that nonlinearity plays a dual role, either enhancing localization effects at lower values or accelerating thermalization at sufficiently high nonlinear strengths.

To quantitatively assess these effects and confirm the observed transitions, we now turn to the spectral entropy of the system.

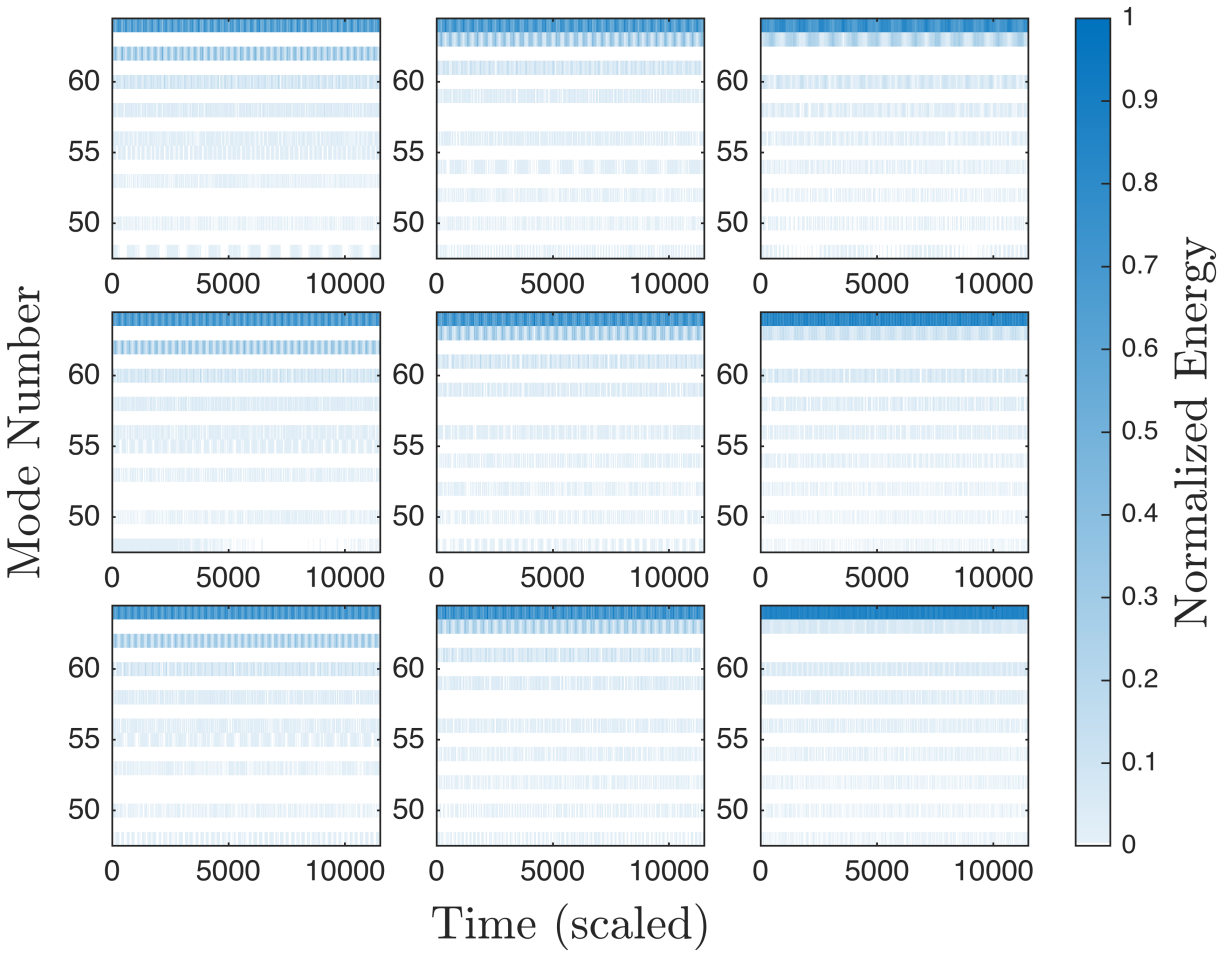

Fig. 2.19: Normalized energy per mode over time for a system of $N = 64$ particles with periodic boundary conditions. The columns represent different mass difference levels: $\Delta m = 0.3, 0.6, 0.9$ (left to right). The rows correspond to varying nonlinearity strengths: $\alpha = 0.3, 0.6, 0.9$ (top to bottom). The system is initialized with energy localized in the second mode with an initial amplitude of $A = 0.1$.

In the α-FPUT system (Fig. 2.21), the entropy values remain remarkably low, growing linearly rather than saturating. Notably, $\Delta m = 0.9$ cases consistently show the highest entropy values.

The β-FPUT system (Fig. 2.22) exhibits more conventional behavior, with entropy approaching asymptotic values. Again, $\Delta m = 0.9$ configurations reach the highest entropy levels, supporting the energy cascade hypothesis at large mass differences.

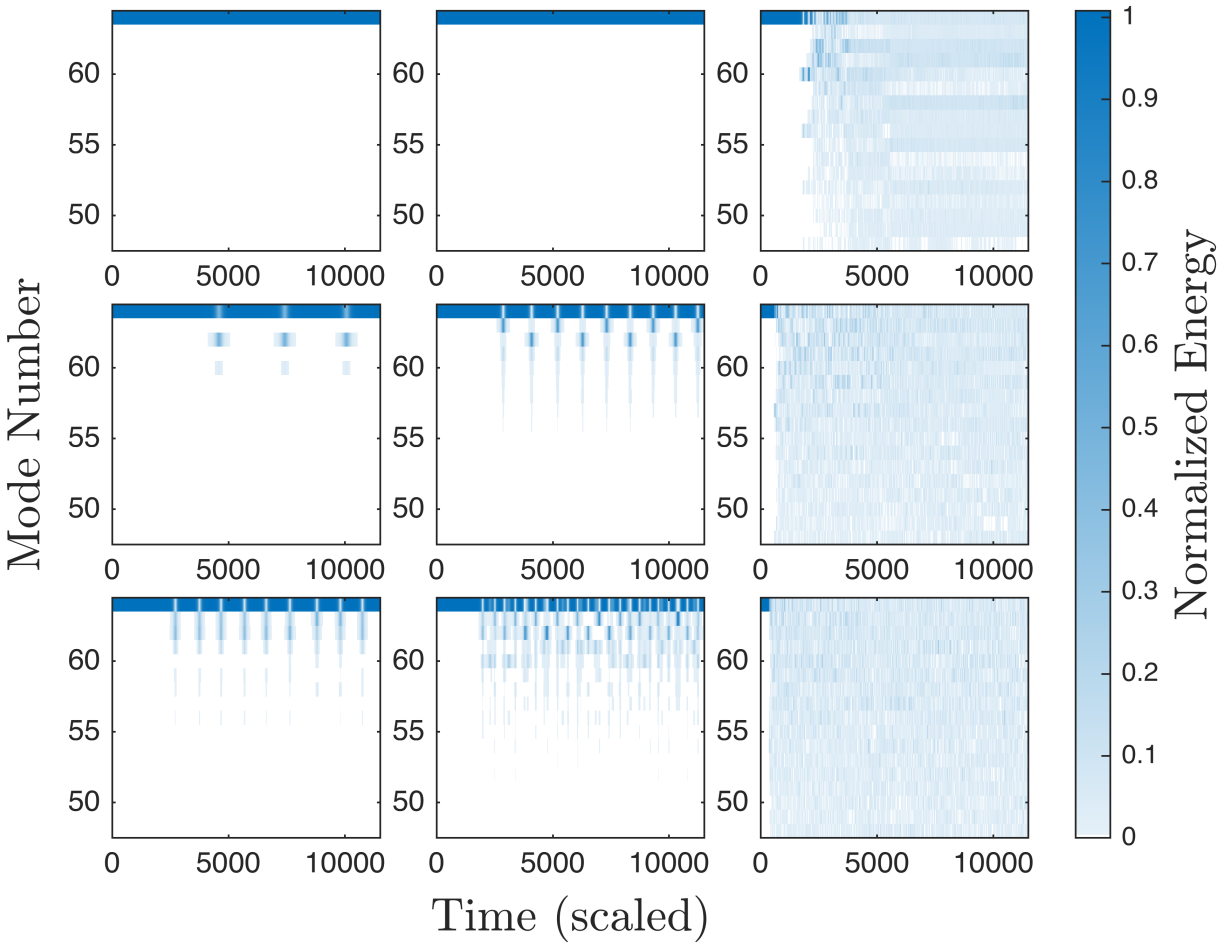

Fig. 2.20: Normalized energy per mode over time for a system of $N = 64$ particles with periodic boundary conditions. The columns represent different mass difference levels: $\Delta m = 0.3, 0.6, 0.9$ (left to right). The rows correspond to varying nonlinearity strengths: $\beta = 1.0, 3.0, 5.0$ (top to bottom). The system is initialized with energy localized in the second mode with an initial amplitude of $A = 0.1$.

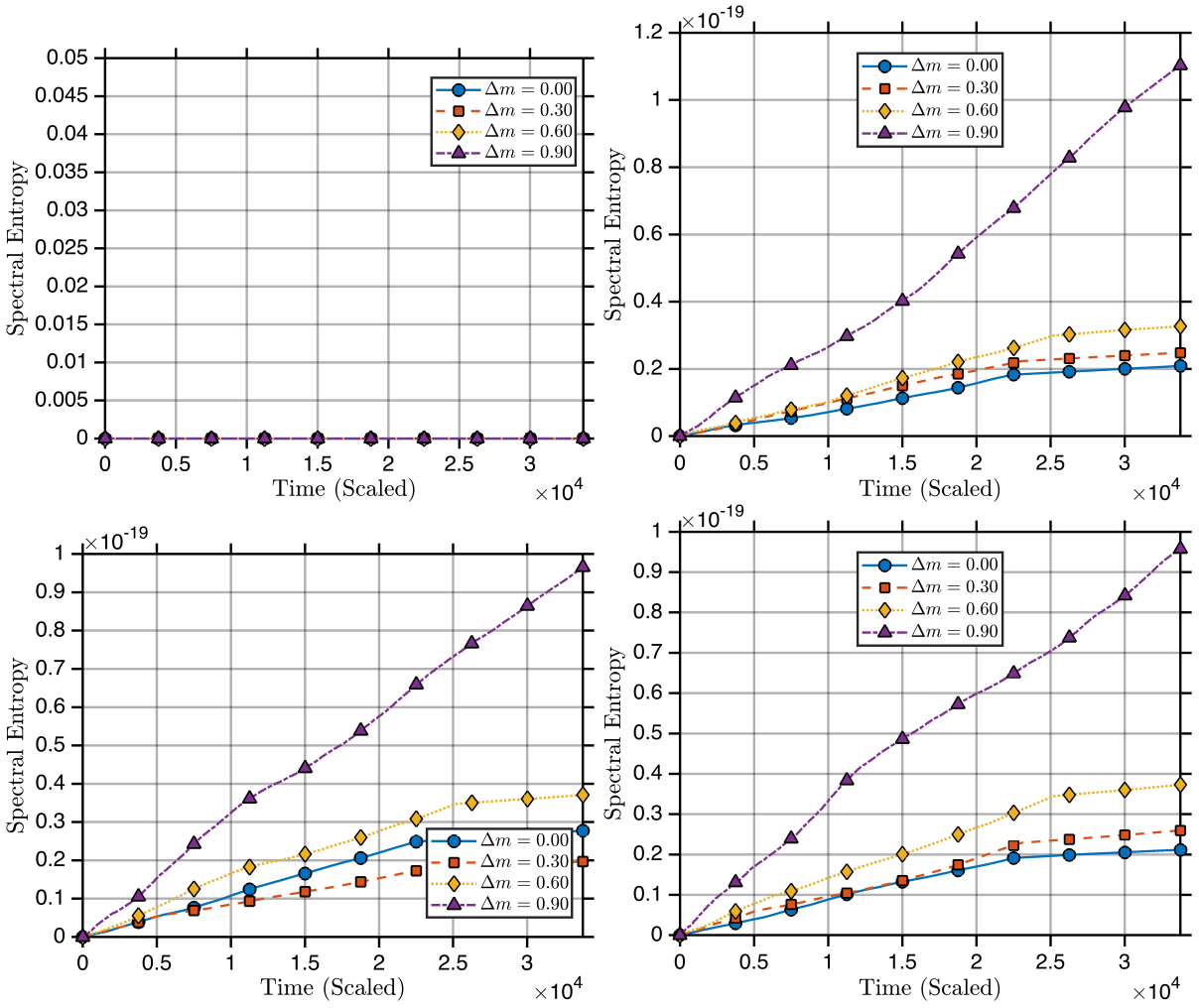

Fig. 2.21: Time evolution of the spectral entropy for a system of $N = 64$ particles with periodic boundary conditions, showing the variation of the spectral entropy for different values of Δm. Each panel corresponds to different values of the nonlinear parameter α, increasing from left to right and top to bottom: $\alpha = 0, 0.3, 0.6, 0.9$. The system is initialized with an excitation in the last mode, with an initial amplitude of $A = 0.1$.

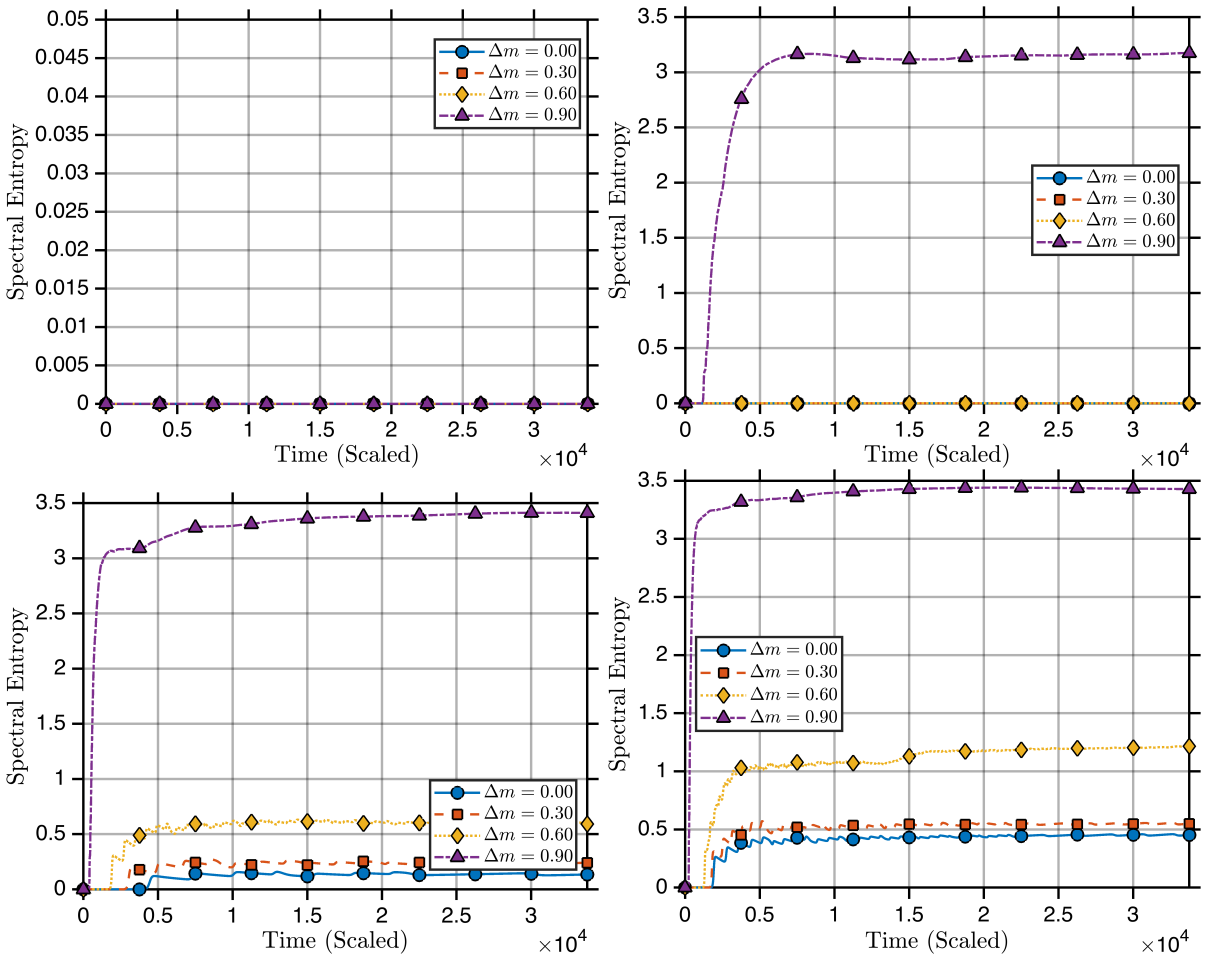

Fig. 2.22: Time evolution of the spectral entropy for a system of $N = 64$ particles with periodic boundary conditions, showing the variation of the spectral entropy for different values of Δm. Each panel corresponds to different values of the nonlinear parameter β, increasing from left to right and top to bottom: $\beta = 0, 1, 3, 5$. The system is initialized with an excitation in the second mode, with an initial amplitude of $A = 0.1$.

Capítulo 3

On the relaxation for the case of different springs

Following the analysis of mass heterogeneity, this chapter extends the study to the case of alternating spring constants. While less explored than the case of varying masses, this scenario presents distinct challenges and opportunities for understanding energy transport and thermalization in nonlinear lattices. Its relevance extends to various real-world applications, including disordered materials, biological systems, and engineered structures, as highlighted in the Introduction. Additionally, the interplay between nonlinearity and spring alternance provides a compelling framework for addressing fundamental questions in statistical mechanics and dynamical systems.

Unlike previous studies, this work considers a system where nonlinear parameters are not homogeneous, allowing for a more comprehensive exploration of the effects of varying spring constants. However, this generalization introduces additional computational complexity. By systematically varying both the alternance strength and nonlinearity parameters, we examine the system's thermalization dynamics, energy localization, and spectral entropy. Our results demonstrate how variations in spring constants influence energy transport and thermalization, offering new insights into the role of heterogeneity in nonlinear systems.

3.1. Fixed Boundary Conditions

3.1.1. Low Frequency Mode Dynamics and Its effects on Thermalization

As in Chapter 2, we begin with fixed boundary conditions, focusing on the behavior of low-frequency modes. For the α-FPUT system, introducing alternance in spring constants shortens recurrence times and leads to minor excitations of higher modes. However, spring alternance increases system stiffness, which can cause numerical instabilities and requires careful handling in simulations, such as reducing time steps or using adaptive algorithms.

For the α-FPUT chain, as nonlinearity increases, energy distributes more evenly across modes. For example, at $\alpha = 0.9$ and $\Delta\kappa = 0.3$, the recurrence phenomenon appears to vanish but

reemerges as $\Delta\kappa$ increases. Notably, higher values of $\Delta\kappa$ strengthen recurrence, reducing the time between cycles.

High levels of nonlinearity, combined with weak spring alternance, promote partial thermalization, where energy gradually redistributes across modes. In contrast, stronger spring alternance enhances energy localization, delaying or preventing thermalization altogether. These findings underscore the significant role of spring alternance in shaping thermalization dynamics, complementing the well-studied effects of mass alternance.

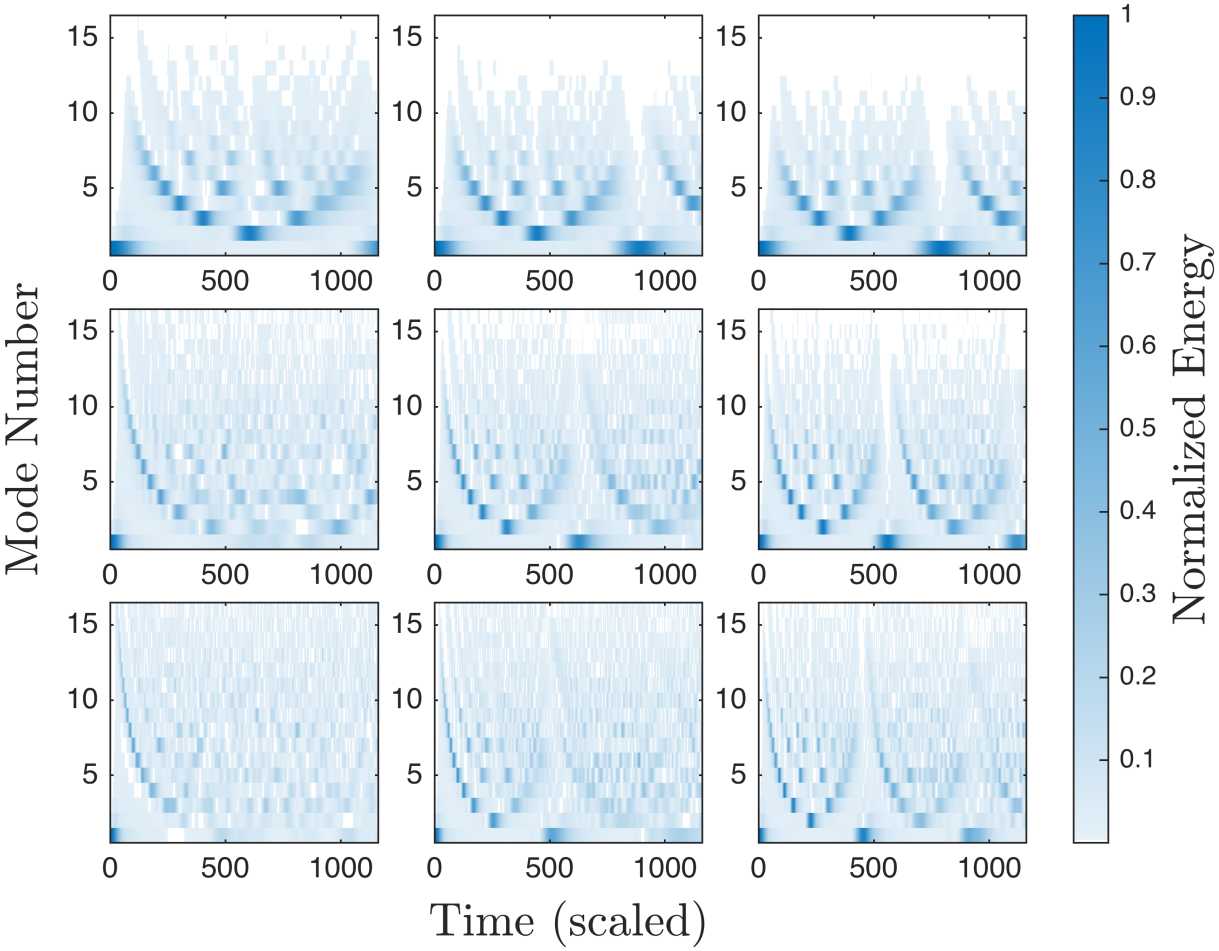

Fig. 3.1: Normalized energy per mode over time for a system of $N = 64$ particles. The columns represent different spring difference levels: $\Delta\kappa = 0.3, 0.6, 0.9$ (left to right). The rows correspond to varying nonlinearity strengths: $\alpha = 0.3, 0.6, 0.9$ (top to bottom). The system is initialized with energy localized in the second mode with an amplitude of $A = 5$.

Turning to the β-FPUT chain, we can see that as $\Delta\kappa$ increases, recurrence time decreases. On the other hand, as β increases, the excitation of higher modes is more prominent. For $\beta = 5.0$. and $\Delta\kappa = 0.6$, the recurrence seems to disappear for long times, showing that for high values of β and medium values of $\Delta\kappa$, thermalization occurs faster.

To further explore these dynamics, we compute the spectral entropy for the system. This analysis illuminates how thermalization evolves across different values of $\Delta\kappa$ and β, revealing the interplay between spring alternance, nonlinearity parameters (α and β), and thermalization rates.

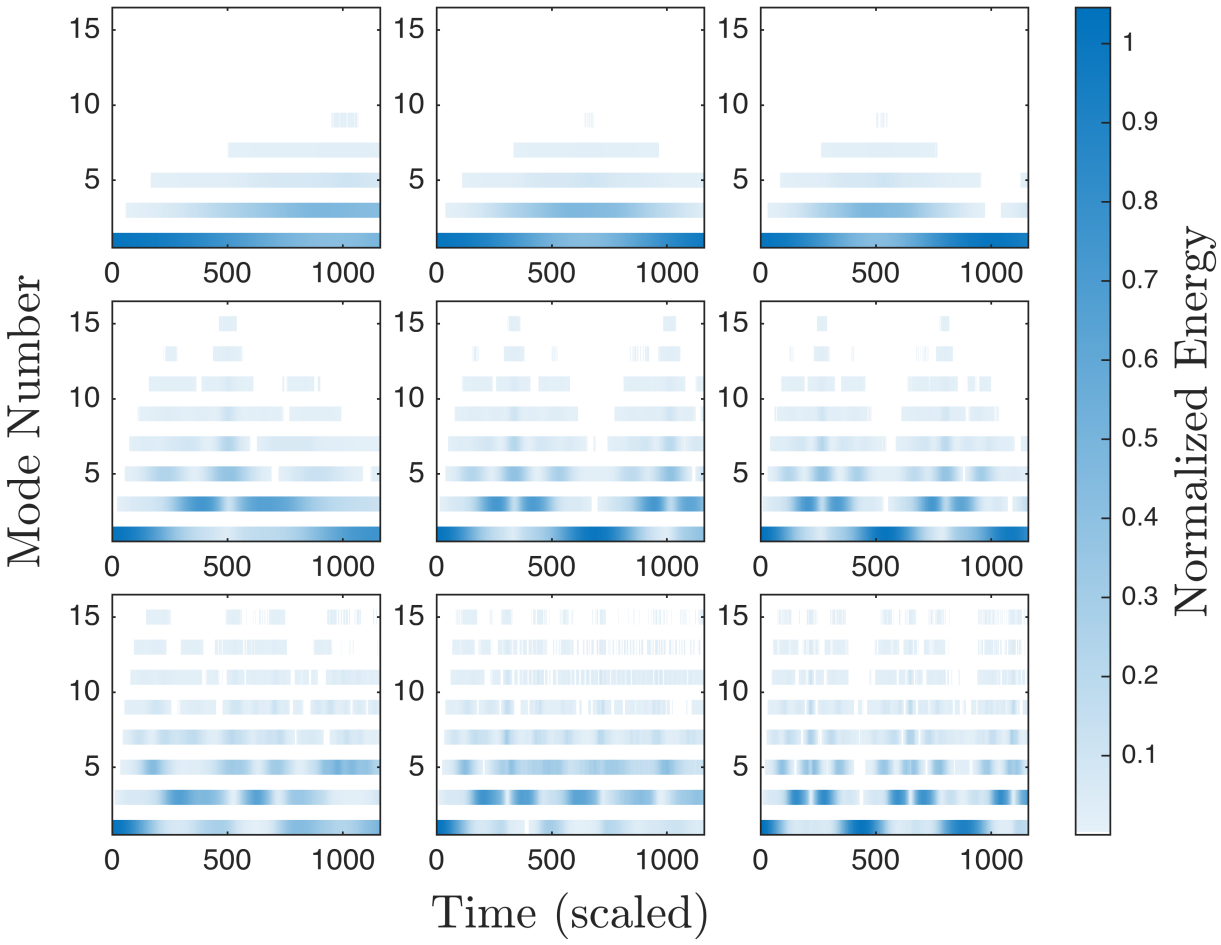

Fig. 3.2: Normalized energy per mode over time for a system of $N = 64$ particles with fixed boundary conditions. The columns represent different spring difference levels: $\Delta\kappa = 0.3, 0.6, 0.9$ (left to right). The rows correspond to varying nonlinearity strengths: $\beta = 1, 3, 5$ (top to bottom). The system is initialized with energy localized in the second mode with an amplitude of $A = 10$.

Starting with the α-FPUT system, Fig. 3.3 reveals key insights about the α-FPUT system under spring alternation ($\Delta\kappa$). At $\Delta\kappa = 0.3$, we observe a behavior qualitatively similar to mass difference cases, where greater differences typically reduce entropy values. For $\Delta\kappa = 0.3$, entropy values initially approximate those of $\Delta\kappa = 0$, but ultimately tend to exceed the homogeneous case ($\Delta\kappa = 0$). This pattern persists across multiple α values, suggesting a systematic effect. The observed entropy enhancement implies spring alternation may facilitate energy redistribution. This effect becomes more pronounced over time. It also contrasts with mass difference cases, where entropy typically decreases.

Nevertheless, difficulty for getting numerical stability, and therefore, for getting reliable results, becomes increasingly a challenge for the study.

On the other hand, for the β-FPUT case, the results are shown in Fig. 3.4. In particular, for the case of $\beta = 3$, we observe an apparent stabilization of entropy at early times, followed by an increase at later times. Interestingly, this late-time excitation is not clearly visible in the heatmaps shown in Figures 3.1 and 3.2. To fully understand this behavior, further refinements in numerical

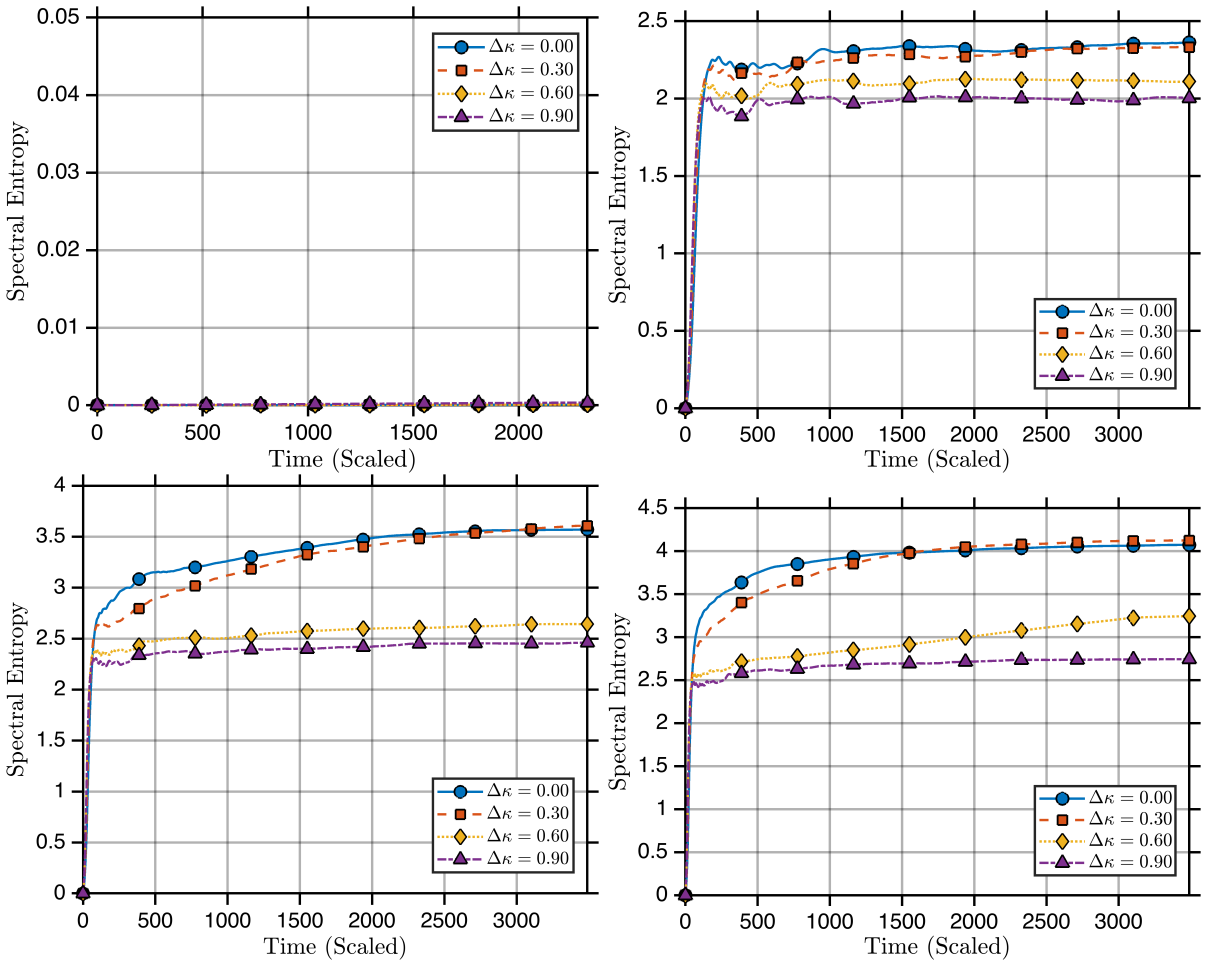

Fig. 3.3: Time evolution of the spectral entropy for a system of $N = 64$ particles with fixed boundary conditions, showing the variation of the spectral entropy for different values of $\Delta\kappa$. Each panel corresponds to different values of the nonlinear parameter α, increasing from left to right and top to bottom: $\alpha = 0, 0.3, 0.6, 0.9$. The system is initialized with an excitation in the first mode, with an initial amplitude of $A = 10$.

methods are necessary. These improvements will help distinguish between numerical flaws and genuine physical phenomena, ensuring the reliability of our observations and conclusions. Another possibility is the existence of a 'phase transition' behavior for the case $\beta = 3$ and $\Delta\kappa = 0.9$, but further studies are necessary. Due to a lack of literature for this case, a conclusion is rather bold in this case.

3.1.1.1. Thermalization Time Analysis

Using the latest spectral entropy results, we compute the reached values of spectral entropy when the system is thermalized, and thermalization time as previously done for the case of different masses with fixed boundary conditions.

The results for the thermalization time are shown in Figure 3.6, while the results for the values of the spectral entropy are shown in 3.5.

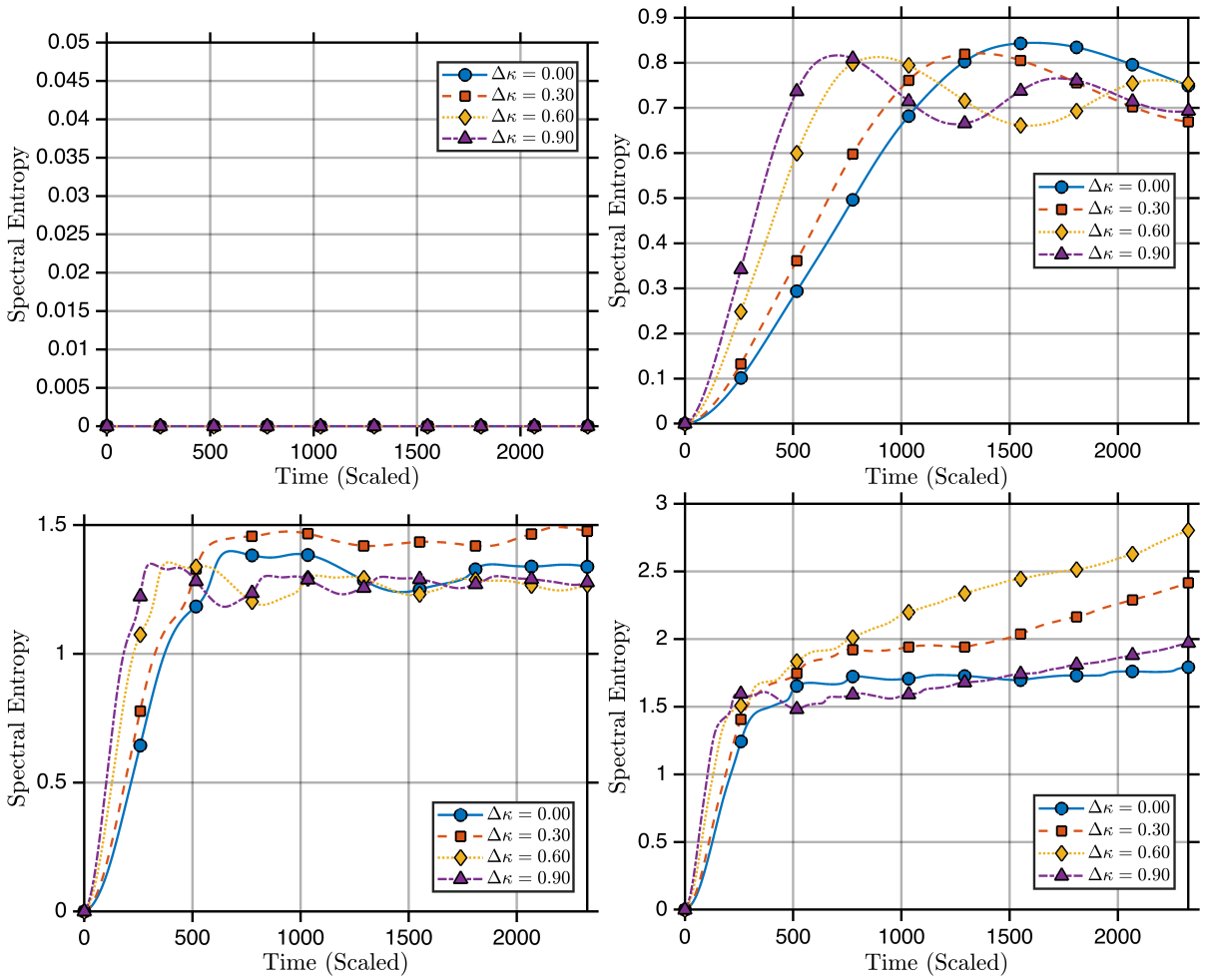

Fig. 3.4: Time evolution of the spectral entropy for a system of $N = 64$ particles with fixed boundary conditions, showing the variation of spectral entropy for different values of $\Delta\kappa$. Each panel corresponds to different values of the nonlinear parameter β, increasing from left to right and top to bottom: $\beta = 0, 1.0, 3, 5$. The system is initialized with an excitation in the first mode, with an initial amplitude of $A = 10$.

The spectral entropy $S(\tau_{th})$ as a function of spring constant heterogeneity $\Delta\kappa$ reveals distinct behaviors between the α and β-FPUT systems. On one hand, the α-FPUT system (Fig. 3.5a)) exhibits a more systematic trend: entropy decreases monotonically with increasing Δm across all values of α. Notably, higher nonlinearity (α=0.9) leads to initially elevated entropy values that decline more steeply with heterogeneity. These results suggest that spring alternance effectively suppresses thermalization in the α-FPUT model, promoting energy localization over a broad range of nonlinearities.

On the other hand, the β-FPUT system (Fig. 3.5b)) displays a more abrupt, non-monotonic response. A sharp drop in entropy occurs only at intermediate nonlinearity (β=3.0), indicating a threshold-like transition toward localization as alternance increases. In contrast, for weak ($\beta = 1.0$) and strong ($\beta = 5.0$) nonlinearities, entropy remains nearly constant, suggesting limited sensitivity to spring heterogeneity in those regimes.

In summary, the α-FPUT system exhibits a clear suppression of thermalization as spring

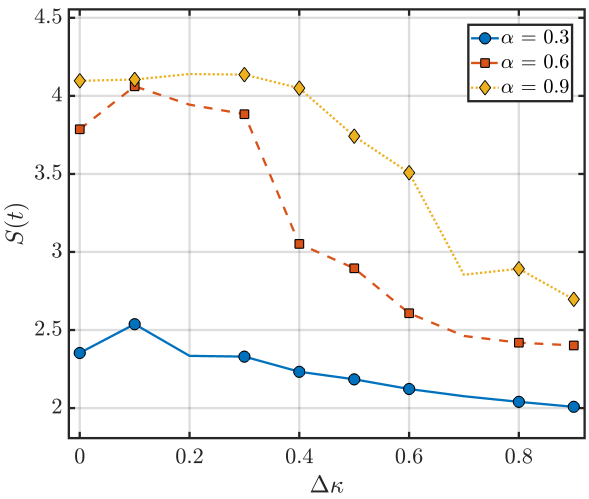

a) Spectral entropy at equilibrium times vs different values of $\Delta\kappa$ for different values of $\alpha = 0.3, 0.6, 0.9$ for fixed boundary conditions. The initial conditions are the same as Fig. 3.1.

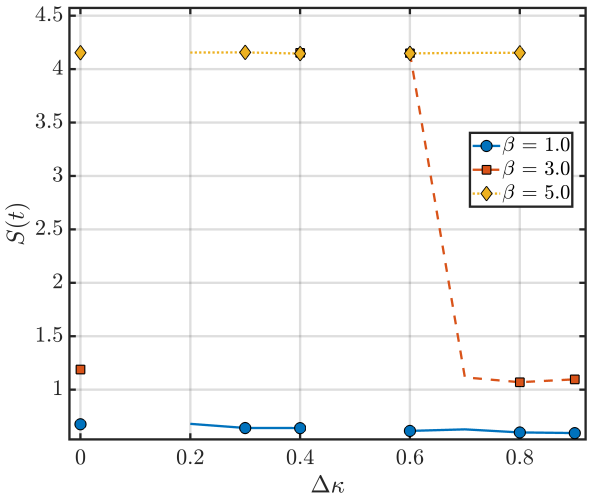

b) Spectral entropy at equilibrium times vs different values of $\Delta\kappa$ for different values of $\beta = 1.0, 3.0, 5.0$ for fixed boundary conditions. Initial conditions are the same as Fig. 3.2.

Fig. 3.5: Values of spectral enetropy when thermalization time is reached for different values of $\Delta\kappa$ with fixed boundary conditions. (a) Varying α values. (b) Varying β values.

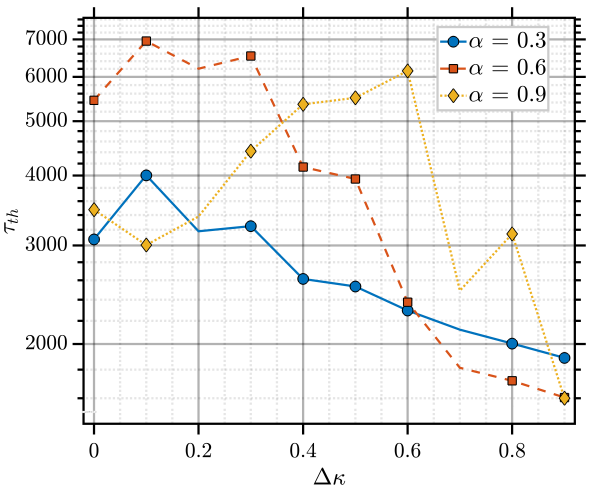

a) Thermalization time vs different values of $\Delta\kappa$ for different values of $\alpha = 0.3, 0.6, 0.9$ for fixed boundary conditions. The initial conditions are the same as Fig. 3.1.

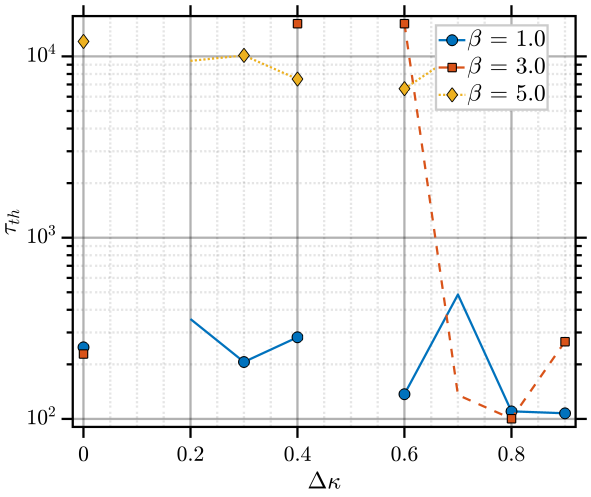

b) Thermalization time vs different values of $\Delta\kappa$ for different values of $\beta = 1.0, 3.0, 5.0$ for fixed boundary conditions. Initial conditions are the same as Fig. 3.2.

Fig. 3.6: Thermalization time for different values of $\Delta\kappa$ with fixed boundary conditions. (a) Varying α values. (b) Varying β values.

alternance increases, with entropy decreasing steadily across all nonlinearities. In contrast, the β-FPUT system shows this effect only at intermediate nonlinearity, suggesting a threshold behavior. These differences reflect how each type of nonlinearity uniquely mediates the impact of spring difference on energy localization.

Once this explored, we analyze now the thermalization times.

For the α-FPUT system (Fig. 3.6a))) we can see a similar pattern to the Δm case. We can see a clear tendency for decreasing thermalization time around all values of Δm for the cases $\alpha = 0.3$ and $\alpha = 0.6$. However, for the case of $\alpha = 0.9$, we can see two different regimes, the first

one between $\Delta\kappa = 0.1$ and $\Delta\kappa = 0.6$, in which thermalization time increases, and another regime where thermalization time decreases for the rest of values of $\Delta\kappa$.

For the β-FPUT system (Fig. 3.6b)) a tendency is harder to see. The stiffness of the system shows that thermalization time reaches orders from 10^2 up to 10^4. In particular, for $\beta = 3.0$ we can see an abrupt fall in thermalization time for $\Delta\kappa = 0.7$. While for low values of $\Delta\kappa$, thermalization time is beyond 10^4, reaching this regime for $\Delta\kappa = 0.4$. For other cases, we can see an oscillating behavior, mainly in $\beta = 1.0$, where thermalization time increases, decreases and increases, for finally decreasing again. For the case of $\beta = 5.0$ we can see a tendency to decrease thermalization time for low to intermediate values of $\Delta\kappa$, but the absence of thermalization times for some values of $\Delta\kappa$ indicates that thermalization time is beyond the scope of 10^4 shown in the figure, giving clues for an oscillating behavior for $\beta = 5.0$.

These results suggest that nonlinearity and alternance interact in fundamentally different ways depending on the dominant nonlinear term. To gain deeper insight into this interplay, we now turn our attention to the behavior of high-frequency (optical) modes, where additional complexities arise due to their distinct dynamical properties.

As a final result of this section, we can plot τ_{th}/τ_0, where τ_0 is the thermalization time for the homogeneous case exploring the regime for weak spring alternance $\Delta\kappa$, similar to the case with different masses.

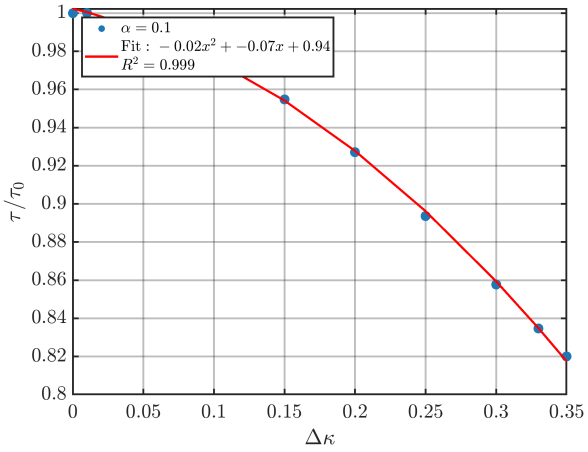

a) Thermalization time τ_{th} as a function of $\Delta\kappa$ for low values of α and $\Delta\kappa$. Initial conditions correspond to those in Fig. 3.6a)

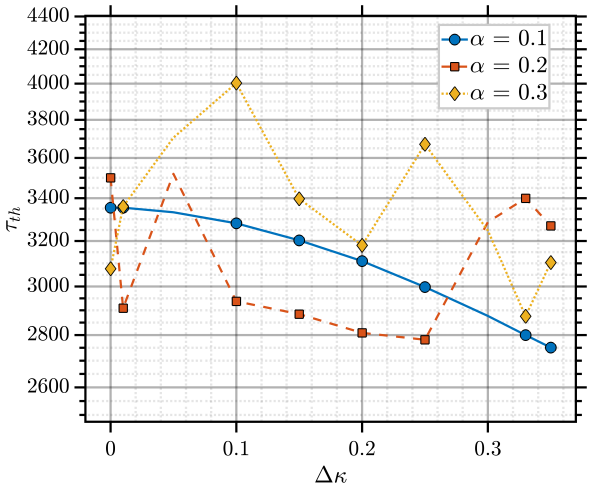

b) Normalized thermalization time $\tau_{th}/\tau_{th}(\Delta\kappa = 0)$ versus $\Delta\kappa$ for $\alpha = 0.1$ (low $\Delta\kappa$ regime). A polynomial fit is included, with data points extracted from Fig. 3.7a).

Fig. 3.7: Thermalization dynamics in the low-parameter regime. (a) Dependence of τ_{th} on $\Delta\kappa$; (b) Normalized thermalization time with polynomial fit.

For the case of $\Delta\kappa$, we observe a pattern similar to the previous one: at $\alpha = 0.1$ and low Δm, the thermalization time τ_{th} exhibits a smooth decay. This suggests that the underlying mechanism responsible for the decay is analogous in both cases—despite differences in masses and spring constants—and is initially approximated by Eq. (1.83). Further studies are needed to determine the limiting behavior of this phenomenon, as discussed in Chapter 1.

3.1.2. Exploration of High Frequency Mode Dynamics

The analysis of optical modes introduces additional numerical complexities, yet reveals consistent patterns in respect to previous cases.

The α-FPUT system (Fig.3.8) exhibits distinct recurrence patterns depending on nonlinearity strength. At $\alpha = 0.3$, recurrence is completely absent, while for $\alpha = 0.6$ it only emerges at the maximum spring alternation ($\Delta\kappa = 0.9$). The $\alpha = 0.9$ case reveals an inverse relationship between $\Delta\kappa$ and recurrence time - a surprising contrast to the $\alpha = 0.6$ behavior that warrants further investigation.

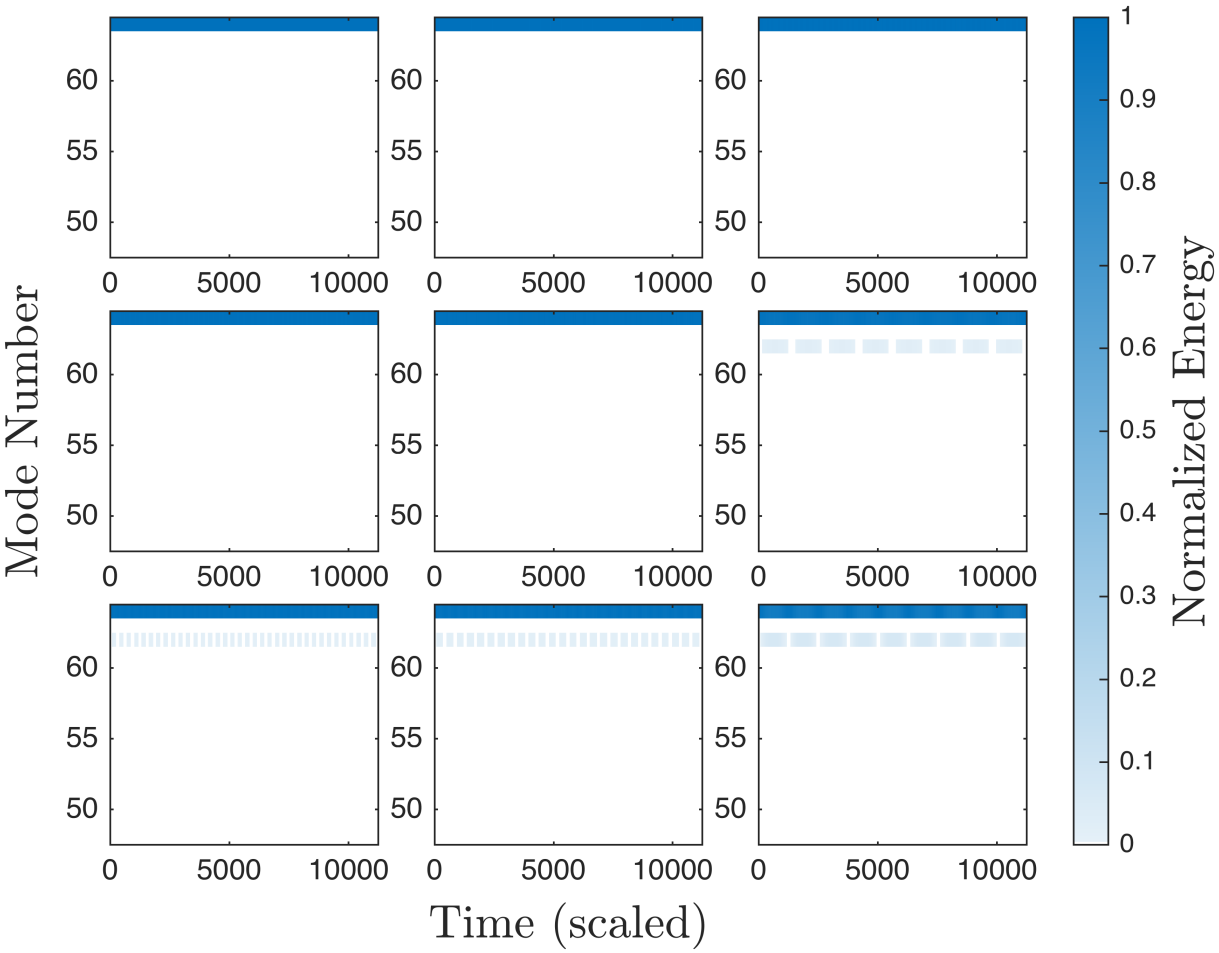

Fig. 3.8: Normalized energy per mode over time for a system of $N = 64$ particles with fixed boundary conditions. The columns represent different spring difference levels: $\Delta\kappa = 0.3, 0.6, 0.9$ (left to right). The rows correspond to varying nonlinearity strengths: $\alpha = 0.3, 0.6, 0.9$ (top to bottom). The system is initialized with energy localized in the last mode with an amplitude of $A = 0.1$.

The β-FPUT system (Fig. 3.9) demonstrates progressive changes with increasing β and $\Delta\kappa$. Higher β values excite additional modes while shortening recurrence times, though these effects diminish in extreme parameter regimes. Most notably, the $\beta = 3$, $\Delta\kappa = 0.9$ configuration exhibits partial recurrence breakdown, where an emerging energy cascade coexists with intermittent mode-specific energy oscillations - suggesting a transitional state between localized and delocalized energy dynamics. Alternative analysis or further refinements on numerical methods are necessary

for a clear distinction on the study of this case.

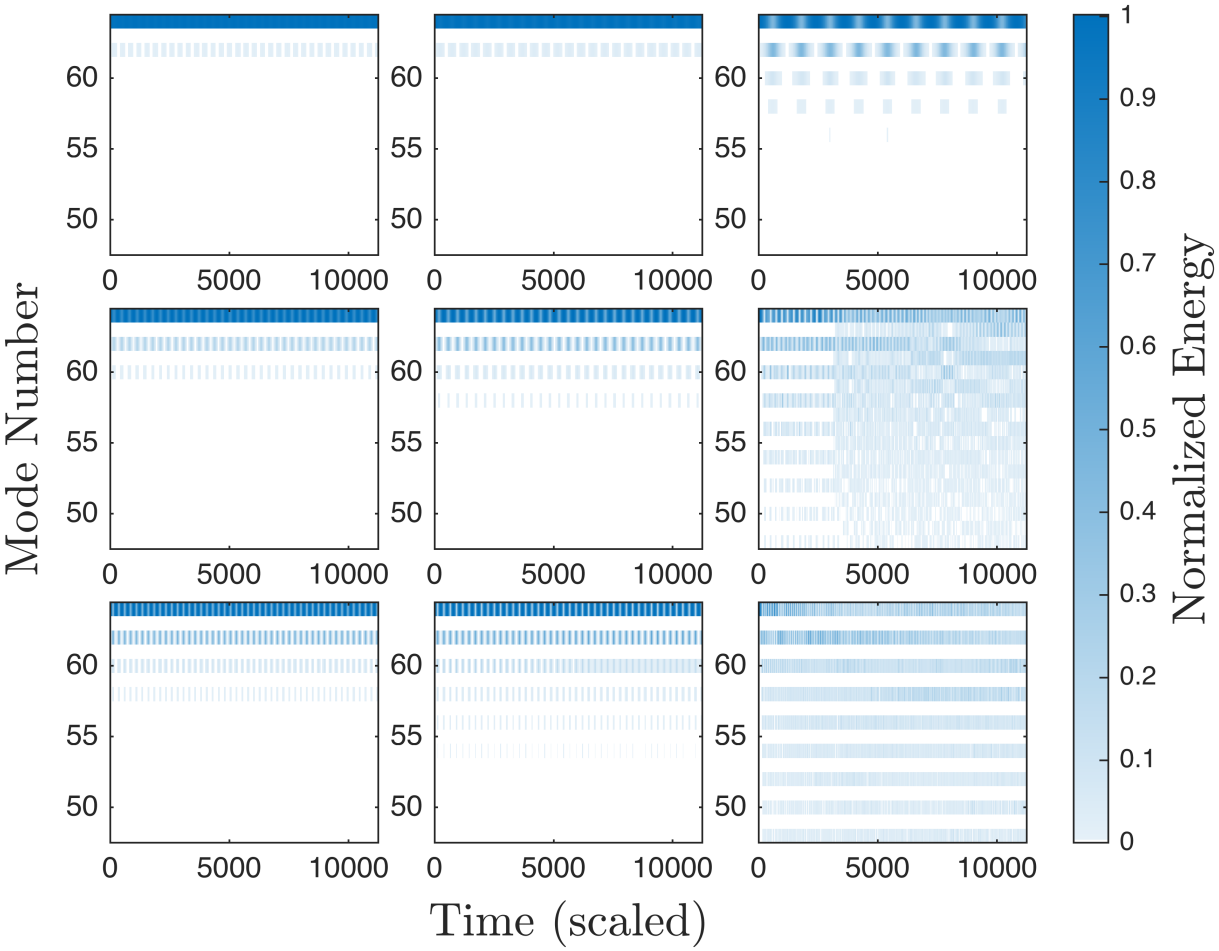

Fig. 3.9: Normalized energy per mode over time for a system of $N = 64$ particles with fixed boundary conditions. The columns represent different spring difference levels: $\Delta\kappa = 0.3, 0.6, 0.9$ (left to right). The rows correspond to varying nonlinearity strengths: $\beta = 1, 3, 5$ (top to bottom). The system is initialized with energy localized in the last mode with an amplitude of $A = 0.1$.

The analysis of the spectral entropy of this case, is represented in Fig. 3.10 for the $\alpha \neq 0$ case.The spectral entropy analysis for the $\alpha \neq 0$ case reveals consistent patterns in high-frequency mode dynamics. Most notably, configurations with $\Delta\kappa = 0.9$ consistently achieve the highest entropy values across all parameter sets. These cases exhibit pronounced oscillatory behavior, particularly strong in early time evolution before weakening, potentially indicating recurrent dynamics prior to system equilibration.

For the $\beta \neq 0$ case, the results are shown in 3.11. For this case, we observe analogous behavior at $\beta = 1$, with $\Delta\kappa = 0.9$ again yielding maximum entropy values. However, this oscillatory pattern diminishes with increasing β, converging toward the entropy evolution characteristics observed in low-frequency cases. The analysis further demonstrates that greater $\Delta\kappa$ values systematically enhance entropy production, suggesting that spring alternation significantly promotes energy equipartition when high-frequency modes are initially excited.

Having examined the fixed boundary condition cases, we now turn to periodic boundary

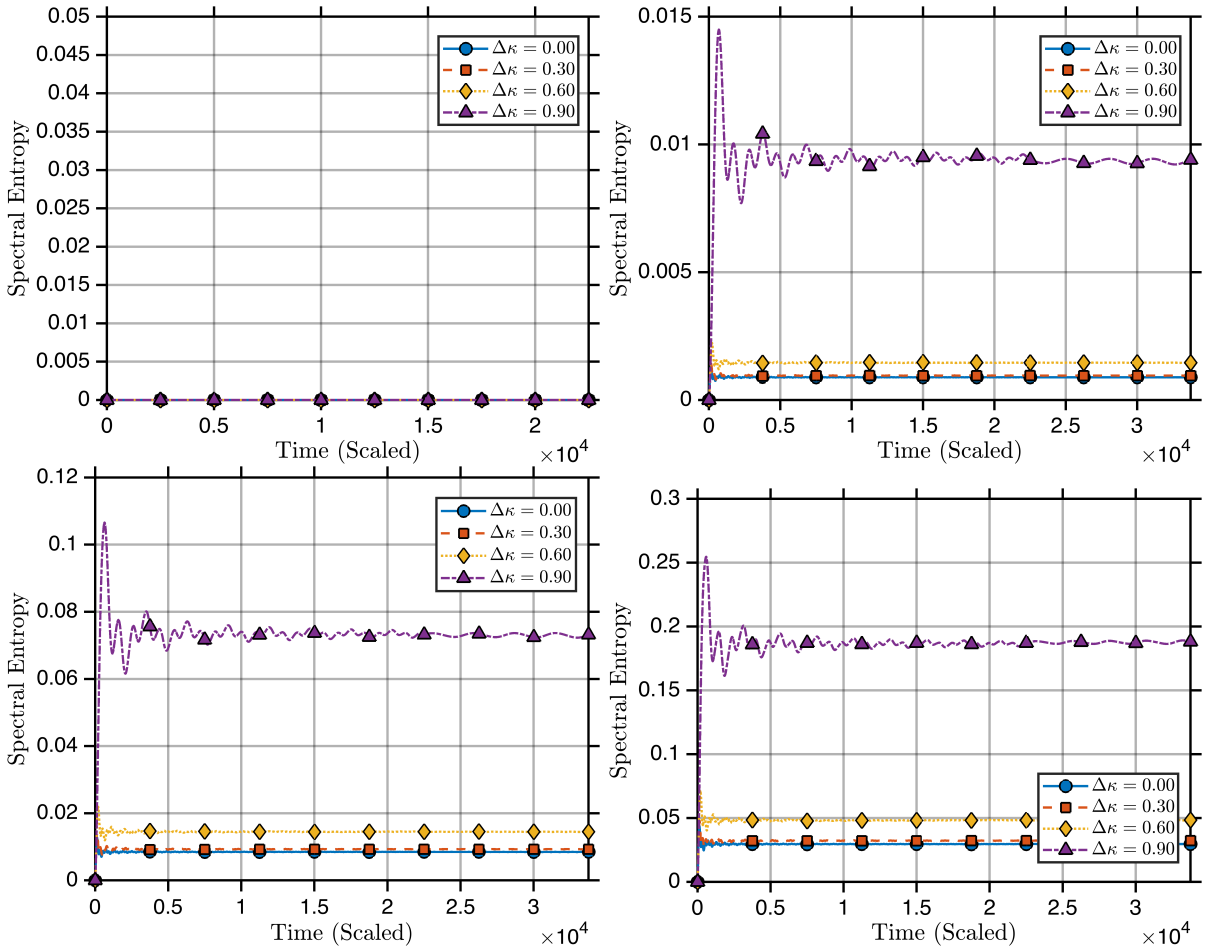

Fig. 3.10: Time evolution of the spectral entropy for a system of $N = 64$ particles with fixed boundary conditions, showing the variation of spectral entropy for different values of $\Delta\kappa$. Each panel corresponds to different values of the nonlinear parameter α, increasing from left to right and top to bottom: $\alpha = 0, 0.3, 0.6, 0.9$. The system is initialized with an excitation in the last mode, with an initial amplitude of $A = 0.1$.

conditions to investigate how system confinement affects these dynamics.

3.2. Periodic boundary conditions

3.2.1. Low Frequency Mode Dynamics and Its Effects

We begin our analysis with the α-FPUT system. The result can be visualized in Fig. 3.12. A notable behavior emerges for $\alpha = 0.3$: as $\Delta\kappa$ increases, fewer modes become excited, leading to energy localization in the lowest-frequency modes. However, this trend does not persist for larger values of α. For higher nonlinearities, an increase in $\Delta\kappa$ results in a greater number of excited modes, facilitating energy redistribution.

In particular, for $\alpha = 0.9$ and $\Delta\kappa = 0.3$ (Fig. 3.12, the system exhibits what appears to be a more chaotic energy transfer for times exceeding $t \approx 0.05$. In contrast, for lower values of α,

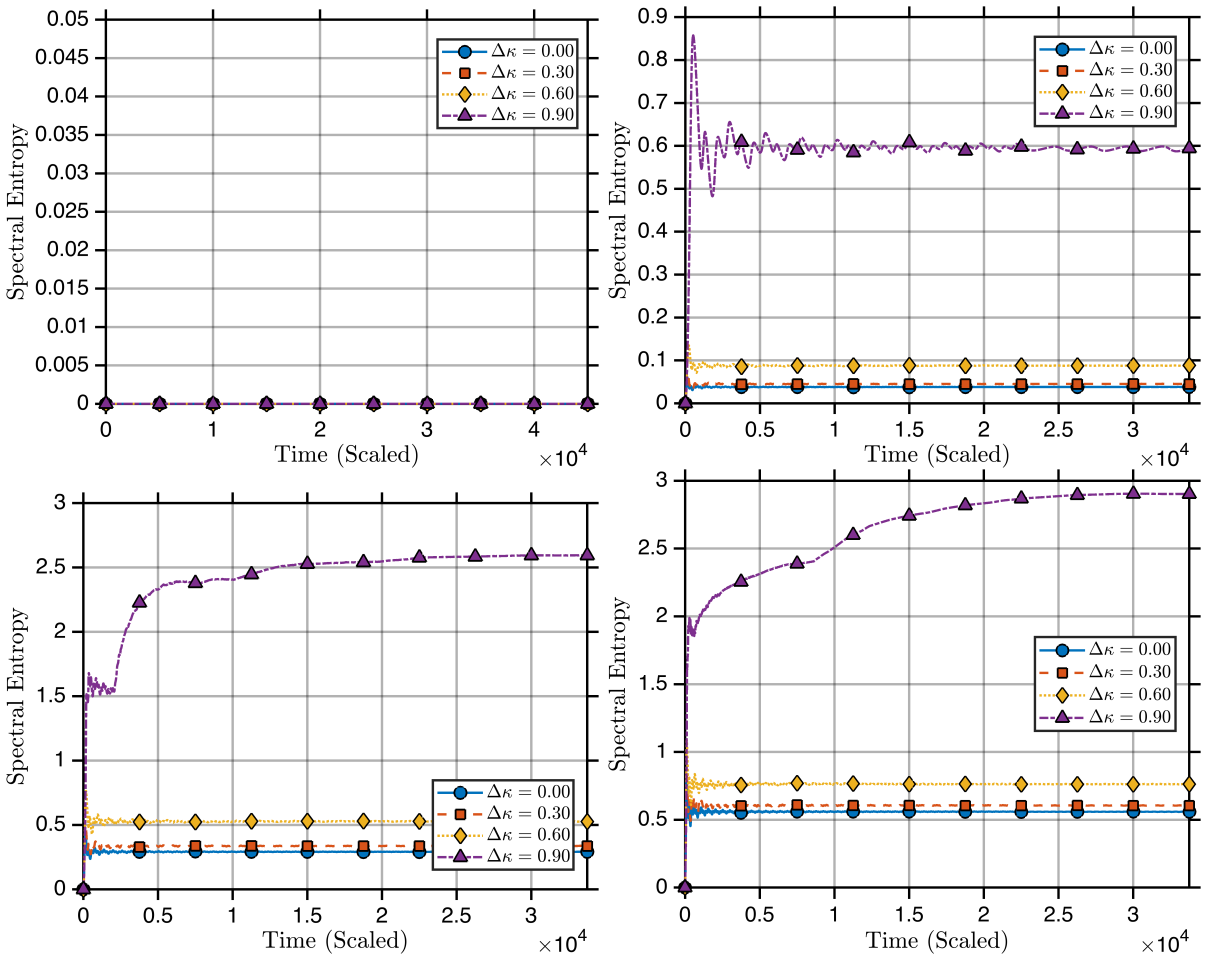

Fig. 3.11: Time evolution of the spectral entropy for a system of $N = 64$ particles with fixed boundary conditions, showing the variation of spectral entropy for different values of $\Delta\kappa$. Each panel corresponds to different values of the nonlinear parameter β, increasing from left to right and top to bottom: $\alpha = 0, 1, 3, 5$. The system is initialized with an excitation in the last mode, with an initial amplitude of $A = 0.1$.

energy follows a more structured pattern: it is initially transferred from the first mode to higher modes, then redistributed to the second excited mode, repeating this cycle before returning to the first mode.

Now, for the β-FPUT system, the result is shown in 3.13. For this system, another intriguing behavior is observed for $\beta = 1$, where only two modes are initially excited. As $\Delta\kappa$ increases, the recurrence time decreases for $\Delta\kappa = 0.6$, while for $\Delta\kappa = 0.9$, a lower-frequency mode becomes excited. Furthermore, as β increases, a progressively larger number of modes participate in the energy redistribution process.

As with other cases, we decided to explore spectral entropy with the objective to give an idea of the thermalization of the system. For the α-FPUT case, results are obtained in 3.14. For $\alpha = 0.3$, we see a similar pattern viewed on the case of Δm with fixed boundary conditions, in which as we increase $\Delta\kappa$, entropy tends to reach lower values. However, as before, for $\Delta\kappa = 0.3$, it seems like entropy tends to reach the values of the case $\Delta\kappa = 0$ and getting bigger on the long run. Now, this last observation tends to be more remarkable as α becomes bigger. For the case

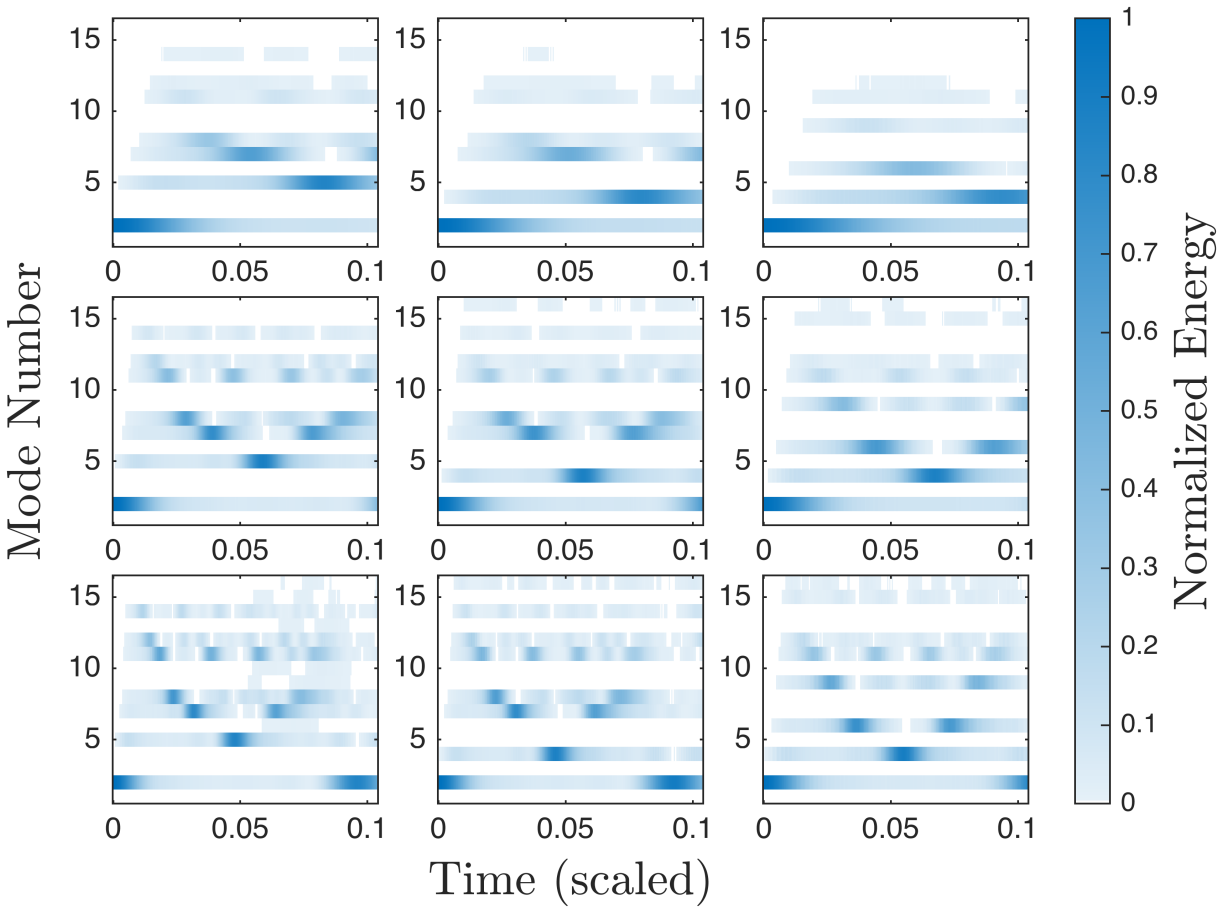

Fig. 3.12: Normalized energy per mode over time for a system of $N = 64$ particles with periodic boundary conditions. The columns represent different spring difference levels: $\Delta\kappa = 0.3, 0.6, 0.9$ (left to right). The rows correspond to varying nonlinearity strengths: $\alpha = 0.3, 0.6, 0.9$ (top to bottom). The system is initialized with energy localized in the second mode with an amplitude of $A = 5$.

of $\alpha = 0.9$, we can see that for $\Delta\kappa = 0.3$, entropy values are beyond the rest of the other cases of $\Delta\kappa$, showing a difference with respect to other cases, and what could be a 'phase transition' around $\Delta\kappa = 0.3$.

With respect to other cases, numerical stability becomes a major problem due to introduction of stiffness. This reflects the results of these figures. Further refinements on numerical methods are necessary for this, in light to help discern numerical errors or if we are appreciating a real behavior of the system.

For the β-FPUT system, results are shown in 3.15. For one hand, for $\beta = 1$, we can observe a similar pattern observed before, in which as we increase $\Delta\kappa$, entropy values decreases. This is not the case for the other values of β. For the cases of $\beta = 3$ and 5, we can observe an apparent stability of entropy just for increasing at later times, as we observed before for the case of fixed boundary conditions. This reflects an initial recurrence and trapped states, for later, possibly exciting other modes, not observed in figures 3.12 and 3.13.

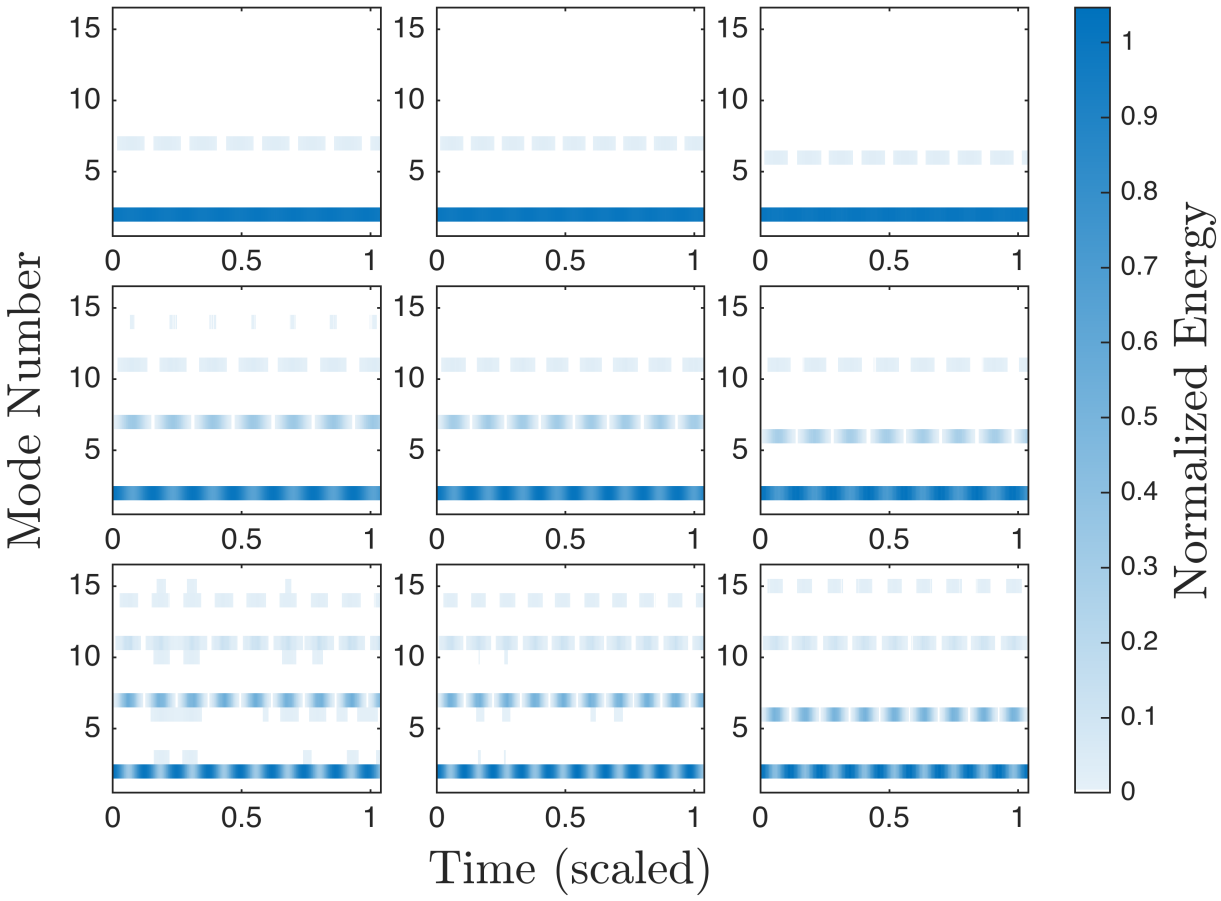

Fig. 3.13: Normalized energy per mode over time for a system of $N = 64$ particles with periodic boundary conditions. The columns represent different spring difference levels: $\Delta\kappa = 0.3, 0.6, 0.9$ (left to right). The rows correspond to varying nonlinearity strengths: $\beta = 1, 3, 5$ (top to bottom). The system is initialized with energy localized in the second mode with an amplitude of $A = 5$.

3.2.2. Exploration on High Frequency Modes

A complete characterization of the system's nonlinear dynamics requires examination of both acoustic (low-frequency) and optical (high-frequency) modes. However, periodic boundary conditions introduce significant numerical constraints that shape our analytical approach. For the $\beta \neq 0$ case, simulations remain numerically stable across physically relevant amplitude ranges, yielding reliable results. In contrast, the $\alpha \neq 0$ case presents substantial computational challenges - only at very small amplitudes ($A \approx 0.05$, as the case of β) could stable simulations be performed, which revealed trivial linear behavior without energy equipartition transitions, as a consequence of a low energy initial condition.

The simulation results are presented in Fig. 3.16, revealing distinct behaviors compared to previous cases. Notably, for $\beta = 1$, recurrence phenomena are entirely absent, even as $\Delta\kappa$ increases. As β grows, small energy cascades emerge, where energy briefly redistributes among neighboring modes before repeating the process ($\Delta\kappa = 0.3, 0.6$). For $\Delta\kappa = 0.9$, a clear energy cascade develops, disrupting recurrence and transferring energy predominantly among low-frequency modes. A similar pattern appears for $\alpha = 0.9$, reinforcing these observations.

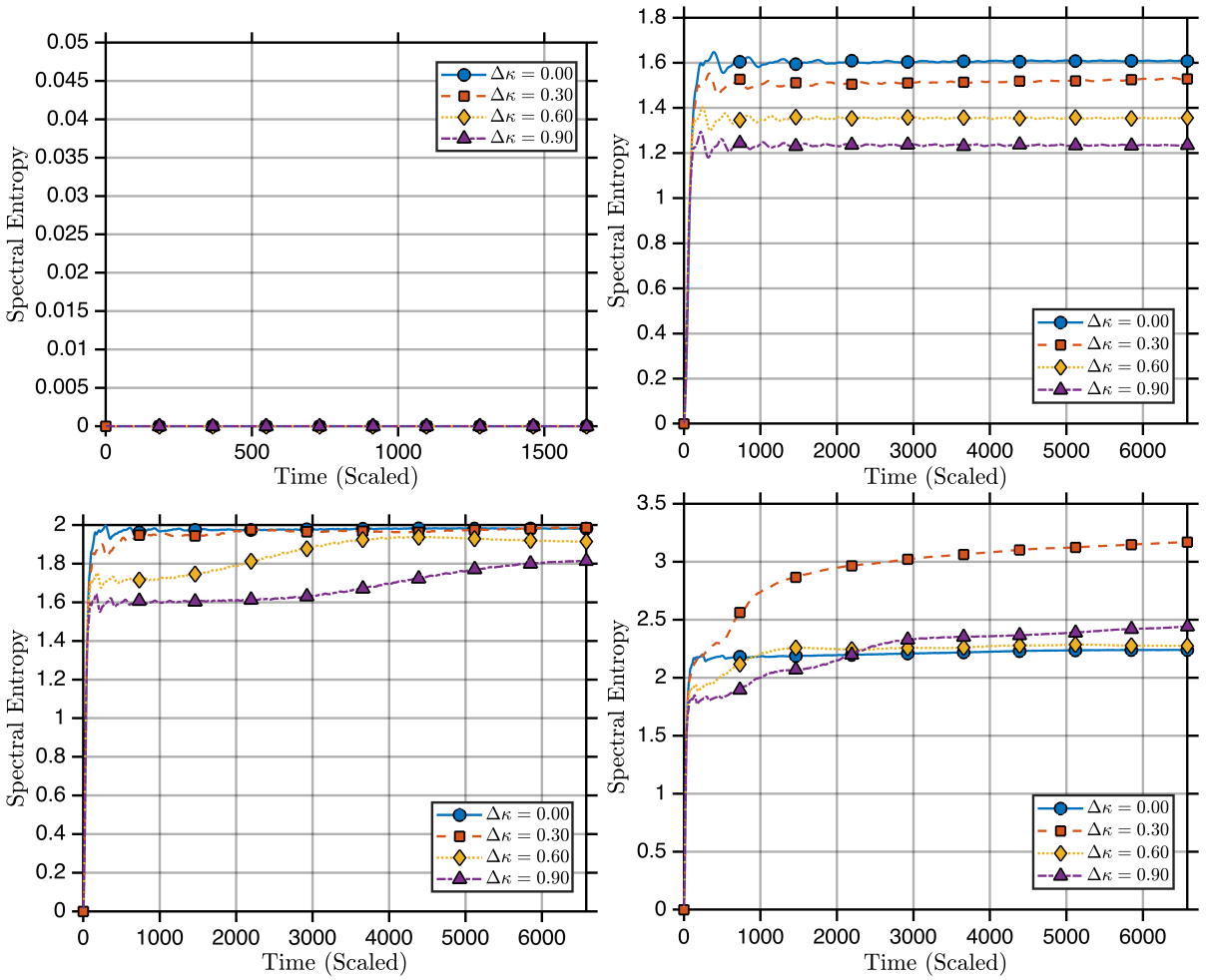

Fig. 3.14: Time evolution of the spectral entropy for a system of $N = 64$ particles with periodic boundary conditions, showing the variation of spectral entropy for different values of $\Delta\kappa$. Each panel corresponds to different values of α, increasing from left to right and top to bottom: $\alpha = 0, 0.3, 0.6, 0.9$. The system is initialized with an excitation in the second mode, with an initial amplitude of $A = 5$.

To quantify these effects, we compute the spectral entropy (see Figure 3.17). For $\beta = 1$, recurrence remains absent within the observed timeframe, but for $\Delta\kappa = 0.9$, the entropy exhibits a sharp increase, followed by oscillations and gradual growth. Lower $\Delta\kappa$ values display a more stable trend. For $\beta = 0.6$, the entropy evolves more smoothly for $\Delta\kappa = 0.9$, trending toward higher values over time, while other cases oscillate but suggest a tendency toward equilibrium. At $\beta = 5$, entropy rises even more smoothly for $\Delta\kappa = 0.9$, indicating a well-developed energy cascade (Figure 3.16). This suggests faster partial thermalization with minimal recurrence effects.

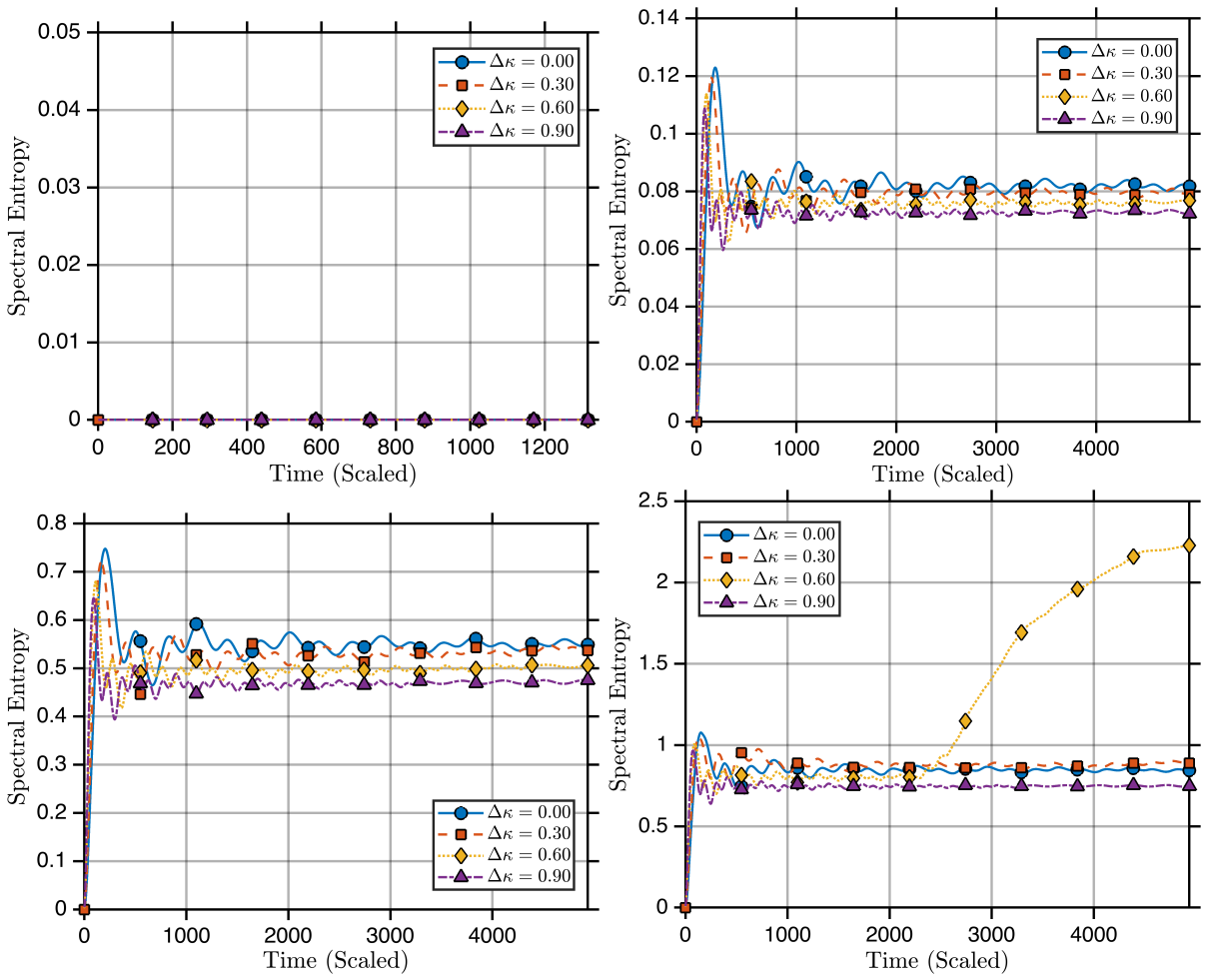

Fig. 3.15: Time evolution of the spectral entropy for a system of $N = 64$ particles with periodic boundary conditions, showing the variation of spectral entropy for different values of $\Delta\kappa$. Each panel corresponds to different values of β, increasing from left to right and top to bottom: $\beta = 0, 1, 3, 5$. The system is initialized with an excitation in the second mode, with an initial amplitude of $A = 5$.

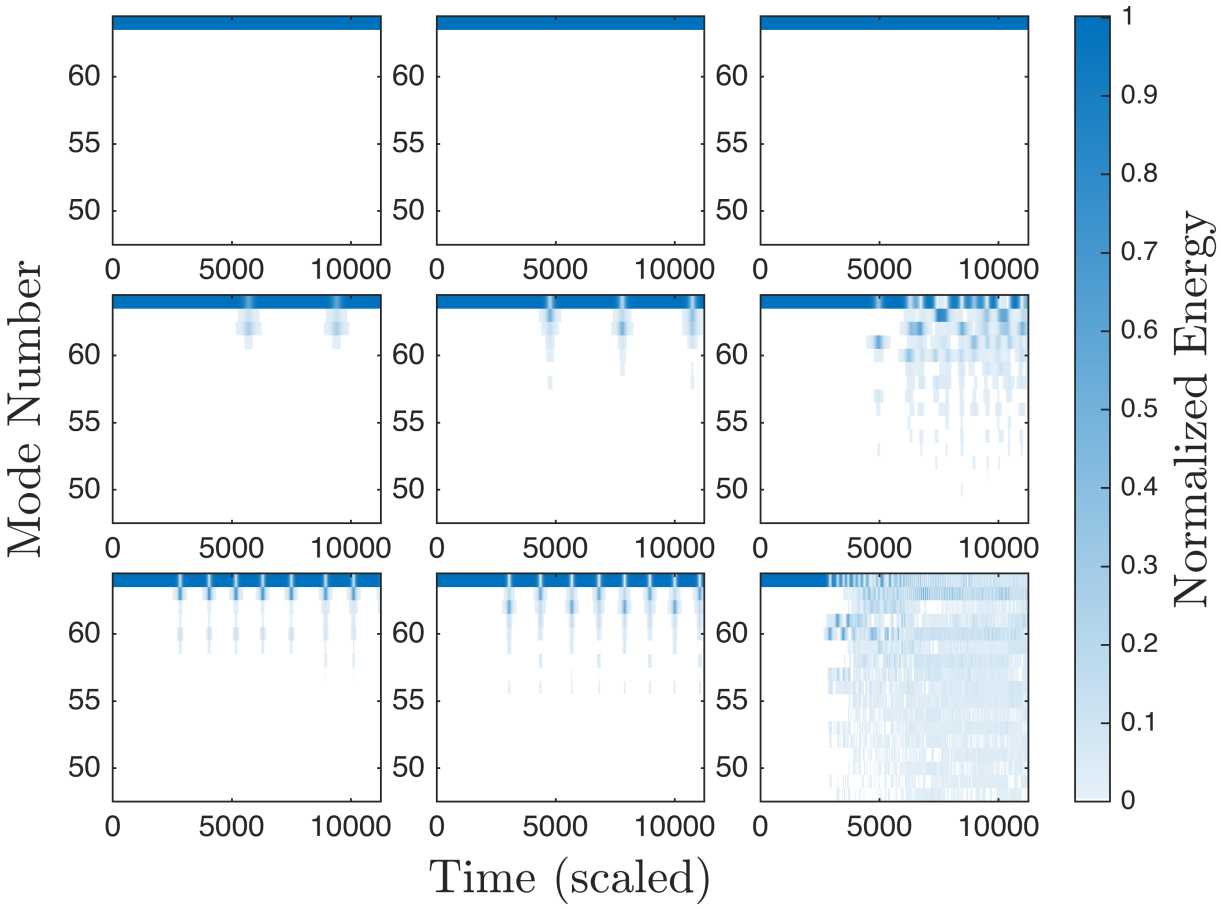

Fig. 3.16: Normalized energy per mode over time for a system of $N = 64$ particles with periodic boundary conditions. The columns represent different spring difference levels: $\Delta\kappa = 0.3, 0.6, 0.9$ (left to right). The rows correspond to varying nonlinearity strengths: $\beta = 1, 3, 5$ (top to bottom). The system is initialized with energy localized in the last mode with an amplitude of $A = 0.5$.

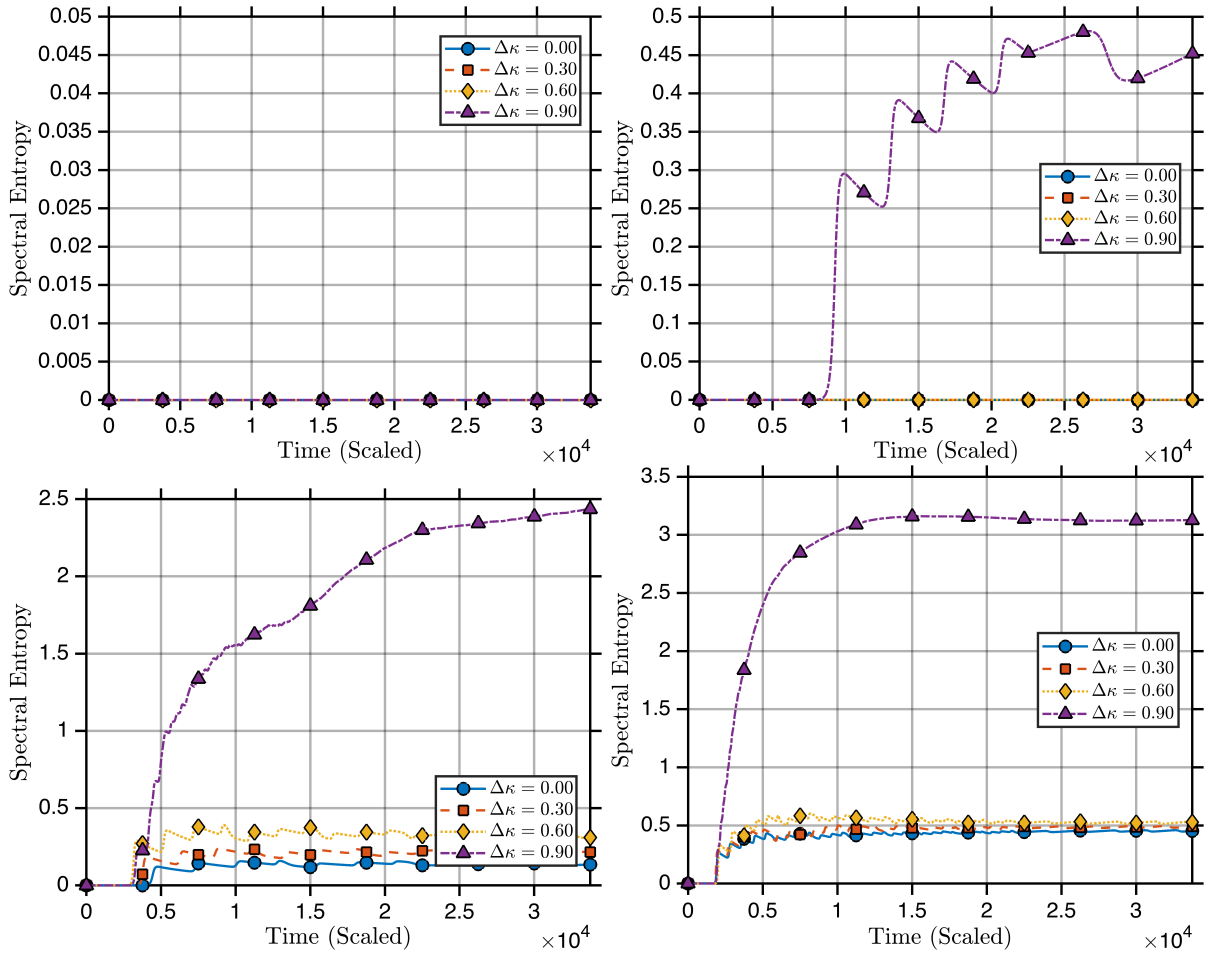

Fig. 3.17: Time evolution of the spectral entropy for a system of $N = 64$ particles with periodic boundary conditions, showing the variation of spectral entropy for different values of $\Delta\kappa$. Each panel corresponds to different values of β, increasing from left to right and top to bottom: $\beta = 0, 1, 3, 5$. The system is initialized with an excitation in the last mode, with an initial amplitude of $A = 0.05$.

Conclusions

This work presents a generalization of the Fermi-Pasta-Ulam-Tsingou (FPUT) model, incorporating site-dependent mass and spring distributions. Two specific cases were analyzed: a system with alternating masses and a system with alternating spring constants. While the case of alternating masses has been previously studied in the literature, the case of varying spring constants remains largely unexplored. This latter scenario is particularly relevant as a model for polymeric chains and topological insulators, offering new perspectives on wave propagation in structured materials.

For both cases, different initial conditions (ranging from low- to high-frequency modes) and boundary conditions (fixed and periodic) were explored. The results indicate that introducing local variations modifies recurrence behavior and thermalization dynamics in a nontrivial way, with the effects strongly dependent on the type and strength of the nonlinearity.

A central result is that the role of alternating mass-spring distributions varies with the nonlinearity parameters α and β, as well as the imposed boundary conditions. The key observations are:

- For weak nonlinearities ($\alpha = 0.3, \beta = 1$), in both fixed and periodic boundary conditions, introducing weak alternation in masses or springs leads to enhanced recurrence and delayed thermalization, as evidenced by the persistence of low spectral entropy values over long timescales. Energy remains confined to a few low-frequency modes, and equipartition is significantly inhibited.
- For weak nonlinearities of α and weak values of Δm, $\Delta\kappa$ the existence of a regime where thermalization time decreases as a function of Δm up to a quadratic term is given.
- For intermediate to strong nonlinearities, the impact depends on both the type of nonlinearity and boundary conditions:
  - In the α-FPUT case, energy redistribution remains slow, but nonlinear interactions gradually compensate for the frequency mismatch introduced by alternating masses or springs, leading to a progressive increase in entropy. This effect is particularly pronounced for periodic boundary conditions, where entropy increases more rapidly than in the homogeneous case ($\Delta m = 0, \Delta\kappa = 0$).
  - In the β-FPUT case, stronger nonlinearities ($\beta = 3, 5$) facilitate energy transfer across modes. For different values of β, thermalization accelerates despite disorder, as seen

in spectral entropy dynamics, which initially stabilizes before increasing significantly over time. Similar to the α case, this behavior emerges around a threshold of Δm or $\Delta\kappa$, and is more pronounced under periodic boundary conditions.

These findings challenge the conventional assumption that mass and spring alternance always inhibits thermalization. Instead, our results suggest that nonlinearity can counteract site variability-induced localization, restoring energy mixing and facilitating equipartition in certain regimes, while in others can inhibit it. This interplay between site variability, nonlinearity, and thermalization time highlights the importance of considering both mass and spring alternance when modeling wave turbulence and energy transport in complex systems.

Several open problems and extensions emerge from this study, offering promising avenues for future work:

- A further study of the limit case for weak α and Δm, $\Delta\kappa$, where α values around 0.1 are taken, and the exploration of low β values is also necessary.
- Higher-dimensional generalizations: Investigating whether the observed recurrence and localization effects persist in two- and three-dimensional lattices, where additional degrees of freedom may modify relaxation behavior.
- Chaotic vs. recurrent behavior: Examining the transition between localized and ergodic regimes in disordered nonlinear systems, using Lyapunov exponents and chaos indicators to classify dynamical phases.
- Extensions to different topologies: Exploring randomly disordered networks, quasicrystals, and non-periodic lattice structures, to determine whether disorder-enhanced or suppressed thermalization is a universal phenomenon.
- Connections to quantum analogs: Investigating potential links between classical nonlinear lattices and quantum many-body localization (MBL), particularly the role of Anderson localization and topological states in energy transport.
- Advanced numerical techniques: Developing more efficient computational methods for long-term integration of nonlinear and disordered systems, including machine learning-based models, symplectic integrators, and parallelized algorithms.

To address these questions, we propose the following methodological approach:

- Performance of more numerical simulations around the values $\alpha = 0$ and $\alpha = 0.2$, looking for the limit of α where quadratic dependence of Δm breaks for low and high values of Δm and experimenting with β values.
- Numerical and analytical studies in higher dimensions: Extend the current analysis to 2D and 3D lattices, comparing relaxation times and recurrence behavior with the 1D case. Implement high-performance computing techniques using Julia or C/C++ to handle large-scale simulations.

- Characterization of chaos and phase transitions: Apply Lyapunov exponent analysis to quantify the transition between regular, recurrent, and chaotic dynamics in nonlinear disordered systems.
- Graph-theoretical approaches to disorder: Investigate randomly disordered networks using graph theory and spectral analysis, to characterize energy redistribution and localization phenomena.
- Cross-disciplinary collaborations: Work with quantum physicists to explore classical-quantum correspondences, particularly regarding MBL and Anderson localization.

By pursuing these research directions, this study aims to contribute to a deeper understanding of nonlinear energy transport, disorder-induced localization, and thermalization dynamics. The results have broad implications in fields such as condensed matter physics, materials science, and quantum computing, providing a foundation for further explorations of nonlinear wave dynamics in structured media.

Apéndice A

MATLAB Code for numerical simulations

Listing A.1: MATLAB Simulation Code

```
% ----------------- Tests -------------------------------------
clear all;
close all;

% ---------------------- Parameters ----------------------
N = 32;              % Number of particles
alpha = 0.25;        % Nonlinear parameter alpha
beta = 0.0;          % Nonlinear parameter beta
TMAX = 12000;          % Maximum simulation time
DT = 20;          % Time step
tspan = 0:DT:TMAX;  % Time range for simulation
delta_t = 0.5; %Delta t for time averaged quantities

%------------------ Spring constants and masses ----------
DeltaMass = 0.0; % Alternating masses
DeltaK = 0.0;

%  Spring constants and alternating masses for numerical simulation
k = 1 + DeltaK * ((-1).^mod((0:N)', 2)); % Alternating masses
m = 1 + DeltaMass * ((-1).^mod((0:N-1)', 2)); % Alternating masses

% ---------------------- Normal Modes ----------------------
% Compute normal modes and frequencies
[frequencies, normal_matrix] = find_normal_modes(k, m); %Find
   normal modes
sqrt_inv_mass = diag(sqrt(1./ m)); % Find Normal Matrix
U_matrix = sqrt_inv_mass*normal_matrix;

% --------------------- Initial conditions ------------------
%Original state
q0 = sin(pi* (1:N)' / (N + 1));  % Initial positions
```

```
%q0 = -10*U_matrix(:, 1);
%5q0 = -U_matrix(:, N);
p0 = zeros(N, 1);                   % Initial momenta

state0 = [q0; p0];      % Combined initial state [q; p]
% ---------------------- ODE Solver ----------------------
%options = odeset('RelTol', 1e-12, 'AbsTol', 1e-15, 'MaxStep', DT);
    % Optimized tolerances
options = odeset('RelTol', 1e-9, 'AbsTol', 1e-12, 'MaxStep', DT); %
    For equal masses
%options = odeset('RelTol', 1e-6, 'AbsTol', 1e-9, 'MaxStep', DT); %
    For equal springs it should be fine
[T, Y] = ode78(@(t, state) yoshida_rhs(t, state, k, m, alpha, beta)
   , tspan, state0, options);

% Extract positions (q) and momenta (p)
q = Y(:, 1:N)';
p = Y(:, N+1:end)';

% ---------------------- Energy Computation ----------------------

% Compute scaled time using the first eigenvalue of the dynamical
   matrix
scaled_time = T * sqrt(frequencies(1)) / (2 * pi);
%scaled_time = T * sqrt(frequencies(1)) / (2 * pi);

energies_per_modes = find_energies(p, q, frequencies, normal_matrix
   , m);
%
% % ---------------------- Plotting ----------------------

% ---------------------- Optimized Grayscale-Friendly Plot
   ----------------------
indices = 1:5;  % First 5 modes to plot
figure;
hold on;

% Define different line styles & markers for better distinction
line_styles = {'-', '--', ':', '-.', '--'};
marker_styles = {'o', 's', 'd', '^', 'v'};

% Select fewer points for markers
num_markers = 10;
marker_indices = round(linspace(1, length(scaled_time), num_markers
   ));

for idx = 1:length(indices)
```

```
    i = indices(idx);

    % Plot with fewer markers
    plot(scaled_time, energies_per_modes(i, :), 'LineStyle',
       line_styles{idx}, ...
         'LineWidth', 2.0, 'Marker', marker_styles{idx}, '
            MarkerSize', 7, ...
         'MarkerIndices', marker_indices, 'Color', [0 0 0], ...
         'DisplayName', sprintf('Mode %d', i));

    % Compute label position
    last_x = scaled_time(end);
    last_y = energies_per_modes(i, end);

    % Offset labels for visibility
    offset = max(energies_per_modes(i, :)) * 0.15 * (-1)^idx;
    label_y = last_y + offset;
    label_y = max(label_y, min(energies_per_modes(i, :)) * 1.05);

    % Add labels slightly above the last point
    %text(last_x, label_y, sprintf('%d', i), 'FontSize', 14, '
       FontWeight', 'bold', ...
    %     'HorizontalAlignment', 'left', 'VerticalAlignment', '
       bottom', 'Color', [0 0 0]);
end

% Formatting for grayscale
xlabel('Time (scaled)', 'Interpreter', 'latex', 'FontSize', 18, '
   FontWeight', 'bold');
ylabel('Energy', 'Interpreter', 'latex', 'FontSize', 18, '
   FontWeight', 'bold');
legend('show', 'Location', 'best', 'Interpreter', 'latex');
set(gca, 'FontSize', 13, 'LineWidth', 1.5, 'GridAlpha', 0.5, '
   XColor', [0 0 0], 'YColor', [0 0 0]);
grid off;
box on;
hold off;

% ---------------------- Plot Total Energy ----------------------

% ---------------------- Total Energy Computation
   ----------------------

% Compute total energy using the defined functions
total_energy_over_time = compute_energy(p, q, m, k);

figure;
```

```
plot(T, total_energy_over_time, 'LineWidth', 1.5);
title('Total Energy Over Time');
xlabel('Time');
ylabel('Total Energy');

grid on;

% ---------------------- Compute and Plot Cumulative Average Energy
    -----------------------
avg_energies = average_energy_cumulative(energies_per_modes,
   scaled_time, delta_t);
plot_average_energy(avg_energies, scaled_time);

% ---------------------- RHS Function ----------------------
function dstate = yoshida_rhs(~, state, k, m, alpha, beta)
    N = length(m);  % Number of particles
    q = state(1:N);  % Positions
    p = state(N+1:end);  % Momenta
    forces = zeros(N,1);

    % Compute forces (dp)
    diff_q_left = q(2:end-1) - q(1:end-2); %[0; q(2:end-1) - q(1:
       end-2)];  % Left spring elongations
    diff_q_right = q(3:end) - q(2:end-1); % [q(3:end) - q(2:end-1);
        0]; % Right spring elongations

    % Forces calculation
    forces(2:end-1) = k(3:end-1) .* diff_q_right - k(2:end-2) .*
       diff_q_left + ...
          alpha * (k(3:end-1) .* diff_q_right.^2 - k(2:end-2) .*
              diff_q_left.^2) + ...
          beta * (k(3:end-1) .* diff_q_right.^3 - k(2:end-2) .*
             diff_q_left.^3);


    % Boundary conditions for left and right springs
    forces(1) = -k(1) * q(1) + k(2) * (q(2) - q(1)) + ...
                alpha * (k(2) * (q(2) - q(1))^2 - k(1) * q(1)^2) +
                   ...
                beta * (k(2) * (q(2) - q(1))^3 - k(1) * q(1)^3);

    forces(end) = -k(end) * q(end) + k(end-1) * (q(end-1) - q(end))
        + ...
                  alpha * (-k(end-1) * (q(end-1) - q(end))^2 - k(
                     end) * q(end)^2) + ...
                  beta * (k(end-1) * (q(end-1) - q(end))^3 - k(end)
                      * q(end)^3);
```

```
    dq = p ./ m;  % Velocity
    dp = forces;  % Forces

    % Combine derivatives
    dstate = [dq; dp];

    % Spectral Entropy
    spectral_entropy = find_spectral_entropy(avg_energies);
    % Compute derivative of entropy
    %dS_dt = abs(diff(spectral_entropy) ./ max(diff(scaled_time), 1
       e-5));
    dS = abs(diff(spectral_entropy));

    % Find first index where entropy change stabilizes
    %equilibrium_index = find(movmean(dS_dt, window_size) <
       threshold, 1);
    equilibrium_index = find(dS < threshold, 1)+1;

    % Fix: Ensure equilibrium_index is valid before indexing
       scaled_time
    if ~isempty(equilibrium_index) && equilibrium_index <= length(
       scaled_time)
        equilibrium_times(i, j) = scaled_time(equilibrium_index);
        fprintf("Equilibrium reached at t=%.2f for alpha =%.2f,
           Delta K=%.2f\n", ...
            equilibrium_times(i, j), alpha, DeltaK);
    else
        equilibrium_times(i, j) = NaN;  % Assign NaN if no valid
           equilibrium found
        fprintf("Equilibrium not reached for alpha =%.2f, Delta K
           =%.2f\n", alpha, DeltaK);
    end

end

function D = build_dynamical_matrix_fixed(k, m)
    N = length(m); % Number of particles
    D = zeros(N, N); % Initialize the matrix

    % Fill the diagonal and off-diagonal elements
    for i = 1:N
        D(i, i) = D(i, i) + k(i) / m(i); % Contribution from left
           spring
        if i > 1
            D(i, i-1) = -k(i) / sqrt(m(i) * m(i-1)); % Off-diagonal
                term (coupling)
```

```
        end
        D(i, i) = D(i, i) + k(i+1) / m(i); % Contribution from
            right spring
        if i < N
            D(i, i+1) = -k(i+1) / sqrt(m(i) * m(i+1)); % Off-
                diagonal term (coupling)
        end
    end
end

function [frequencies, normal_coordinates] = find_normal_modes(k, m
    )
    % Find the normal modes (frequencies and eigenvectors)
    D = build_dynamical_matrix_fixed(k, m);  % Dynamical matrix
    [V, Lambda] = eig(full(D));  % Eigen decomposition
    frequencies = sqrt(diag(Lambda));  % Eigenvalues (frequencies
        squared)
    normal_coordinates = V;  % Eigenvectors (normal coordinates)
end

function energies_per_modes = find_energies(p, q, frequencies,
    normal_matrix, m)
    % Compute energies for each mode
    [N_particles, total_time] = size(q);
    energies = zeros(N_particles, total_time);  % Preallocate

    sqrt_inv_mass = diag(sqrt(1./m));
    U_matrix = sqrt_inv_mass*normal_matrix;
    v = p ./ m;

    for i = 1:total_time
        normal_q = U_matrix \ q(:, i);
        normal_v = U_matrix \ v(:, i);

        energies(:, i) = 0.5 * (normal_v.^2 + (frequencies.^2 .*
            normal_q.^2));
    end

    energies_per_modes = energies;
end

function avg_energies = average_energy_cumulative(energies, t,
    delta_t)
    [num_modes, time_steps] = size(energies);
    avg_energies = NaN(num_modes, time_steps);

    for i = 1:time_steps
```

```
        t_min = max(t(1), t(i) - t(i)*delta_t);
        t_max = min(t(end), t(i) + t(i)*delta_t);
        indices = find(t_min <= t & t <= t_max);
        if ~isempty(indices)
            avg_energies(:, i) = mean(energies(:, indices), 2);
        end
    end

end

function plot_average_energy(avg_energies, scaled_time)
    figure;
    hold on;

    % Define grayscale-friendly line styles and markers
    line_styles = {'-', '--', ':', '-.', '--'};
    marker_styles = {'o', 's', 'd', '^', 'v'};

    % Select fewer points for markers
    num_markers = 10;
    marker_indices = round(linspace(1, length(scaled_time),
       num_markers));

    % Loop through modes and apply grayscale-friendly styles
    for i = 1:min(5, size(avg_energies, 1))
        plot(scaled_time, avg_energies(i, :), 'LineStyle',
           line_styles{i}, ...
             'LineWidth', 2.0, 'Marker', marker_styles{i}, '
                MarkerSize', 6, ...
             'MarkerIndices', marker_indices, 'Color', [0 0 0], ...
             'DisplayName', sprintf('Mode %d', i));
    end

    % Improve readability for grayscale
    xlabel('Time (scaled)', 'Interpreter', 'latex', 'FontSize', 18,
        'FontWeight', 'bold');
    ylabel('Average Energy (Normalized)', 'Interpreter', 'latex', '
       FontSize', 18, 'FontWeight', 'bold');
    legend('show', 'Location', 'best', 'Interpreter', 'latex');
    set(gca, 'FontSize', 14, 'LineWidth', 1.5, 'GridAlpha', 0.5, '
       XColor', [0 0 0], 'YColor', [0 0 0]);
    grid off;
    box on;
    hold off;
end

function plot_particle_positions(time_steps, positions)
```

```
    figure;
    hold on;

    % Define grayscale-friendly markers
    markers = {'o', 's', 'd', '^', 'v', 'p', 'h'};
    num_markers = length(markers);

    % Loop through time steps and plot with different markers
    for i = 1:length(time_steps)
        marker_style = markers{mod(i - 1, num_markers) + 1}; %
           Cycle through markers
        scatter(1:size(positions, 1), positions(:, i), ...  % X:
           particle index, Y: displacement
                50, 'k', marker_style, 'filled', 'DisplayName',
                   sprintf('$t = %.1fs$', time_steps(i)));
    end

    % Labels and formatting
    xlabel('Mass Position', 'Interpreter', 'latex', 'FontSize', 18)
       ;
    ylabel('Displacement', 'Interpreter', 'latex', 'FontSize', 18);
    legend('show', 'Location', 'best', 'Interpreter', 'latex');
    set(gca, 'FontSize', 14, 'LineWidth', 1.5, 'GridAlpha', 0.5, '
       XColor', [0 0 0], 'YColor', [0 0 0]);
    grid off;
    box on;
    hold off;
end

plot_particle_positions([1, 55, 267, 504, 600], q);

% ---------------------- Heat Map of Energies per Mode
   ------------------------

% **Heat Map of Energies per Mode with Custom 'sky' Colormap and
   White Lowest Value**
figure;
set(gcf, 'Color', 'w'); % Set figure background to white
ax = gca;
ax.Color = 'w'; % Ensure axes background is also white
initial_total_energy = sum(energies_per_modes(:, 1));
normalized_energies = energies_per_modes / initial_total_energy;

%imagesc(scaled_time, 1:10, normalized_energies); %Low frequency
imagesc(scaled_time, 1:N ,normalized_energies); %High frequency
set(gca, 'YDir', 'normal');
```

```
% Get the 'sky' colormap and modify the lowest value to white
cmap = colormap('sky'); % Get current colormap
cmap(1, :) = [1 1 1]; % Set lowest value to white
colormap(cmap);

colorbar;
xlabel('Time (scaled)', 'Interpreter', 'latex', 'FontSize', 18);
ylabel('Mode Number',  'Interpreter', 'latex', 'FontSize', 18);
c = colorbar;
c.Label.String = 'Normalized Energy';

% ---------------------- Total Energy Functions
   ----------------------
% Compute kinetic energy
function T = kinetic_energy(p, m)
    T = 0.5 * sum(p.^2 ./ m);
end

% Compute potential energy
function V = potential_energy(q, k)
    diff = q(2:end) - q(1:end-1);
    V = 0.5 * sum(k(2:end-1) .* diff.^2);
    V = V + 0.5 * (k(1) * q(1)^2 + k(end) * q(end)^2); % k(end) * (
       q(1) - q(end))^2;
end

% Compute total energy
function E = total_energy(q, p, m, k)
    T = kinetic_energy(p, m);
    V = potential_energy(q, k);
    E = T + V;
end

% Compute energy over time
function energies = compute_energy(p, q, m, k)
    total_time = size(q, 2);
    energies = zeros(1, total_time);

    for t = 1:total_time
        energies(t) = total_energy(q(:, t), p(:, t), m, k);
    end
end


% ------------- Functions for periodic boundary conditions --------

clear all;
```

```
close all;

% ---------------------- Parameter Sweep Setup
   ----------------------
N = 64;
alpha = 0.9;
beta = 0.0;
TMAX = 10000;
DT = 20;
tspan = 0:DT:TMAX;

DeltaMass = 0.0;
DeltaK = 0.9;

k = 1 + DeltaK * ((-1).^mod((0:N-1)', 2)); % Alternating masses
m = 1 + DeltaMass * ((-1).^mod((0:N-1)', 2)); % Alternating masses

% ------------- Normal Modes --------------------
% Compute normal modes and frequencies
[frequencies, normal_matrix] = find_normal_modes(k, m);
sqrt_inv_mass = diag(sqrt(1 ./ m));
U_matrix = sqrt_inv_mass * normal_matrix;

% -------------------- Initial Conditions ----------------------
q0 = -5*U_matrix(:, 2);  % Initial positions
p0 = zeros(N, 1);          % Initial momenta
state0 = [q0; p0];

%------------------------ Dynamical Matrix --------------
function D = build_dynamical_matrix_periodic(k, m)
    N = length(m);  % Number of particles
    D = zeros(N, N);  % Initialize dynamical matrix

    for i = 1:N
        % Previous and next indices with periodic boundary
           conditions
        iprev = mod(i-2, N) + 1;  % i-1 in MATLAB indexing (cyclic)
        inext = mod(i, N) + 1;    % i+1 in MATLAB indexing (cyclic)

        % Diagonal term
        D(i, i) = (k(i) + k(iprev)) / m(i);

        % Off-diagonal terms (coupling with neighbors)
        D(i, inext) = -k(i) / sqrt(m(i) * m(inext));
        D(i, iprev) = -k(iprev) / sqrt(m(i) * m(iprev));
    end
end
```

```
% ----------------------- Functions for spectral entropy
    -------------
function spectral_entropy = find_spectral_entropy(average_energies)
    total_energy = sum(average_energies, 1);
    normalized_energies = average_energies ./ total_energy;
    spectral_entropy = -sum(normalized_energies .* log(
        normalized_energies));
end


% Define stability threshold
threshold = 1e-7; % Stability criterion
window_size = 10; % Moving window for stability check
equilibrium_times = NaN(length(alpha_values), length(DeltaK_values)
    );
```

Bibliografía

[1] T. Dauxois. Fermi, Pasta, Ulam, and a mysterious lady. *Physics today*, **61**(1):55-57, 2008 (citado en la pág. 1).

[2] J. Ford. The Fermi-Pasta-Ulam problem: paradox turns discovery. *Physics Reports*, **213**(5):271-310, 1992 (citado en las págs. 1, 5, 6).

[3] E. Fermi, P Pasta, S. Ulam y M. Tsingou. Studies of the nonlinear problems. Informe técnico, Los Alamos National Laboratory (LANL), Los Alamos, NM (United States), 1955 (citado en las págs. 1, 18, 19).

[4] G. Gallavotti. *The Fermi-Pasta-Ulam problem: a status report*, volumen 728. Springer Science & Business Media, 2007 (citado en las págs. 1, 6, 19).

[5] J. Romero-Arias y G. G. Naumis. Thermal relaxation and low-frequency vibrational anomalies in simple models of glasses: A study using nonlinear Hamiltonians. *Physical Review E—Statistical, Nonlinear, and Soft Matter Physics*, **77**(6):061504, 2008 (citado en la pág. 1).

[6] G. G. Naumis. Low-Frequency Vibrational Modes Anomalies and Rigidity: A Key to Understanding the Glass and the Electronic Properties of Flexible Materials from a Topological Perspective. *Frontiers in Materials*, **2**, jun. de 2015. ISSN: 2296-8016. DOI: 10.3389/fmats.2015.00044. URL: http://dx.doi.org/10.3389/fmats.2015.00044 (citado en la pág. 1).

[7] X. Fang, W. Lacarbonara y L. Cheng. Advances in nonlinear acoustic/elastic metamaterials and metastructures. *Nonlinear Dynamics*, sep. de 2024. ISSN: 1573-269X. DOI: 10.1007/s11071-024-10219-4. URL: http://dx.doi.org/10.1007/s11071-024-10219-4 (citado en la pág. 1).

[8] D. Sholl. Modal coupling in one-dimensional anharmonic lattices. *Physics Letters A*, **149**(5-6):253-257, 1990 (citado en la pág. 5).

[9] L. Peng, W. Fu, Y. Zhang y H. Zhao. Instability dynamics of nonlinear normal modes in the Fermi–Pasta–Ulam–Tsingou chains. *New Journal of Physics*, **24**(9):093003, 2022 (citado en la pág. 5).

[10] C. G. Goedde, A. J. Lichtenberg y M. A. Lieberman. Chaos and the approach to equilibrium in a discrete sine-Gordon equation. *Physica D: Nonlinear Phenomena*, **59**(1-3):200-225, 1992 (citado en la pág. 6).

[11] R. Livi, M. Pettini, S. Ruffo, M. Sparpaglione y A. Vulpiani. Equipartition threshold in nonlinear large Hamiltonian systems: The Fermi-Pasta-Ulam model. *Physical Review A*, **31**(2):1039, 1985 (citado en la pág. 6).

[12] K. A. Reiss y D. K. Campbell. The Metastable State of Fermi–Pasta–Ulam–Tsingou Models. *Entropy*, **25**(2):300, 2023 (citado en la pág. 6).

[13] F. Verhulst. Variations on the Fermi-Pasta-Ulam chain, a survey. En *Chaotic Modeling and Simulation International Conference*, páginas 1025-1042. Springer, 2020 (citado en las págs. 9, 21).

[14] W. van der Kallen y F. Verhulst. Explorations for alternating FPU-chains with large mass. *International Journal of Non-Linear Mechanics*, **137**:103809, 2021 (citado en las págs. 9, 21).

[15] A. Dhar y K. Saito. Heat conduction in the disordered Fermi-Pasta-Ulam chain. *Physical Review E—Statistical, Nonlinear, and Soft Matter Physics*, **78**(6):061136, 2008 (citado en la pág. 9).

[16] C. Giardina, R. Livi, A Politi y M Vassalli. Finite thermal conductivity in 1D lattices. *Physical review letters*, **84**(10):2144, 2000 (citado en la pág. 10).

[17] M. Onorato, Y. V. Lvov, G. Dematteis y S. Chibbaro. Wave Turbulence and thermalization in one-dimensional chains. *Physics Reports*, **1040**:1-36, 2023 (citado en las págs. 10, 14-16).

[18] W. Fu, Y. Zhang y H. Zhao. Nonintegrability and thermalization of one-dimensional diatomic lattices. *Physical Review E*, **100**(5):052102, 2019 (citado en las págs. 10, 16).

[19] A. Ponno. The Fermi-Pasta-Ulam problem in the thermodynamic limit: Scaling laws of the energy cascade. En *Chaotic Dynamics and Transport in Classical and Quantum Systems: Proceedings of the NATO Advanced Study Institute on International Summer School on Chaotic Dynamics and Transport in Classical and Quantum Systems Cargèse, Corsica 18–30 August 2003*, páginas 431-440. Springer, 2005 (citado en las págs. 10, 14, 15).

[20] S. H. Simon. *The Oxford solid state basics*. OUP Oxford, 2013 (citado en la pág. 11).

[21] N. J. Zabusky y M. D. Kruskal. Interaction of"solitonsïn a collisionless plasma and the recurrence of initial states. *Physical review letters*, **15**(6):240, 1965 (citado en las págs. 13, 14).

[22] H. Christodoulidi, C. Efthymiopoulos y T Bountis. Energy localization on q-tori, long-term stability, and the interpretation of Fermi-Pasta-Ulam recurrences. *Physical Review E—Statistical, Nonlinear, and Soft Matter Physics*, **81**(1):016210, 2010 (citado en las págs. 13, 14).

[23] V. Z. V. L'vov y G Falkovich. Kolmogorov Spectra of Turbulence I, 1992 (citado en las págs. 13, 15).

[24] D. Shepelyansky. Low-energy chaos in the Fermi-Pasta-Ulam problem. *Nonlinearity*, **10**(5):1331, 1997 (citado en la pág. 13).

[25] A Pezzi, G Deng, Y Lvov, M Lorenzo y M Onorato. Three-wave resonant interactions in the diatomic chain with cubic anharmonic potential: theory and simulations. *arXiv preprint arXiv:2103.08336*, 2021 (citado en las págs. 14, 15, 31, 32).

[26] M. Onorato, L. Vozella, D. Proment e Y. V. Lvov. Route to thermalization in the α-Fermi–Pasta–Ulam system. *Proceedings of the National Academy of Sciences*, **112**(14):4208-4213, 2015 (citado en la pág. 15).

[27] Y. V. Lvov y M. Onorato. Double scaling in the relaxation time in the β-Fermi-Pasta-Ulam-Tsingou model. *Physical review letters*, **120**(14):144301, 2018 (citado en la pág. 15).

[28] F. Novkoski, C.-T. Pham y E. Falcon. Evidence of experimental three-wave resonant interactions between two dispersion branches. *Physical Review E*, **107**(4):045101, 2023 (citado en las págs. 15, 27).

[29] F. Israiljev y B. V. Chirikov. The statistical properties of a non-linear string. Informe técnico, SCAN-9908053, 1965 (citado en la pág. 19).

[30] J. Q. Toledo-Marín y G. G. Naumis. Escape time, relaxation, and sticky states of a softened henon-heiles model: Low-frequency vibrational mode effects and glass relaxation. *Physical Review E*, **97**(4):042106, 2018 (citado en la pág. 21).

[31] L. Deng, H. Yu, Z. Zhu, W. Fu, Y. Wang y L. Huang. q-Breathers in the diatomic β-Fermi-Pasta-Ulam-Tsingou chains. *New Journal of Physics*, 2025 (citado en la pág. 27).